



Universitat Autònoma de Barcelona

**ADVERTIMENT.** L'accés als continguts d'aquesta tesi queda condicionat a l'acceptació de les condicions d'ús establertes per la següent llicència Creative Commons:  [http://cat.creativecommons.org/?page\\_id=184](http://cat.creativecommons.org/?page_id=184)

**ADVERTENCIA.** El acceso a los contenidos de esta tesis queda condicionado a la aceptación de las condiciones de uso establecidas por la siguiente licencia Creative Commons:  <http://es.creativecommons.org/blog/licencias/>

**WARNING.** The access to the contents of this doctoral thesis it is limited to the acceptance of the use conditions set by the following Creative Commons license:  <https://creativecommons.org/licenses/?lang=en>

# **Study of the cooperative effect of UVR, BRAF and LKB1 in Melanoma**

---

PhD thesis

PhD student: Elena González Sánchez

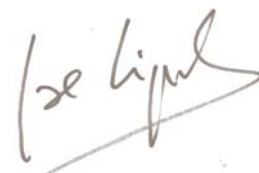
Thesis director: Dr. Juan Ángel Recio Conde  
Tutor Director: Dr. José Miguel Lizcano de Vega  
Biochemistry, Molecular Biology and Biomedicine PhD program  
Biochemistry and Molecular Biology Department  
Autonomous University of Barcelona (UAB)  
2019



Elena González Sánchez  
PhD Student



Juan Ángel Recio Conde, PhD  
Thesis Director



José Miguel Lizcano de Vega, PhD  
Thesis Tutor

# SUMMARY

Understanding the molecular mechanisms related with melanomagenesis is key in order to find new preventive and therapeutical approaches against this lethal disease. Epidemiology indicates that there are genetic- and environmental-factors associated with melanoma development and progression. In this study, we have generated the B/L/UV animal model that allows us to study the cooperation between the oncogene, *Braf*<sup>V600E</sup>, the environmental insult, ultraviolet radiation (UVR), and the loss of a tumor suppressor, *Lkb1*.

In summary, the B/L/UV animal model presented here is a strong system to study the melanoma pathogenesis. This animal model demonstrates the important role of UVR in preventing the *Braf*<sup>V600E</sup>-induced senescence, a requisite in melanoma progression in this specific mutational context. Moreover, a patent fact is the importance of *Lkb1* in *in vivo* induction of this disease, which has a relevant effect in the tumors, affecting its onset, its genetic instability, and its histological heterogeneity. The genetic analysis of tumors highlights the important role of Rho-, Netrin1- and SAPK/JNK-signaling pathway in melanomagenesis.

# RESUMEN

Entender los mecanismos moleculares relacionados con la melanomagénesis es clave a la hora de encontrar nuevas estrategias preventivas y terapéuticas contra esta letal enfermedad. La epidemiología indica que hay factores genéticos y medioambientales asociados con el desarrollo y la progresión del melanoma. En este estudio, hemos generado el modelo animal B/L/UV que nos permite estudiar la cooperación entre el oncogén, *Braf*<sup>V600E</sup>, el factor medioambiental, de la radiación ultravioleta (UVR) y la pérdida del supresor tumoral, *Lkb1*.

En resumen, el modelo animal B/L/UV presentado aquí es un potente sistema para estudiar la patogénesis del melanoma. Este modelo animal demuestra el importante rol de la UVR en la prevención de la senescencia inducida por *Braf*<sup>V600E</sup>, un requisito imprescindible en la progresión del melanoma en este específico contexto genético. Además, otro hecho evidente en la importancia de *Lkb1* en la inducción *in vivo* de esta enfermedad, que tiene un efecto relevante en los tumores, afectando su iniciación, inestabilidad genética y su heterogeneidad histológica. El análisis genético de los tumores destaca el papel de las vías de señalización Rho, Netrin1 y SAPK/JNK en la melanomagénesis.

*Gracias a todas las personas que me han ayudado a llegar hasta aquí.*

*Sin su apoyo no hubiese sido posible.*

*Elena González Sánchez*

# **INDEX**

<b>INTRODUCTION</b> .....	<b>7</b>
1. CANCER .....	8
2. CUTANEOUS MELANOMA.....	8
a. <i>Melanocyte development</i> .....	9
3. MELANOMAGENESIS .....	10
a. <i>Benign lesions: Common Acquired and dysplastic nevi</i> .....	10
b. <i>Malignant lesions</i> .....	10
i. Radial-growth phase .....	10
ii. Vertical-growth phase .....	11
iii. Metastatic melanoma .....	11
iv. De novo melanoma.....	11
4. MELANOMA RISK FACTORS .....	12
a. <i>Environmental Factor: Ultraviolet radiation (UVR)</i> .....	12
b. <i>Genetic Factors</i> .....	13
c. <i>Somatic mutations</i> .....	14
5. MAPK SIGNALING DEREGULATION IN MELANOMA .....	15
a. <i>The extracellular regulated kinase pathway</i> .....	15
b. <i>BRAF<sup>V600E</sup> a melanoma oncogene</i> .....	17
i. Oncogene-induced senescence (OIS).....	17
i. BRAF <sup>V600E</sup> as a therapeutic target for melanoma patients .....	17
6. PI3K-AKT SIGNALING DEREGULATION .....	18
a. <i>Tumor suppressor: LKB1</i> .....	19
i. LKB1:STRAD:MO25 complex .....	19
ii. LKB1 kinase signaling .....	20
iii. LKB1/AMPK pathway in cancer.....	20
iv. LKB1 role in DNA damage.....	21
7. MELANOMA ANIMAL MODELS .....	22
<b>HYPOTHESIS</b> .....	<b>25</b>
<b>OBJECTIVES</b> .....	<b>26</b>
<b>RESULTS</b> .....	<b>27</b>
1. <i>BRAF<sup>V600E</sup>-EXPRESSION INDUCES THE ABNORMAL PROLIFERATION OF DERMAL MELANOCYTES</i> .....	28
2. <i>A SINGLE DOSE OF NEONATAL UVR COOPERATES WITH BRAF<sup>V600E</sup> IN MELANOMA PROGRESSION IN OUR MOUSE MODEL</i> .....	29
3. <i>UVB IRRADIATION PREVENTS BRAF<sup>V600E</sup>-INDUCED SENESCENCE IN VIVO AND IN VITRO</i> .....	30
4. <i>LOSS OF LKB1 INCREASES MELANOMA INCIDENCE AND TUMOR LAG TIME IN BRAF<sup>V600E</sup> MICE</i> .....	32
5. <i>HISTOLOGIC ANALYSIS OF TUMORS UNVEILS MORPHOLOGIC TUMOR HETEROGENEITY</i> 34	
6. <i>LKB1 LOSS INCREASES THE GENETIC INSTABILITY FAVORING THE MELANOMA HISTOLOGIC HETEROGENEITY</i> .....	36
7. <i>MELANOMA TUMORS SHOWED BOTH mTORC1 AND mTORC2 SIGNALING PATHWAYS ACTIVATION</i> .....	38
8. <i>AN IMPORTANT PERCENTAGE OF HUMAN BRAF<sup>V600E</sup>-MUTATED CUTANEOUS MELANOMAS SHOWS LOW OR NONE LEVELS OF LKB1</i> .....	39
9. <i>DIFFERENTIAL PROGNOSIS OF HUMAN BRAF AND NRAS MUTANT MELANOMAS DEPENDING ON ASSOCIATED LKB1 GENETIC ALTERATIONS</i> .....	41
10. <i>LKB1 REGULATES cMET EXPRESSION IN MICE AND HUMAN MELANOMA CELLS, WHICH HAS AN EFFECT IN VITRO CELL PROLIFERATION</i> .....	41
11. <i>HUMAN MELANOMA ANALYSIS CONFIRMS THE POSITIVE CORRELATION BETWEEN THE LKB1 AND cMET EXPRESSION LEVEL</i> .....	44
12. <i>GENETIC PROFILING OF MOUSE TUMORS UNVEILS ALTERATIONS IN EXTRACELLULAR MATRIX INTERACTIONS, NEURAL DIFFERENTIATION AND RHO-SIGNALING PATHWAYS</i> .....	44

13. B/L/UV ANIMAL TUMORS HARBOR MUTATIONS FOUND IN SIMILAR ANIMAL MODELS AND THE HUMAN DISEASE .....	50
14. MAPK-, TNF $\alpha$ , NF $\kappa$ B, AND P38-SIGNALING PATHWAYS ARE KEY IN <i>BRAF</i> <sup>V600E</sup> -MEDIATED MELANOMA PROGRESSION .....	53
15. DOWNREGULATION OF SAPK/JNK SIGNALING PATHWAY COMPONENTS MODIFIED THE <i>IN VIVO</i> PROLIFERATION RATES IN <i>BRAF</i> <sup>V600E</sup> HUMAN MELANOMA CELLS .....	56
16. COMBINED STUDY OF THE DIFFERENT <i>BRAF</i> <sup>V600E</sup> -INDUCED MOUSE WITH THE TCGA DATA CONFIRMED THAT B/L/UV ANIMAL MODEL RECAPITULATES HUMAN MELANOMA GENETIC ALTERATIONS .....	57
<b>CONCLUSIONS .....</b>	<b>69</b>
<b>MATERIAL AND METHODS .....</b>	<b>70</b>
1. CONSTRUCTS.....	71
a. <i>Plasmid Generation</i> .....	71
i. Digestion and ligation procedures .....	71
ii. Transformation in NEB® Stable Competent E. coli .....	71
2. CELL CULTURE.....	71
a. <i>Cell lines</i> .....	71
b. <i>Cell quantification</i> .....	72
c. <i>Subculture Procedure</i> .....	72
d. <i>Cryopreservation procedure</i> .....	73
3. CELL GENERATION.....	73
a. <i>Lentiviral Particles Production and infection</i> .....	73
b. <i>Cell Sorting</i> .....	74
4. PROTEIN ANALYSIS TECHNIQUES.....	74
a. <i>Cell Lysis</i> .....	74
b. <i>Protein Quantification</i> .....	74
c. <i>Western Blot</i> .....	75
d. <i>Immunofluorescence protocol</i> .....	76
i. Specific immunohistochemistry .....	76
ii. Specific immunofluorescence.....	76
iii. Chromogenic assay for Whole Skin $\beta$ -Galactosidase activity .....	78
5. RNA ANALYSIS TECHNIQUES .....	78
a. <i>RNA isolation</i> .....	78
b. <i>RNA quantification and quality control</i> .....	79
c. <i>Quantitative-Reverse Transcriptase Polymerase Chain Reaction (qRT-PCR)</i> .....	79
6. DNA ANALYSIS TECHNIQUES.....	80
a. <i>Whole Exome Sequencing (WES)</i> .....	80
b. <i>Global genomic DNA repair assay</i> .....	80
7. PROLIFERATION ASSAY .....	80
8. IN VIVO ASSAY .....	80
c. <i>Transgenic mice</i> .....	81
d. <i>UV irradiation</i> .....	81
9. MELANOCYTE ISOLATION.....	81
<b>SUPPLEMENTARY.....</b>	<b>82</b>
<b>INFORMATION .....</b>	<b>82</b>
1. ABBREVIATIONS.....	83
2. BUFFER RECIPE COMPILATION.....	85
<b>BIBLIOGRAPHY .....</b>	<b>99</b>

# **INTRODUCTION**



## 1. Cancer

Cancer is second leading cause of death worldwide. It was responsible for 8.8 million deaths in 2015, nearly 1 in 6 deaths globally. Among skin cancers, melanoma represents only about the 1%, but it causes the vast majority of skin cancer deaths. According to the World Health Organization (WHO), melanoma incidence is continuing to rise worldwide, with an estimation of 23.6 million of new cases predicted in 2030.

It is difficult to define cancer in absolute terms. Tumors are usually phenotypically recognized by the fact that their cells show abnormal growth patterns and are no longer under the control of normal homeostatic growth controlling mechanism. This unrestrained proliferation arises through the accumulation of genetic alterations in the cells.

Several evidences indicate that tumorigenesis is a multistep process and that these steps reflect genetic alterations that drive the progressive transformation of normal cells into malignant derivatives. In 2000, Hanahan and Weinberg (1) highlighted six biological capabilities acquired during the progression of the neoplastic disease. These are (a) sustaining proliferative signaling, (b) evading growth suppressors, (c) resisting cell death, (d) enabling replicative immortality, (e) inducing angiogenesis, and (f) activating invasion and metastasis. Underlying these hallmarks is genome instability, which generates the genetic diversity that accelerates their acquisition, and inflammation, which promotes multiple cancer functions. In 2011, an updating review (2) includes three more biological abilities required in the progression of the disease: the reprogramming of energy metabolism, the evasion of immune system and the important effect of the tumor microenvironment. The complexity of the biology of tumors shows us how important is to unveil the mechanisms involved in tumorigenesis, so that different strategies for the treatment of cancer can be envisaged.

## 2. Cutaneous Melanoma

Melanoma is the 6<sup>th</sup> most common cancer in the developed world with an increasing incidence that affects both young and older populations; accounting for more than 47,000 deaths worldwide annually (3). Although melanoma is the less frequent type of skin cancer, it is the most lethal form, being the cause of 75% of deaths of this kind of neoplasms (3). According to epidemiological data, 132,000 new cases of melanoma and 50,000 melanoma-related deaths are diagnosed worldwide each year (4). Current rise in melanoma incidence can be explained partly by altered patterns of sun exposure, which is related to increased popularity of sun-tanning and the relative ease of global travel or migration of fair-skinned individuals to more sun-intensive regions (5).

Malignant melanoma is considered the most aggressive and treatment resistant human skin cancer (6,7). At present, prevention and early detection of this disease is a requisite for the overall survival of the patients. Surgical removal is the gold standard treatment option for patient with primary cutaneous melanomas with negative sentinel regional

lymph node. Advanced melanoma has traditionally been associated with a poor prognosis, resistance to cytotoxic chemotherapy, and limited treatment options. Hence, any effort in understanding the genetic alterations that trigger melanomagenesis would allow the scientific community to find novel therapeutic approaches against this disease.

#### a. Melanocyte development

Melanoma arises from the malignant transformation of the pigment-producing melanocytes. Melanocytes are neural crest-derived cells. During the embryonic development the dorsolateral pathway generates melanoblasts, the precursors of differentiated melanocytes, which colonize the skin and few other tissues throughout the body (the meninges, the uveal- and the anogenital-tract) (8,9).

In human skin, the melanocytes reside mainly in the (a) dermo-epidermal junction and (b) hair follicles. *Epidermal* melanocytes rarely proliferate, but produce melanin pigment to provide keratinocytes located in the basal and superficial layers, through arborizing dendritic processes. This fact offers protection from ultraviolet light radiation (UVR). Each melanocyte transfers pigment-containing melanosomes via these dendrites to approximately 36 basal and suprabasal keratinocytes (known as the *epidermal melanin unit*) (5). On the other hand, differentiated *hair follicles* melanocytes repeatedly proliferate and differentiate every hair cycle from non-pigment-producing melanocyte stem cells (MCSCs) located in the hair follicle bulge. These differentiated melanocytes contribute melanin to the hair shaft (10,11). In mouse skin, melanocytes are located mainly in the hair follicles, with the exception of the murine tail that contains interfollicular melanocytes and pigmented epidermis (11,12).

Two different chemically types of pigment can be found in human: eumelanin (brown/black) and pheomelanin (red/yellow). Eumelanin is the photoprotective pigment that provides UVR attenuation and it is present in higher concentrations in dark-skinned individuals (7). Although pheomelanin is also present in higher concentrations in the melanocytes of dark-skinned individuals, its relative abundance is much higher in individuals with light complexion, who have lower amounts of eumelanin. Pheomelanin has a diminished UV-light protective capacity and produces metabolites that are believed to be mutagenic and cytotoxic (5).

Pigment synthesis is stimulated by the binding of  $\alpha$ -melanocyte-stimulating hormone ( $\alpha$ -MSH) to melanocortin 1 receptor (MC1R) on melanocytes. MC1R activates cyclic adenosine monophosphate (cAMP) production and cAMP response element-binding protein (CREB)-mediated transcriptional activation of MITF. MITF in turn promotes transcription of pigment synthesis genes and melanin production. MC1R is a major determinant of pigmentation. Loss-of-function polymorphisms of this receptor result in impaired eumelanin production, producing red hair and fair skin (5).

### 3. Melanomagenesis

Melanocytes neoplasms range from benign lesions, termed melanocytic nevi, to malignant ones, named melanomas. This disease comprises multiple biologically distinct categories, which differ in cell origin, clinical and histologic presentation, pattern of metastasis, causative role of UVR, and pattern of germ-line or somatic mutations (13).

One of the most accepted model of melanomagenesis is the Clark's model (10), which describes histologic and morphologic changes that attend the progression from normal melanocytes to malignant melanoma (Figure 1). These biological changes in the melanoma progression could be related with acquisition of particular mutations. However, it should be emphasized that a portion of melanomas cannot be unequivocally placed in any of the categories.

#### a. Benign lesions: Common Acquired and dysplastic nevi

Melanomagenesis can begin with the development of either dysplastic or benign nevi. Nevi are clonal benign proliferations of melanocytes. They are unlikely to progress to melanoma; but their high prevalence makes them contributors to a considerable proportion of melanomas. These neoplasms are initiated by gain-of-function mutations in one of several primary oncogenes, which typically lead to benign melanocytic nevi with characteristic histologic features. Approximately, 80% of this benign neoplasm frequently harbors the oncogenic BRAF<sup>V600E</sup> mutation (14). The acquisition of this mutation is characterized by an initial phase of melanocyte growth, followed by a near-complete cessation of proliferative activity and the expression of senescence markers, which can be maintained for decades (3,8). The lack of telomere attrition in the nevi argue in favor of an active oncogene-driven senescence (OIS) process (15).

Dysplastic nevi are characterized by the presence of cytologic atypia, which may arise from preexisting nevi or as new lesions. The molecular abnormalities at this stage of progression affect cell growth, DNA repair, and the susceptibility to cell death. The overall mutation burden in this neoplasm subtype is intermediate between the benign and malignant lesions. Some of the driver mutations in dysplastic nevi include mutations that activate MAPK signaling or affect *TERT* promoter (8). Additionally, these lesions can also carry losses of heterozygosity of the *CDKN2A* and *TP53* loci (8,10). Dysplastic nevi present a long-lasting balance between slow melanocyte proliferation and attritional factors that clear the lesion.

#### b. Malignant lesions

##### i. Radial-growth phase

Radial-growth phase (RGP) or primary melanoma spreads progressively within or just beneath the epidermis. In this stage, malignant melanocytes require keratinocytes or their products for survival, and can grow only in or near the epidermis. This category could be

classified as *in situ* or invasive. In the latter case, cells may have acquired the ability to invade and survive in the dermis. RGP does not metastasize in the vast majority of cases (16).

### *ii. Vertical-growth phase*

The final stage in melanoma progression is the vertical growth phase (VGP), which defines tumors that acquire proliferative capacity, grow vertically, invade basement membrane and dermis, and are metastasis competent (13). Progression from RGP to VGP requires mutations that suppress apoptosis, contributing to the keratinocyte-independence proliferation of the melanocytes. This stage is also marked by: (a) loss of E-cadherin, (b) aberrant expression of N-cadherin, and (c) stimulation of the  $\beta$ -Catenin signaling pathway.

### *iii. Metastatic melanoma*

Metastatic melanoma develops when tumor cells dissociate from the primary lesion, migrate through the surrounding stroma, invading blood- and lymphatic-vessels to form a tumor at a distant site. As many solid tumors, metastatic dissemination progress serially, affecting first in the lymph nodes close to the primary lesion and latter in distant visceral sites. Despite the mutations that promote the departure from the primary melanoma are unknown; there are anecdotal genetic evidence that implicates the activation of the WNT signaling in this step (8). Moreover, alterations in cell adhesion are a requisite that contribute to tumor invasion and tumor-stroma interactions.

Approximately 4% of melanomas arise as apparent metastases without any detectable primary tumor, known as melanomas of unknown primary (MUP) (8). MUPs have a high mutation burden with UVR-induced mutations, indicating that they originated from sun-exposed skin.

### *iv. De novo melanoma*

Almost 50% melanomas do not arise from a benign lesion. Melanoma progression is typically depicted as a linear stepwise process in which metastasis occurs as a late event. However metastatic spread can also be initiated earlier, even before than the primary tumor formation, leading to the model of *parallel metastatic progression* (8,17). Several studies sustain that melanoma cells leave primary tumors early and evolve in different sites in parallel. It has been shown that the lymphatic dissemination occurs shortly after dermal invasion of the primary lesion at a median thickness of 0.5 mm and with common genetic changes, including *BRAF* mutations and gained or lost regions comprising genes like *cMET* or *CDKN2A* (17).

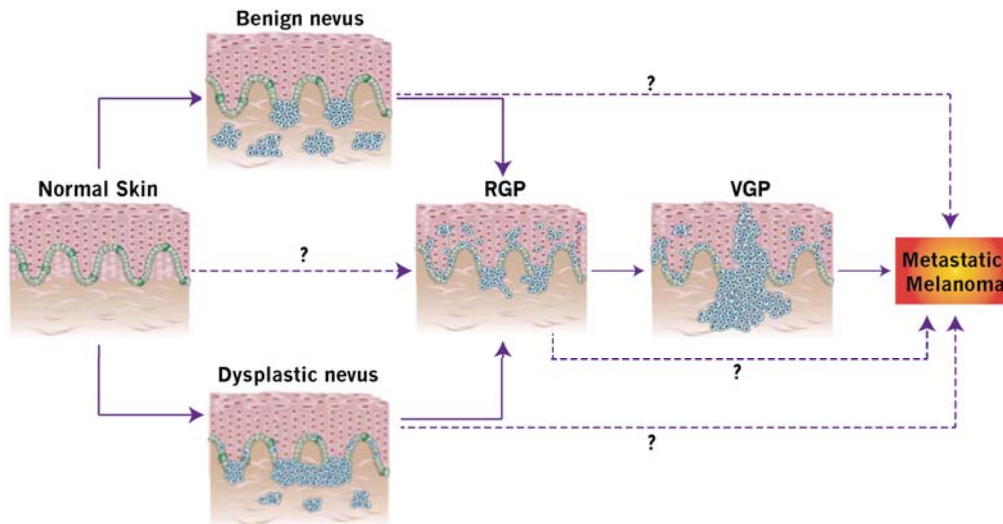


**Figure 1: Melanoma histologic classification.** Clark's model is a histological method that classified melanoma according to the location and stage of progression of the disease. There are five distinct proposed stages: common and acquired and congenital nevi without dysplastic changes; dysplastic nevi with structural and architectural atypia; radial-growth phase (RGP) and vertical-growth phase (VGP); and metastatic melanoma. Lines indicate the putative lesion progression. Figure adapted from (5).

## 4. Melanoma Risk Factors

### a. Environmental Factor: Ultraviolet radiation (UVR)

Melanoma incidence is influenced by pigmentation of the population and geographical parameters, such as latitude and altitude, indicating that UVR has a causal role in melanoma development (3,5). Solar radiation reaching the Earth's surface is a range of electromagnetic radiation composed by two ranges of UV wavebands, 5% of ultraviolet B (UVB, 280-320nm) and 95% ultraviolet A (UVA, 320-400nm) (18,19). These two different wavelengths have different roles in their capacity to initiate DNA damage, cell signaling pathways and immune alterations (20).

UVB has been considered the principal melanoma carcinogen (20). The predominant UVB-induced photo-lesions are the DNA cyclobutane pyrimidine dimers (CPDs)<sup>1</sup>, pyrimidine-6, 4-pyrimidone photoproducts (6,4-PPs)<sup>2</sup> and Dewar photoproducts<sup>3</sup>. These helix-distorting DNA lesions are repaired exclusively by a nucleotide excision repair (NER) system in human. If unrepaired, these mutations at dipyrimidine sites induce the characteristic C>T transition, known as "UV-signature mutation" (10). On the other hand, UVA wavelengths interact with cellular photosensitizers to generate reactive oxygen species (ROS) and ROS-mediated oxidative damage to DNA (19). Although to

<sup>1</sup> CPDs contains a four membered ring arising from the coupling of the C=C double bonds of pyrimidines. Such dimers interfere with base pairing during DNA replication

<sup>2</sup> 6-4PPs occur at one third the frequency of CPDs but are more mutagenic

<sup>3</sup> Valence isomer of (6-4) photoproduct in photodamaged DNA

be uncommon, UVR also has the capacity to induce other types of DNA alterations, including: protein-DNA crosslinks, oxidative base damage, single-strand breaks, chromosomal aberrations, and epigenetic changes (5).

UVR exposition results in a broad spectrum of cellular reactions as epidermal hyperplasia, cutaneous inflammation, and migration of MCSCs to the interfollicular epidermis (IFE) in both mice and human (12). Epidemiological observations indicate that melanoma occurs most frequently after intermittent exposure to the sun and in people with frequent sunburns, especially during childhood (10,21). Indoor artificial tanning devices have also been linked to dose-dependent melanoma risk (7). Nevertheless, chronic or low-grade exposures to UVR induce protection against DNA damage, owing to increased skin thickness and melanin production that result from chronic ultraviolet exposure (10,18,22).

### b. Genetic Factors

The usual melanoma patient is characterized by having a pale-skinned complexion, red or blonde hair, blue eyes and high number of large and irregular nevus, that directly correlates with the UVR exposure. Familial melanomas, which represent 8-12% of all melanoma cases, are indicated to identify melanoma susceptibility genes implicated not only in the familiar disease, but also the sporadic cases (5,23). Genetic studies in patients with Familial Atypical Mole-Melanoma (FAMM) syndrome identified four melanoma predisposition genes, which could be classified in high- and low-penetrance genes.

Within the high-penetrance genes, the best characterized is the *CDKN2A* gene located on chromosome 9p21, which is known as the familial melanoma locus. About 45% of familial melanomas harbor germline mutation in this gene, which encodes two distinct proteins: p16<sup>INK4A</sup> and p14<sup>ARF</sup> (p19<sup>ARF</sup> in mice) (5). Interestingly, one third of all melanoma patients carry *CDKN2A* inactivating mutations or deletions. Generally, these mutations affects p16<sup>INK4a</sup> alone or p16<sup>INK4a</sup> together with p14<sup>ARF</sup>; only in rare cases p14<sup>ARF</sup> alone is affected (6).

Functional p16<sup>INK4a</sup> acts after DNA damage and blocks cell cycle at G1-S phase checkpoint inhibiting CDK4 (22,24). Some studies implicate p16<sup>INK4A</sup> in the oncogene-induced senescent response, where its loss has been linked with tumor progression (25). Moreover, p16<sup>INK4A</sup> loss is reported in almost all established melanoma cell lines and 15-28% of primary uncultured sporadic melanoma samples (5). On the other hand, p14<sup>ARF</sup> induces G1 and G2 phase arrest via the p53 pathway, allowing DNA damage repair or apoptosis (24).

The third high-penetrance melanoma predisposition gene is the cyclin-dependent kinase 4 (*CDK4*), which is located on chromosome 12q13. Punctual mutations in *CDK4* have been identified in melanoma. These mutations impede the binding of *CDK4* with *INK4A*, thus activating constitutively cell cycle progression (22).

Conversely, the low penetrance gene is the *MC1R*, the melanocortin receptor gene, situated on 16q24.3. This is the receptor of the melanocyte-stimulating hormone ( $\alpha$ MSH), the hormone synthesized after sun exposure that promotes the production of eumelanin. *MC1R* is highly polymorphic, which impedes to discern between polymorphism and melanoma-associated mutations (11). Certain variants in *MC1R* have been associated with pheomelanin synthesis, responsible of: red hair color, poor tanning ability, and, importantly, increased risk for melanoma (14,22). This melanin intermediate product contributes to malignancy by increasing the oxidative stress that promotes mutagenesis.

### c. Somatic mutations

Many oncogenes and tumor suppressors are linked to the disruption of the accurate control of transduction of cell signaling pathways. Signaling transduction is the complex system of communication that governs cellular activities and coordinate cell actions. Deregulation of this complex network can promote the acquisition of cancer-phenotypes. Cell signaling pathways are important for understanding cell growth and death, migration, metabolism, and angiogenesis; processes tightly involved also in cancer.

Melanoma is a genetic complex disease. The most frequent genetic alterations in melanoma affect genes in key signaling pathways that governs (a) proliferation (*BRAF*, *NRAS* and *NF1*); (b) growth and metabolism (*PTEN*, *STK11* and *KIT*), (c) resistance to apoptosis (*TP53*); (d) cell cycle control (*CDKN2A*) and (e) replicative response (*TERT*) (Table 1). Also, master regulators of melanocyte biology can be altered, as *MITF*.



**Table 1: Selected genetic alterations predominant in human cutaneous melanoma.** In this table, it is shown: the functional gene classification, gene ID, gene alteration frequency in melanoma, common type of alteration, effector pathways affected, and some relevant melanoma literature references of these genes. Abbreviations: MAPK, mitogen-activated protein kinase; PI3K, phosphoinositide 3-kinase; RB pathway, retinoblastoma pathway.

Functional gene classification	Gene ID	Melanoma alteration frequency (%)	Type of alteration	Effector pathways affected	Reference
<b>Oncogenes</b>	<i>BRAF</i>	50-70	Mutation	MAPK pathway	(26)
	<i>NRAS</i>	15-30	Mutation	MAPK pathway	(26,27)
	<i>AKT3</i>	43-60	Overexpression	PI3K pathway	(28)
<b>Tumor Suppressor</b>	<i>CDKN2</i>	30-70	Deletion or mutation	RB pathway (via p16), p53 pathway via p14 <sup>ARF</sup> )	(29)
	<i>PTEN</i>	5-20	Deletion or mutation	PI3-kinase	(27)
	<i>TP53</i>	10	Deletion or mutation	p53 pathway	(30)
	<i>STK11</i>	10	Mutation	PI3K- and mTORC-pathway	(31)
<b>Other</b>	<i>MC1R</i>	-	Polymorphism	Melanin synthesis pathway	(32)
	<i>MITF</i>	10-16	Amplification	Upregulation of transcriptional targets ( <i>MET</i> , <i>BCL2</i> , <i>CDK2</i> )	(33)

## 5. MAPK signaling deregulation in melanoma

The mitogen-activated protein kinase (MAPK) family is composed of three major groups: (a) the extracellular regulated kinases (ERKs), (b) the c-Jun N-terminal kinases (JNKs), and (c) the p38 MAPKs (34). The ERK-pathway primarily directs proliferation and survival programs. On the other hand, JNK-pathway promotes either proliferation or apoptosis, whereas p38-signaling is activated upon cellular stress and engages pathways that block proliferation or promote apoptosis (35).

### a. The extracellular regulated kinase pathway

The ERK-MAPK signaling is one of the best-characterized signal transduction pathways inside the cell. MAPKs are protein Serine (Ser)/Threonine (Thr) kinases that convert



extracellular stimuli into a cellular response. MAPK cascade is one of the most evolutionary-conserved transduction pathways that coordinate and regulate gene expression, cell division, metabolism, motility, survival, differentiation, and apoptosis.

MAPK is described as a canonical signaling cascade composed of (a) the small GTPase RAS (HRAS, KRAS or NRAS); (b) downstream kinases (ARAF, BRAF or CRAF, MAPKKK level); (c) MAP/ERK-kinase (MEK1 and MEK2, MAPKK level); and (d) MAPK (ERK1 and ERK2). ERK cascade begins when ligands, such as growth factors, bind to their respective receptor tyrosine kinase (RTK). Receptor dimerization triggers the intrinsic tyrosine-kinase activity of the receptor and activates RAS small G protein, which activates the signaling cascade by phosphorylating a MAPKKK. RAF proteins, in turn, phosphorylate MAPKK, which phosphorylates MAPK. Activated ERK protein can translocate into the nucleus, where they can phosphorylate specific substrates that are involved in the regulation of proliferation, differentiation, senescence and survival (Figure 3).

The MAPK cascade is considered the most relevant in the melanoma progression and one of the principal therapeutic targets in this disease. ERK protein kinase is hyperactivated in 90% of human melanomas by growth factors and genetic alterations of upstream effectors, as *NF1*, *RAS*, and *RAF* (mutated in 10-13%, 30% and 70% of malignant melanomas, respectively) (3). One of the most common mutations in this disease includes: *BRAF*<sup>V600E</sup> (50% of melanomas) and *NRAS*<sup>Q61L/R</sup> (15-20% of melanomas) (3). BRAF and NRAS mutations are mutually exclusive in these neoplasms, which strongly indicates that RAF–MAPK is the relevant downstream mediator of RAS activity in human melanoma. It is likely that the choice of downstream effectors for the transformation activity of RAS is also context- and cell type-dependent (5). These mutations, although they lack typical UV-signature, could be produced by secondary mutagens related with UVR (10). As indicated before, the high frequency of these mutations in the benign melanocytic neoplasm, suggest that these mutations represent primary steps in the melanomagenesis, which lead to Oncogene-Induced Senescence (OIS). So full development of malignant melanoma requires secondary or tertiary mutations to overcome or prevent senescence and become malignant (1).

In the melanocytic lineage, proliferation, differentiation and survival are tightly regulated and require synergistic paracrine stimulation by growth factors that signal from both G-protein coupled receptors (GPCRs) and Tyrosine kinase receptors (RTKs), such as endothelin-1/3,  $\alpha$ -melanocyte stimulating hormone ( $\alpha$ -MSH), basic fibroblast growth factor (bFGF) and hepatocyte growth factor/scatter factor (HGF/SF) (5). The ability to transduce and possibly integrate converging signals from RTKs and GPCRs might explain the frequent involvement of the MAPK signaling cascade in cancer, so activating mutations in RAS or RAF might mimic mitogenic signals from both pathways, leading to decoupling of growth from extracellular growth-factor regulation.

## b. BRAF<sup>V600E</sup> a melanoma oncogene

In melanoma, the most common BRAF mutation correspond to the T1799A transversion in exon 15, which results in a single phosphomimetic substitution of a glutamate for valine at position 600 in the BRAF kinase domain (from now on BRAF<sup>V600E</sup>) (36). This change produces the 500-fold constitutive activation of the MAPK signaling, stimulating the growth and viability of melanoma cells harboring this mutation (37).

Melanoma epidemiology shows that 80% of nevi and 50% of melanomas harbor the BRAF<sup>V600E</sup> mutation. Only 30% of these melanomas progress from previous BRAF<sup>V600E</sup>-mutated nevi, while the remaining 20% are not related with any benign lesion. These statistics suggest that under appropriated conditions, OIS can be bypassed or prevented by the acquisition of secondary genetic lesions, which promote malignant tumors progression.

### i. Oncogene-induced senescence (OIS)

Cellular senescence is defined as a permanent cell-cycle arrest brought about by either extensive cell proliferation or certain cellular stresses, such as oncogene overexpression, radiation, or reactive oxygen species (36). In melanoma, the BRAF<sup>V600E</sup>-induced senescence acts as a brake against the malignant transformation of BRAF<sup>V600E</sup>-mutated nevi (38).

The acquisition of BRAF<sup>V600E</sup> initially promotes moderate melanocyte proliferation, which subsequently leads to growth-inhibitory responses associated with classical senescence hallmarks. These characteristics are the stable proliferative arrest, the increased P16<sup>INK4A</sup> expression, and the induction of senescence-associated  $\beta$ -Galactosidase (SA- $\beta$ Gal) activity (15). Low BRAF<sup>V600E</sup> expression also induces the formation of senescence-associated heterochromatin foci (SAHF), which have a role in silencing proliferation-promoting genes (15). There is no evidence on whether nevi melanocytes have a senescence-associated secretory phenotype (SASP), which seems to be linked with the p53 activation, which is not common in nevi lesions (36).

### i. BRAF<sup>V600E</sup> as a therapeutic target for melanoma patients

Since the molecular revolution of the 1980s, it has been discovered and developed novel therapies that target cancer-specific pathways. The main foundation of targeted therapy is the oncogene addiction, that is, the acquired dependence of a cancer cell on the activity of a single oncogenic gene product (39). Certainly, melanoma progression shown a clear dependence on the MAPK signaling, specifically the BRAF<sup>V600E</sup> gene (14).

One of the first drugs that target this pathway was the multikinase inhibitor Sorafenib (BAY46-9006). This drug blocks the autophosphorylation of several RTK (VEGFR1, 2 and 3, PDGFR $\beta$ , cKit and RET), as well as inhibiting downstream RAF kinases isoforms (wildtype CRAF, BRAF and BRAF<sup>V600E</sup>). Unfortunately, as monotherapy, Sorafenib shows only modest activity against melanoma, but combined with carboplatin and paclitaxel the results are more encouraging, but with poor improvement of the patient survival (40–42).

Later, it was designed the first-generation RAF inhibitors: Vemurafenib and Dabrafenib. Vemurafenib, also called PLX4032, is a powerful and specific inhibitor of BRAF<sup>V600E</sup>. During its clinical trial, this inhibitor induced complete or partial tumor regression in 81% patients with melanoma harboring the mutation BRAF<sup>V600E</sup>. This data highlighted its important role in the melanoma treatment (40). On the other hand, Dabrafenib is a reversible, ATP-competitive inhibitor that selectively inhibits BRAF kinase. Both inhibitors present tumor response and a benefit in the overall survival in mutant BRAF<sup>V600E</sup>-driven melanomas. This clinical effectiveness lies in the almost complete abolition of the MAPK pathway output in BRAF-mutated tumors (43). However, these compounds paradoxically activate the MAPK pathway in cells bearing oncogenic RAS or elevated upstream receptor signaling (44).

Trying to overcome this paradoxical MAPK pathway activation, preclinical studies have shown the positive effect of the BRAF- and MEK-inhibitor combination. This combination has an effect in delaying the resistance onset and inducing apoptosis. In the literature the combination of Dabrafenib with Trametinib (CombiDT), a MEK-inhibitor, prolongs progression-free survival, improves response rate, and reduces toxicities associated with paradoxical activation of the MAPK pathway compared with BRAF inhibitor monotherapy (45).

However still, BRAF-directed treatments are associated with some troubles as (a) the interpatient variability in the treatment response, (b) the development of resistance, and (c) the toxicity associated with BRAF inhibition (45). This panorama highlights the need to deep understand RAS–RAF–MEK–ERK cell signaling and to find new therapeutically targets that improve the current precarious situation in the patient treatment.

## **6. PI3K-AKT signaling deregulation**

PI3K pathways is involved in biological processes such as cell proliferation, cell survival, differentiation, motility and metabolism regulation (3,46,47). In the presence of growth factor signaling, the intracellular levels of PIP<sub>3</sub> rises, leading to phosphorylation of AKT which is known to promote cell cycle and inhibit apoptosis. PTEN regulates PIP<sub>3</sub> levels, and its inactivation results in PIP<sub>3</sub> accumulation, AKT hyperphosphorylation, and enhanced cell survival/proliferation (14) (Figure 3).

PI3K pathway plays an important role in melanoma progression, where it seems to be hyperactivated in a high proportion of melanomas (6,14,46). Elevated phospho-AKT levels, considered a melanoma bad prognosis factor, is found in 12% of nevi, 53% of primary melanomas and 67% of malignant melanoma (48). Beside this, 20% and 40% of melanomas have an allelic loss or altered expression of *PTEN*, respectively. Interestingly, *BRAF* and *PTEN* mutations are coincident in nearly 20% of the cases. However, *NRAS* and *PTEN* are mutually exclusive due to the redundant effect of this mutational combination (6).

#### a. Tumor suppressor: LKB1

One of the key tumor suppressors involved in metabolism is LKB1/STK11 (Liver Kinase B1/Serine, Threonine Kinase1). LKB1 is a master ubiquitously serine-threonine kinase that plays diverse roles in multiple cellular processes, including: cell polarity (49), cycle control (50,51), energy metabolism (52,53), and DNA damage checkpoint (54), among other roles. LKB1 was first identified as a tumor suppressor gene through its association with the autosomal dominant inherited cancer disorder, Peutz-Jeghers (PJS) syndrome (55). Later on, somatic mutations on *LKB1* were identified in sporadic cancers.

Human LKB1 locus is mapped in the 19p13.3. STK11 gene is composed of 10 exons, nine of which are coding. There are two isoforms of LKB1; (a) the long version, LKB1, and (b) the short isoform, LKB1<sub>s</sub>, generated by an alternative splicing in the C-terminal sequence, lacking Ser428/431(56). LKB1<sub>s</sub> is highly expressed in testis and in other tissues with low level of activity.

LKB1 protein has a central kinase domain, two N-terminal nuclear leading sequences (NLS) and a C-terminal regulatory domain (Figure 2). LKB1 kinase activity can be regulated either by post-translational modification of LKB1 itself or by the regulation of conformational configuration of its downstream targets. The upstream regulators of LKB1 include ERK, RSK, ATM, and DNA-PK (57).

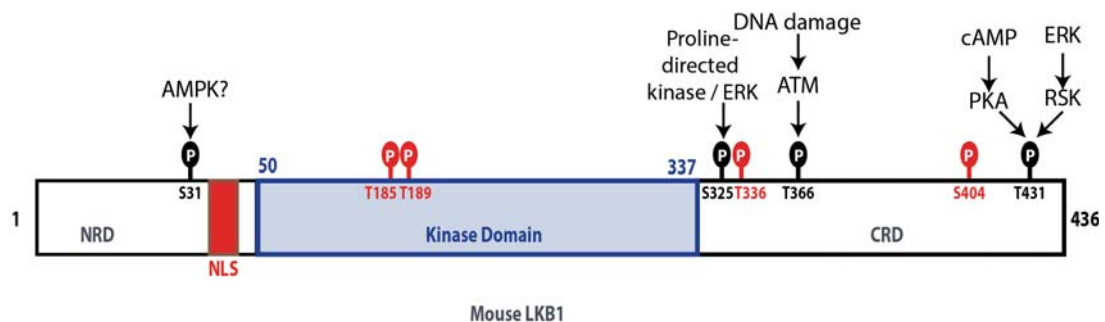


Figure 2: Schema of the mouse LKB1 protein with its posttranslational modification sites. Autophosphorylation sites are represented in red, and the phosphorylation sites by other kinases in black. The non-catalytic domains are symbolized in white, while the kinase domain is light blue. Figure adapted from (58).

#### i. *LKB1:STRAD:MO25* complex

LKB1 is located predominantly in the nucleus due to its nuclear localization signal in the N-terminal non-catalytic region (residues 38 to 43) (59). However, the subcellular localization and activity of LKB1 is controlled through heterotrimeric complexes with the STE20-related adaptor (STRAD $\alpha$  or STRAD $\beta$ ) and the scaffold protein the armadillo repeat-containing mouse protein 25 (MO25 $\alpha$  or MO25 $\beta$ ) (60). In LKB1:STRAD:MO25 complex, all proteins are present in the same stoichiometry, suggesting a high affinity of the individual subunit for each other and are assembled in the cytoplasm (58).

The pseudokinase STRAD, that lacks several residues that are indispensable for intrinsic catalytic activity, has been shown to act as an upstream activator of the LKB1 kinase (61). Moreover, it contributes in the localization of LKB1 in the cytoplasm (61). It has been shown that STRAD regulates LKB1 cytoplasmic localization by blocking access to importin and by association with CRM1 and exportin7, two nuclear protein exportins (59).

On the other hand, the main role of MO25 $\alpha$  in this complex is to stabilize the interaction between LKB1 and STRAD $\alpha$  in the cell cytoplasm, as well as enhancing LKB1 catalytic activity (62). This is achieved by the binding of the MO25 $\alpha$  to the carboxy-terminus of STRAD $\alpha$  and LKB1 (62). The expression of MO25 $\alpha$  is widely expressed in human tissues; on the contrary MO25 $\beta$  expression is more restricted.

### *ii. LKB1 kinase signaling*

LKB1 can phosphorylate at least 12 AMP-activated protein kinases, which includes: AMPKs, BRSKs and MARKs (63). AMPK is one of the best-characterized LKB1 substrate, which linked LKB1 to mTOR regulation through the AMPK-TSC1/TSC2 cascade (63–65). AMPK is recognized as the evolutionary conserved sensor of intracellular energy level. AMPK is switched on during situations in which cellular level of ATP is depleted and the level of AMP is increase. The activation of this protein promotes the stimulation of catabolic pathways and the inhibition of anabolic processes. AMPK is a heterotrimeric complex comprising a catalytic AMPK $\alpha$  subunit and regulatory AMPK $\beta$  and AMPK $\gamma$  subunits. AMP activates the AMPK complex by binding to a pair of cystathionine-beta-synthase (CBS) domains, located on the AMPK $\gamma$  subunit, thereby stimulating phosphorylation of Thr<sup>172</sup> in the T-loop of both mammalian AMPK $\alpha$  catalytic subunits, termed AMPK $\alpha_1$  and AMPK $\alpha_2$  (58). It has been demonstrated that LKB1 efficiently phosphorylated AMPK specifically at Thr<sup>172</sup>.

### *iii. LKB1/AMPK pathway in cancer*

The chronic and often uncontrolled cell proliferation involves not only deregulated control of cell proliferation, but also corresponding adjustments of energy metabolism in order to fuel cell growth and division. Tumors mostly reside in a metabolic stress environment; which promotes the deregulation of the LKB1/AMPK signaling in cancer

cells. Inactivation of LKB1 in human tumors will lead to the deregulation of multiple cellular processes, but its role as metabolic switch in tumorigenesis seems to be a crucial event.

LKB1 has been found mutated particularly in: non-small cell lung cancer (NSCLC) (15-25%), malignant cervical cancer (20%) and malignant melanoma (10%) (66). Separately, the hemizygous loss of chromosome 19p, spanning the *LKB1* locus, is observed in many cancer types. This data correlates with mouse models that suggest the haploinsufficient tumor suppressor role of LKB1 (67,68).

Focusing in the melanoma field, previous studies have reported the connection between the oncogene, BRAF<sup>V600E</sup>, and the metabolic sensor, LKB1. In these reports it has been shown that BRAF<sup>V600E</sup>-mutated melanoma cell lines showed a constitutive phosphorylation of LKB1<sup>Ser325</sup> in an ERK1/2 dependent-manner (52). This network would explain the limited response to metabolic stress under this mutational context.

#### *iv. LKB1 role in DNA damage*

The relevant role of UVR in melanomagenesis, highlight the DNA damage sensor role of LKB1 in this disease. It has been reported in the literature, that cells that lacks *LKB1* expression display increase sensitivity to irradiation, accumulates more DNA double-strand breaks, present defective homology directed DNA repair (HDR) (69). In addition to this, previous result from our group identifies LKB1 as a DNA damage sensor protein involved in the UV-induced DNA damage response. In this report, we demonstrate that LKB1 deficiency leads to the CDKN1A accumulation in response to UVB, promoting defects in DNA repair and resistance to apoptosis (54).

As indicated above, it has been observed that the conserved LKB1<sup>Thr363</sup> (LKB1<sup>Thr366</sup> in mouse) becomes phosphorylated in response to UVR and  $\gamma$ -irradiation by ATM and ATR respectively, as by DNA-PK promoting the nuclear localization of LKB1 (65). In addition to this, LKB1 has been involved in ROS- and IR-induced DNA damage response and repair. It has been shown how LKB1 formed DNA damage-induced nuclear foci and co-localize with DNA damage response proteins as ATM,  $\gamma$ -H2AX and BRCA1 (70) Furthermore, LKB1 not only interact with BRCA1, but also induces its expression (69).



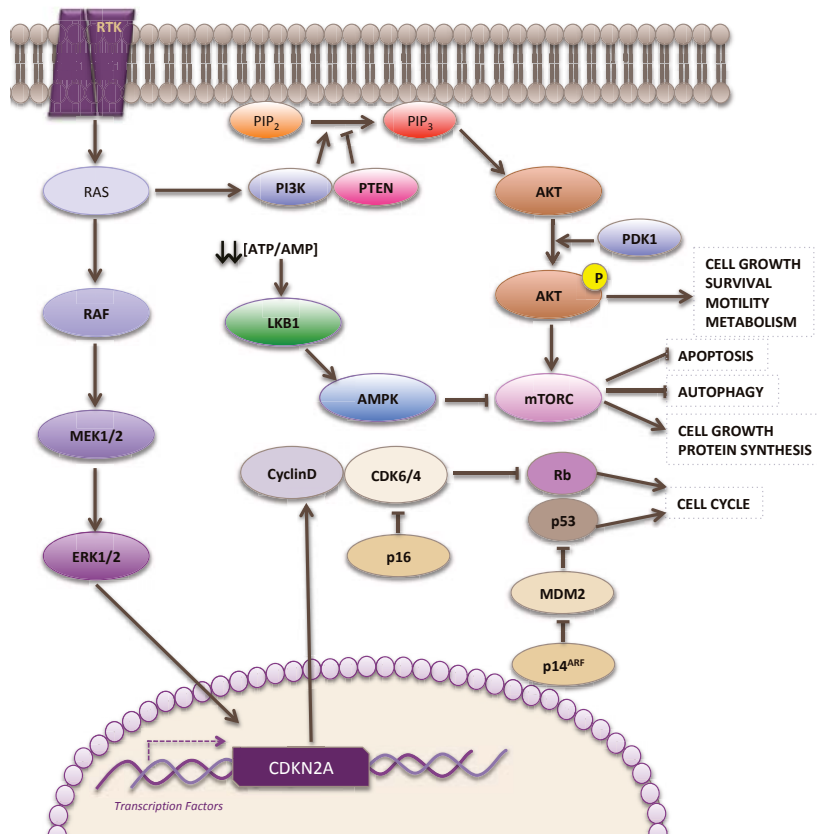


Figure 3: MAPK- and PI3K-pathways and proteins usually altered in human melanoma.

## 7. Melanoma Animal models

Mouse models have provided key insights into cancer initiation, progression and therapy. Currently, there are several mouse models that mimic the genetic evolution of malignant melanoma. The use of these models generates an *in vivo* system to study: (a) melanoma-relevant genes (b) UVR mode and target, (c) gene-gene and gene-environment interactions elucidation, and (d) therapeutic evaluation. Nevertheless, spontaneous melanoma formation is rare in laboratory mice due to the highly UVR-resistance of mouse melanocytes to progress into melanoma, and dermal component of the murine melanomas (71,72).

The first developed animal model that bypassed these limitations was the *HGF/SF* (Hepatocyte Growth Factor/Scatter Factor) transgenic mouse (72). In the skin of these mice, the mouse metallothionein-promoter overexpresses the hepatocyte growth factor/scatter factor (HGF/SF). This genetic background promotes the murine melanocyte localization in the basal layer of epidermal/dermal junction, creating a “humanized” skin. In this model, a single dose of mild sunburn during the neonatal period markedly increases melanoma risk. Although this model shows low penetrance and long latency, 20% of these melanomas developed distal metastasis supporting the importance of the cMET signaling in the tumor progression. This animal model has been a useful model to elucidate the molecular mechanisms linked with UVR.

Recently, the development of new mouse models of human cancer has great emphasis on temporal and spatial control of melanoma-key oncogene expression including BRAF<sup>V600E</sup>, since relatively small variances can promote quiescence, proliferation, or cell cycle arrest-senescence (73).

In order to recapitulate key pathophysiological aspects of the human disease, it was generated transgenic mice with conditional melanocyte-specific expression of *Braf*<sup>V600E</sup> (74). In this animal model, the physiological expression of normal *Braf* is disrupted after Cre-mediated recombination, which induces *Braf*<sup>V600E</sup> expression at same physiological levels. To address this locus recombination specifically in melanocytes, the expression of the 4OHTamoxifen (4OHTx)-activated version of the Cre Recombinase was placed under the control of a tyrosinase enhancer/promoter construct expressed in neural crest-derived cells. This inducible system avoids the lethality associated with the embryonic expression of *Braf*<sup>V600E</sup>, with the exception of one *Braf*<sup>V600E</sup> constitutive model that do not present this specific feature (25). These mice develop benign melanocytic hyperplasia that restrained from malignant progression by engagement of a cell cycle arrest program with features of senescence. The progression to melanoma was achieved with 100% of penetrance and short latency by the concomitant silencing of the PTEN tumor suppressor, a common event in the human disease. Currently, this animal model is used to study the *in vivo* effect of *Braf*<sup>V600E</sup> expression in the latest melanoma reports (11,12,75,76).

Another transgenic mouse strain available is the LSL-*Braf*<sup>V600E</sup> animal model, RM/B/UV model (77,78). In this inducible system, the physiological expression of mutated *Braf*<sup>V600E</sup> off the endogenous *Braf* gene is achieved through the LoxP-stop-LoxP/Cre-recombinase technology, which works similarly to the previous model. The main characteristics of the RM/B/UV animal model are: (a) the skin hyperpigmentation, (b) the appearance of nevi harboring senescence melanocytes, and (c) melanoma development. One striking feature of this strain is that p16<sup>INK4A</sup> is not involved in the melanocyte senescence, but in tumor penetrance and latency (77). Further studies of this group, try to unveil the effect of the UVR in the BRAF-driven melanomagenesis (78). It was shown that 40% BRAF<sup>V600E</sup>-expressing nevi are susceptible to progress into malignancy after UVR through mutations in the *TP53* gene.

Lately another animal model try to unveil the low-penetrance mutations that cooperate with BRAF<sup>V600E</sup> to induce melanomagenesis, the B/SB mice (76). To achieve this purpose it was described transposon-based screen in mice. Transposons can identify genes that are somatically mutated in human cancer, in addition to genes that are deregulated by transcriptional or epigenetic events. One of the limitations in this model is that the vast majority of the genes are putative haploinsufficient tumor suppressor. However, this study allows the scientific community to understand the genes and genetic networks involved in melanomagenesis.



Some mouse models have shown, that constitutive activation of PI3K/Akt signaling through loss of *Pten* relieves OIS induced by Ras/Raf mutations *in vivo* (74). This data correlates with another animal model in which melanomagenesis was linked with the upregulation of the mTOR signaling (79). In this study, the concomitant loss of *Cdkn2a* and *Lkb1* induces rapid formation of melanoma in mice, where *Cdkn2a* loss is associated with mTORC2 and AKT activation, whereas lack of *Lkb1* is linked with the upregulation of the mTORC1.

Moreover, *Lkb1* loss has been shown to cooperate with KRAS activation to induce metastatic melanoma in mice. Furthermore, results from our group demonstrate *in vitro* the LKB1 involvement in the HGF signaling (75). In this article, it was demonstrated that growth factor treatments and in particular oncogenic BRAF<sup>V600E</sup> induces the uncoupling of LKB1-AMPK $\alpha$ , providing a cell mechanism to survive in energy stress conditions, common in tumorigenic environment. Following this data, our group generated *Hgf<sup>Tg</sup>;Lkb1<sup>+/-</sup>* mouse model to study the role of LKB1 suppression in UVB-induced skin cancer with deregulated MAPK signaling. Under this genetic background, *Lkb1* deficiency leads to CDKN1A accumulation in response to UVB radiation, promoting defects in DNA repair and protection against apoptosis. This effect sensitizes these animals to UVB-induced skin cancer, enlightening that the mutational status of *Lkb1* can serve a novel risk factor for UV-induced skin tumors (52).

# HYPOTHESIS

Melanoma is without any doubt the most lethal form of human skin cancer. The BRAF<sup>V600E</sup> acquisition, found in 50% of human melanoma, is considered a central event in the initiation and progression of this disease. Human pathogenesis involves not only this genetic event, but also the cooperation with an environmental factor, as UVB radiation, and additional driver mutations.

Although, UVR has been classified as a melanoma-risk factor, its contribution to melanomagenesis is not fully understood. Moreover, previous results from our group and literature show the relevant role of the tumor suppressor LKB1 in melanoma. Our group unveiled two important roles for LKB1 in tumor development and tumor metabolism: (a) the DNA damage sensor role of this protein sensing the UVR-induced DNA-damage (54), and (b) its contributions to BRAF<sup>V600E</sup>-malignant transformation deregulating the metabolic stress response (54).

This thesis is focused in understanding the effect of UVR in the melanoma progression. Our *in vivo* and *in vitro* data indicates that UVB irradiation prevents *Braf*<sup>V600E</sup>-oncogene induced senescence, leading to melanoma development and progression. On the other hand, our laboratory previous results motivated us to study the cooperation between *Braf*<sup>V600E</sup> expression, the UV environmental factor, and the loss of the tumor suppressor *Lkb1*. Our results suggest that *Lkb1* loss would increase melanoma incidence and genetic instability.

The elucidation of these biological hypotheses would improve our knowledge of melanoma biology, but also would increase the preventive and therapeutics approaches available against this fatal disease.

# OBJECTIVES

1. **Generation of a tissue-specific induced melanocyte mouse model to study the cooperation of oncogenic  $Braf^{V600E}$  and neonatal UVB irradiation in melanomagenesis.**
  - 1.1. Mouse model characterization.
  - 1.2. Study of melanoma incidence in neonatal irradiated and non-irradiated  $Braf^{V600E}$ -induced mice.
  - 1.3. *In vivo* and *in vitro* study of the effect of neonatal UVB radiation in  $Braf^{V600E}$ -induced senescence.
2. **Generation of a tissue-specific induced melanocyte mouse model for the oncogenic  $Braf^{V600E}$  expression with the concomitant loss of the tumor suppressor  $Lkb1$  in melanocytes in order to study its role in neonatal UVR-induced and non-induced melanomagenesis (B/L/UV animal model).**
  - 2.1. Mouse model characterization.
  - 2.2. Study of melanoma incidence in neonatal irradiated and non-irradiated B/L/UV mice.
3. **Genetic characterization of the B/L/UV tumors through the performance of Whole Exome Sequencing.**
  - 3.1. Data analysis from the different experimental groups.
  - 3.2. Comparison of our system genetic alterations with melanoma human data available online.
  - 3.3. Contrast of our model genomic data with other published  $Braf^{V600E}$ -induced animal models.
4. **Analysis of the common genetic alterations observed in all models to discover novel pathways involved in  $Braf^{V600E}$ -induced melanomagenesis.**

# **RESULTS**

## 1. *Braf*<sup>V600E</sup>-expression induces the abnormal proliferation of dermal melanocytes

To investigate the cooperation of the acquisition of BRAF<sup>V600E</sup> mutation early on life with neonatal UVR, we used the conditional mouse model of *Braf*<sup>V600E</sup> (also known as *Braf*<sup>CA</sup>, catalytically active CA) (52). As described above, *Braf*<sup>CA</sup> mice harbor a germline conditional *Braf*<sup>V600E</sup> allele, the expression of which is initiated at physiological levels under a control of Cre recombinase. This enzyme is regulated under a conditional tyrosinase promoter transgenic system (*Tyr::CreER*<sup>T2</sup>), that confines the conditional expression of *Cre* and therefore *Braf*<sup>CA</sup> to melanocytes (Supplementary Appendix Figure 1). In this conditional system, wildtype *Braf* is expressed prior the 4OHTx treatment that activates Cre-mediated recombination at *Braf* locus. At this point, *Braf*<sup>V600E</sup> is expressed in physiological amounts in melanocytes (Figure 4A). It is important to highlight that tyrosinase is expressed in neural crest-derived cells, in this matter *Braf*<sup>CA</sup> expression upon *CreER*<sup>T2</sup> activation at 2.5 days postnatal has been found in unexpected tissues, such as lung (74).

As previously described (80), activation of *Braf*<sup>CA</sup> promoted hyper-keratosis and -pigmentation in glabrous skin of the mice, as pawns, tail and ears (

Figure 4B, D). *Braf*<sup>V600E</sup>-expression in neural crest-derived cells endorsed proliferation of the epidermal melanocytes (nevi), and the meningeal melanocytes (

Figure 4C). Another important characteristic of this animal model was the presence of melanophages in the lymph nodes. Although the biologic significance of dermal melanophages is unknown, they are frequently found in benign melanocytic nevi and malignant melanoma (81). The immunohistochemistry of *Braf*<sup>CA</sup> mice skin showed the presence of abnormal dermal melanocytes, together with the thickening of the keratinocyte layers (

Figure 4D Right-below panel).

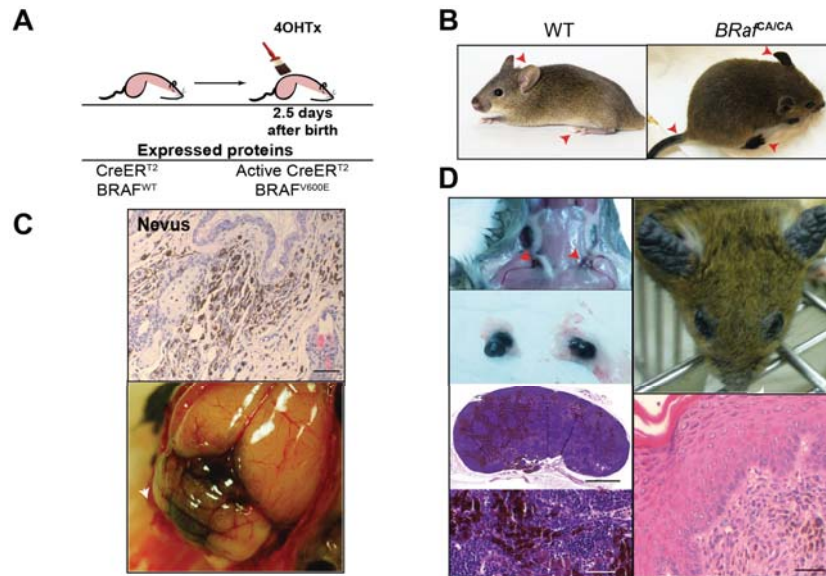


**Figure 4: Phenotypic characterization of *Braf*<sup>V600E</sup>-expressing mice.** (A) Experimental design diagram. Mice carrying conditional alleles of *Braf* (*Braf*<sup>CA</sup>) were crossed to *Tyr::CreER*<sup>T2</sup> mice with melanocyte-specific expression of a hormone-dependent form of Cre recombinase. Activation of *CreER*<sup>T2</sup> by 4OHTx leads to melanocyte-specific conversion of *Braf*<sup>WT</sup> to *Braf*<sup>V600E</sup>. (B) Expression of *Braf*<sup>V600E</sup> leads to highly pigmented skin (red head arrows point out naked skin areas affected with the melanocyte hyperproliferation). (C) Representative image of a nevus (upper panel) and meningeal melanocytes hyperpigmentation (lower panel) developed in *Braf*<sup>V600E</sup>-expressing mice. (D) Left panels, pigmented lymph nodes due to the presence of melanophages, macroscopic and microscopic images are shown. Right panels, hyperkeratosis of skin visualized in the ears and eyelids. Below photograph shows multiple layers of keratinocytes in the epidermis. Insets show a magnification of cells. Bars are 500µm and 50µm.

Thus, neonatal activation of *Braf*<sup>V600E</sup> in murine melanocytes promoted dermal cell hyperproliferation, inducing naevogenesis. However, these pigmented lesions were not able to progress to malignant melanoma, except for one homozygous *Braf*<sup>V600E</sup> old animal out of 16 4OHTx-treated mice.

## 2. A single dose of neonatal UVR cooperates with *Braf*<sup>V600E</sup> in melanoma progression in our mouse model

Epidemiological studies suggest that ultraviolet B exposure (UVR) during childhood is the most important melanoma environmental risk factor (82). For this reason, we investigated the cooperation between *Braf*<sup>V600E</sup> activation and the neonatal UVR in the previously described animal model. To this aim, mice were treated with 4OHTx at 2.5 days post-natal, and the day after, they were irradiated with a single suberythemal dose of UVB radiation (Figure 5A).

As exposed before, *Braf*<sup>V600E</sup>-treated mice developed pigmented lesions that failed to progress into melanoma with a single exception, related to aging (Figure 5B). The UVB-exposure of both *Braf*<sup>CA/+</sup> and *Braf*<sup>CA/CA</sup> animals was enough to significantly induce melanomagenesis at same incidence in both genotypes (Figure 5B,C).

The genetic dose had an effect in the reduction of the tumor onset. While  $Braf^{CA/+}$  animals showed a latency of  $\approx 6$  months, homozygous animals ( $Braf^{CA/CA}$ ) showed a reduced onset to  $\approx 3$  months (Figure 5C). Moreover, UVB-exposed homozygous animals showed a slightly increase in tumor multiplicity (Figure 5D).

Thus, a single dose of neonatal was sufficient to promote  $Braf^{V600E}$ -induced melanomagenesis independently of the genetic dose.

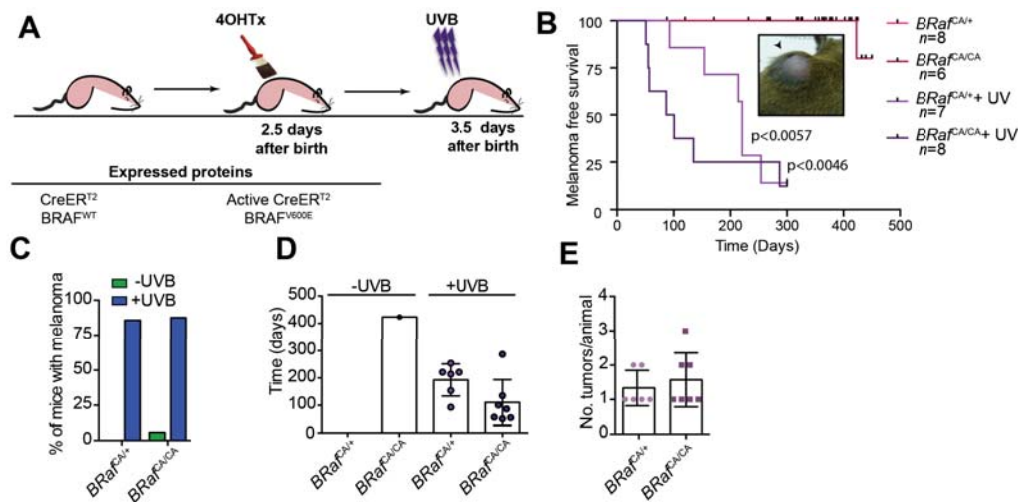


**Figure 5: UVR promotes melanoma progression in  $Braf^{V600E}$ -induced mice. (A)** Experimental design schema. Activation of  $CreER^{T2}$  by 4OHTx led to melanocyte-specific conversion of  $Braf^{WT}$  to  $Braf^{V600E}$ . At 3.5 days, mice were irradiated with a single suberythemal UVB dose. **(B)** Kaplan-Meier survival analysis of 4OHTx-treated  $Tyr::CreER^{T2};Braf^{CA/+}$ ; (n = 8),  $Tyr::CreER^{T2};Braf^{CA/CA}$ ; (n = 6), UVB exposed- $Tyr::CreER^{T2};Braf^{CA/+}$ ; (n = 7), and UVB exposed- $Tyr::CreER^{T2};Braf^{CA/CA}$ ; (n = 8). Photograph of a tumor developed in the back of an UVB-exposed  $Braf^{V600E}$  mouse. **(C)** Percentage of mice with melanoma in UVB-exposed and non-exposed  $Braf^{CA/+}$  and  $Braf^{CA/CA}$ . **(D)** Mean lag-time in UVB-exposed and non-exposed  $Braf^{CA/+}$  and  $Braf^{CA/CA}$ . **(E)** Mean tumors number per animal in UVB exposed- $Braf^{CA/+}$  and UVB exposed-  $Braf^{CA/CA}$ . Error bars show mean  $\pm$  standard deviation.

### 3. UVB irradiation prevents $Braf^{V600E}$ -induced senescence *in vivo* and *in vitro*

As shown before, neonatal  $Braf^{V600E}$  activation in murine melanocytes promotes the development of benign lesions characterized by cell cycle arrest and senescence features, known as nevus. Full malignant transformation of the  $Braf^{V600E}$ -expressing melanocytes was achieved by a single dose of UVR, for this reason we assess the role of this environmental factor preventing  $Braf^{V600E}$ -induced senescence.

In order to monitor the effect of the UVB-irradiation in  $Braf^{V600E}$ -induced melanocytes, the back skin of the 4OHTx-treated and non-treated animals was collected 7 and 27 days after UVB-exposure (Figure 6). To seek the melanocyte proliferation status, we stained the skin sections with the proliferation marker -Ki67-, and the senescence marker -p16.



*Braf*<sup>V600E</sup> activation promotes melanocyte proliferation 7 days after 4OHTx activation. This melanocyte hyperproliferation was located in the matrix and the lower hair follicle region (Figure 6A). At this time point, isolated skin was positive for Ki67 staining, but not for the senescence marker, p16 (Figure 6a). In contrast, 27 days post-activated melanocytes showed signals of cell cycle arrest and senescence. Staining of the proliferative marker - Ki67- was negative, while these cells turned positive for p16<sup>INK4a</sup> (Figure 6c). Clearly, we observed a melanocyte regression, characterized by the presence of melanophages (Figure 6C, upper-left). Intriguingly, by this time point melanocytes started to invade the adjacent dermis, which could be considered as incipient nevi (Figure 6C, down-left). All this data resembled the human BRAF<sup>V600E</sup>-induced nevi, which after a transient proliferative melanocyte state the expression of this oncogene induced its senescence (83). On the other hand, a single erythemogenic dose UVB radiation ensued *Braf*<sup>V600E</sup>-melanocytes to proliferate inside the hair follicle bulbs with melanocytes spreading into the adjacent dermis 7 days after UVR (Figure 6B). The inspection of mice skin, 27 days post UVB-exposure, denoted proliferation and accumulation of melanocytes in the adjacent dermis (Figure 6D). According to the proliferation marker Ki67 and the cell cycle inhibitor p16<sup>INK4a</sup>, UVR has a clear effect in *Braf*<sup>V600E</sup>-induced melanocytes, avoiding cell cycle arrest at 27 days post-irradiation. Irradiated *Braf*<sup>V600E</sup>-induced mouse melanocytes stained positive for Ki67 and negative for p16<sup>INK4a</sup> (Figure 6d). Even though melanocyte regression was detected, we could observe some foci of proliferating tumor cells showing pleomorphic and pyknotic cells in the adjacent dermis. Clearly these cells presented malignant signs as cell division, and loss of pigmentation or tissue structure (Figure 6D). These results indicate that neonatal UVB irradiation prevents *Braf*<sup>V600E</sup> induced senescence promoting malignant tumor progression.

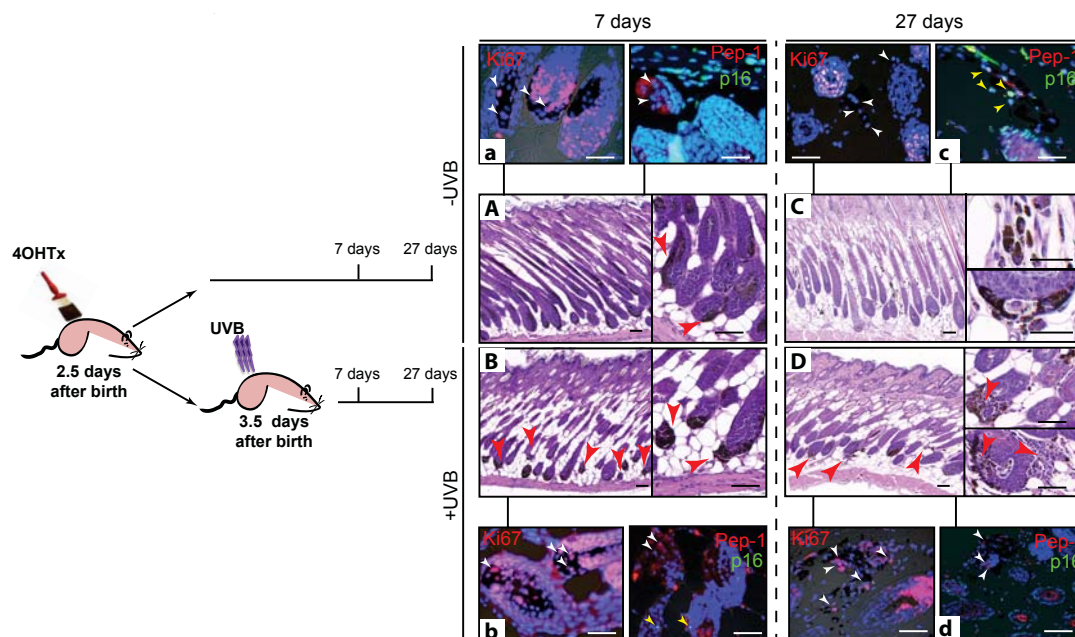


**Figure 6: UVR stimulates the abnormal proliferation of the melanocytes, promoting naevogenesis.** Experimental strategy to study the effect of UVB exposure in *Tyr::CreER<sup>T2</sup>;Braf<sup>CA/CA</sup>* at 7 and 27 days post UVB-irradiation. **(A-D)** Central panel, *Tyr::CreER<sup>T2</sup>;Braf<sup>CA/CA</sup>* animal skin stained with Neutral Red at 7 and



27 days post-UVB irradiation and control skin without irradiation. (a-d) It is shown the immunofluorescence against the proliferation marker (Ki67) and the co-staining of the melanocyte- (PEP1) and the senescence-marker (p16). In the C-upper-left box of 27 days non-irradiated immunohistochemistry, it is shown the melanophages presence, indicating the regression of the melanocyte proliferation. Red arrowhead indicates the melanocyte accumulations. White arrowheads indicate Ki67 and Pep1 positivity, while the yellow arrowheads depicted p16 positivity. Black scale bars are 500 $\mu$ m, 100 $\mu$ m, and 50 $\mu$ m. White scale bars are 500 $\mu$ m.

It is described that sustained expression of *Braf*<sup>V600E</sup> in human melanocytes induced cell cycle arrest, accompanied by the induction of both p16<sup>INK4a</sup> and the senescence-associated acidic  $\beta$ -galactosidase (SA- $\beta$ -Gal) activity (15). We investigated the effect of UVR preventing *Braf*<sup>V600E</sup>-induced senescence *in vitro*. To this end, we isolated melanocytes from the back skin of the neonatal *Tyr::CreER*<sup>T2</sup>;*Braf*<sup>CA/CA</sup> mice. Lineage of isolated cells was previously confirmed by the expression of specific melanocyte markers TRP-2, also known as DCT (Figure 7A). Expression of *Braf*<sup>V600E</sup> in these cells was achieved by addition of 4OHTx. As expected, *Braf*<sup>V600E</sup>-induced melanocytes presented a significant increase of senescence marker p16<sup>INK4a</sup> and SA- $\beta$ -Gal activity seven days after induction. However, irradiation of cells with a single dose of UVB (30J/m<sup>2</sup>) upon *Braf*<sup>V600E</sup>-activation prevented the senescence-like phenotype (Figure 7B).

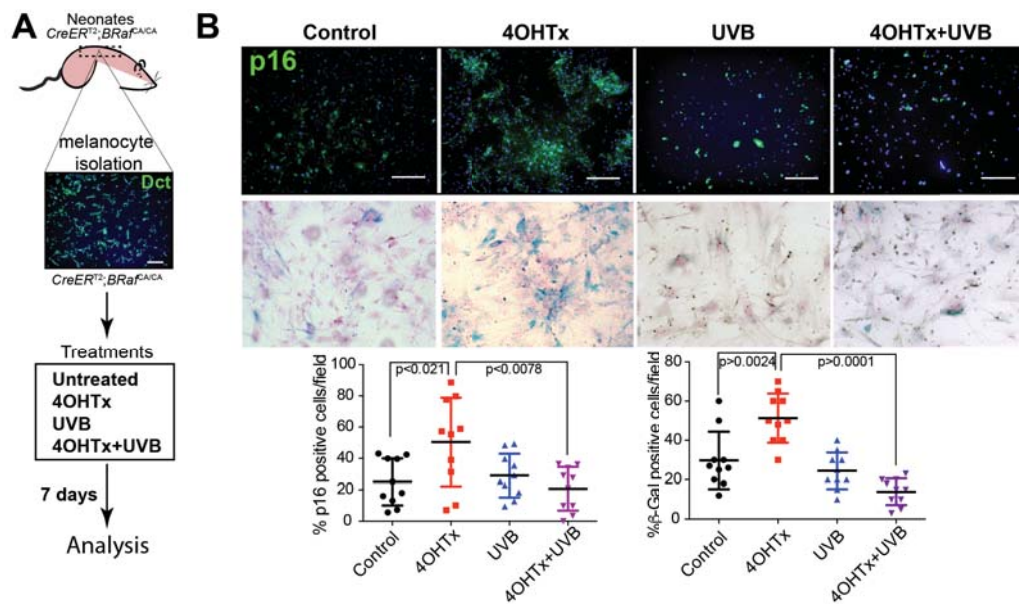


**Figure 7: UVR prevents the expression of senescence markers in the skin of *Braf*<sup>V600E</sup>-induced mice.** (A) Melanocyte isolation from neither non-induced nor irradiated *Tyr::CreER*<sup>T2</sup>;*Braf*<sup>CA/CA</sup> mice experimental scheme. Back skin of 1-2 days old mice was removed and performed the melanocyte isolation following the protocol from (15) to check the different senescence markers. The melanocyte lineage was checked by immunofluorescence against DCT, a melanocyte marker. (B) Top panel, immunostaining for senescence markers (p16<sup>INK4A</sup> and SA- $\beta$ -Gal activity) in melanocytes isolated from neonates back skin. The experimental conditions performed *in vivo* were: control, 4OHTx-induced, UVB-exposed (30J/m<sup>2</sup>) and 4OHTx-induced+UVB-exposed. At the bottom, quantification of the p16<sup>INK4A</sup> signal and SA- $\beta$ -Gal activity immunostaining. Error bars show mean  $\pm$  standard deviation. Scale bars are 50 $\mu$ m.

Altogether, we have confirmed that the expression of *Braf*<sup>V600E</sup> alone was not enough to promote melanomagenesis, due to the induction of the oncogene-induced senescence. Interestingly, a single dose of neonatal UVB radiation prevented *Braf*<sup>V600E</sup>-induced senescence allowing melanoma progression.

#### 4. Loss of *Lkb1* increases melanoma incidence and tumor lag time in *Braf<sup>V600E</sup>* mice

*LKB1* is a tumor suppressor mutated or inactivated in sporadic cancers whose spectrum of tumor type, suggest cooperation with exposure to environmental carcinogens, as melanoma. In our lab, we have previously described a critical role for *Lkb1* in cutaneous squamous cell carcinoma development acting as a DNA-damage sensor upon UVB radiation (75). Thus, we investigated the cooperation among *Braf<sup>V600E</sup>* oncogene, the tumor suppressor *Lkb1* and UVB-radiation in melanoma development. We generated an induced-tissue specific mouse model for the expression of oncogenic *Braf<sup>V600E</sup>* and the concomitant loss of *Lkb1* in melanocytes previously described (54). To this end, we crossed *Tyr::CreER<sup>T2</sup>;Braf<sup>CA/CA</sup>* mouse with *Lkb1<sup>F/F</sup>* mouse to obtain the mendelian-offspring (from now on B/L/UV animal model). Again 4OHTx treatment was performed at 2.5 days after birth, to promote the expression of *Braf<sup>V600E</sup>* with the concomitant loss of *Lkb1*. Then, animals were irradiated one day after with a single suberythemal dose of UVB (Figure 8A).

Loss of one or both copies of this tumor suppressor in combination with *Braf<sup>V600E</sup>* activation induced melanomagenesis independently of UVR (Figure 8B,C). These results correlated with the literature, where either *Cdkn2a* or *Lkb1* loss abrogates *Braf<sup>V600E</sup>*-induced senescence (80). Of note, the genetic dose of *Lkb1* loss slowed down melanoma onset in irradiated *Braf<sup>CA/+</sup>* and *Braf<sup>CA/CA</sup>* animals (Figure 8B,C).

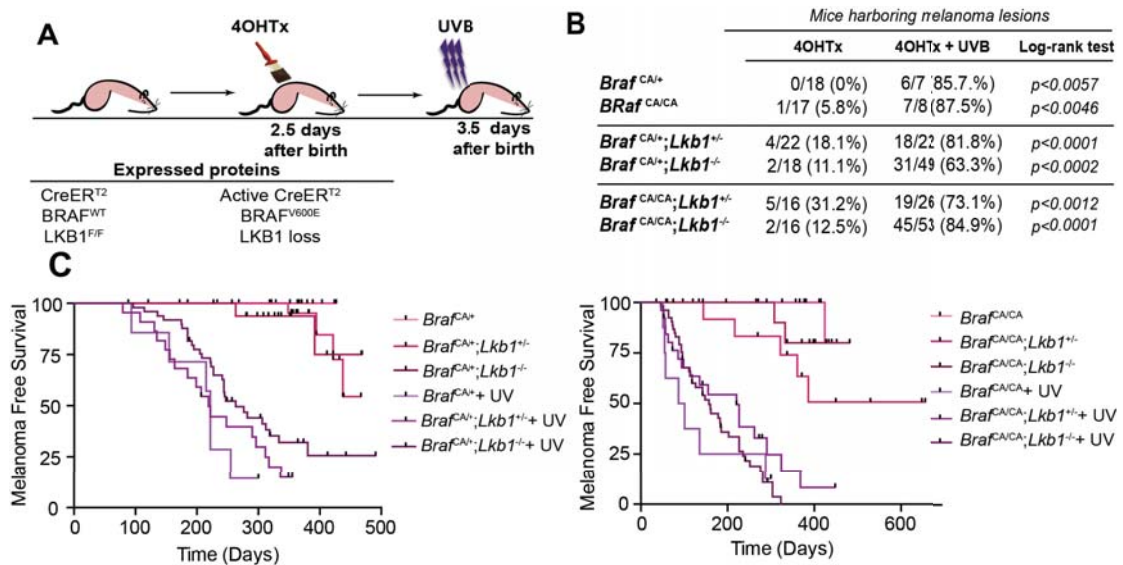


**Figure 8: *Lkb1* loss promotes melanomagenesis in *Braf<sup>V600E</sup>*-mice independently of UVR. (A)** Experimental diagram of mouse treatment and expressed proteins. Same as the scheme presented in Figure 4 with the exception that 4OHTx treatment induced not only the *Braf<sup>CA</sup>* expression, but also the concomitant loss of *Lkb1*. **(B)** Table showing the percentage of mice developing melanoma lesions according to their genotype, 4OHTx-treatment and UVR-exposure. **(C)** In the left, Kaplan-Meier survival analysis of the non-exposed 4OHTx-treated *Tyr::CreER<sup>T2</sup>* animals: *Braf<sup>CA/+</sup>* (n = 18); *Braf<sup>CA/CA</sup>* (n = 17); *Braf<sup>CA/+</sup>;Lkb1<sup>+/-</sup>* (n = 22); *Braf<sup>CA/+</sup>;Lkb1<sup>-/-</sup>* (n = 18); *Braf<sup>CA/CA</sup>;Lkb1<sup>+/-</sup>* (n = 16); and, *Braf<sup>CA/CA</sup>;Lkb1<sup>-/-</sup>* (n = 16). At right, Kaplan-Meier survival analysis of the UVR-exposed 4OHTx-treated *Tyr::CreER<sup>T2</sup>* animals: *Braf<sup>CA/+</sup>* (n = 7); *Braf<sup>CA/CA</sup>* (n = 8); *Braf<sup>CA/+</sup>;Lkb1<sup>+/-</sup>* (n = 22); *Braf<sup>CA/+</sup>;Lkb1<sup>-/-</sup>* (n = 49); *Braf<sup>CA/CA</sup>;Lkb1<sup>+/-</sup>* (n = 26); and, *Braf<sup>CA/CA</sup>;Lkb1<sup>-/-</sup>* (n = 53).

UVR significantly increased melanoma incidence independently of the mice genotype (Figure 9). Furthermore, UVR increased the tumor multiplicity in *Lkb1* genetic dose dependent manner. Interestingly, non-irradiated *Braf*<sup>CA/CA</sup> animals also increase the median tumor number per animal in *Lkb1* dose-dependent manner.

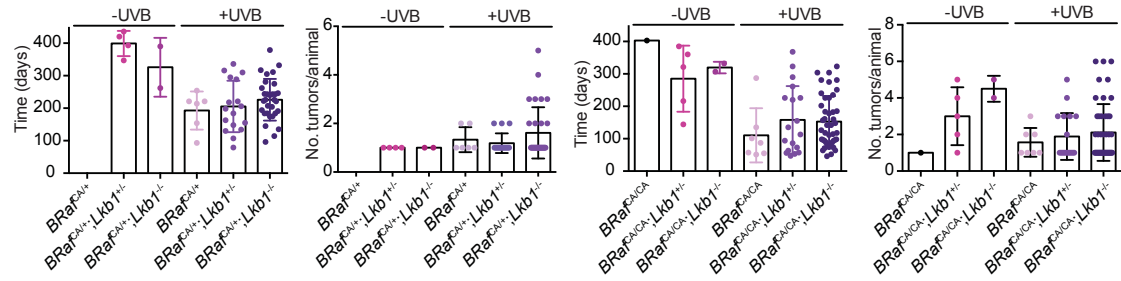


**Figure 9: *Lkb1* haploinsufficiency increased the tumor lag time in irradiated *Braf*<sup>V600E</sup>-tumors.** Percentage of mice with melanoma and the mean tumor number per animal in UVB-exposed and non-exposed and 4OHTx-treated *Tyr::CreER*<sup>T2</sup> animals: *Braf*<sup>CA/+</sup>; *Braf*<sup>CA/CA</sup>; *Braf*<sup>CA/+</sup>;*Lkb1*<sup>+/-</sup>; *Braf*<sup>CA/+</sup>;*Lkb1*<sup>-/-</sup>; *Braf*<sup>CA/CA</sup>;*Lkb1*<sup>+/-</sup>; and, *Braf*<sup>CA/CA</sup>;*Lkb1*<sup>+/-</sup>. Error bars show mean ± standard deviation.

Thus, *Lkb1* loss promotes *Braf*<sup>V600E</sup>-melanomagenesis with a penetrance that ranges from 20-50%, independently of UVR. The lack of this tumor suppressor increased the melanoma onset and the tumor multiplicity in irradiated and non-irradiated animals.

## 5. Histologic analysis of tumors unveils morphologic tumor heterogeneity

Whereas there are an increasing number of publications performed with *Braf*<sup>V600E</sup>-induced animal models focused in melanomagenesis, the histologic classification of the melanoma lesions has not been routinely performed. For this reason, we performed hematoxylin and eosin tumor staining to evaluate the tumor histological components from the different experimental groups.

The histological analysis of the B/L/UV melanomas revealed that many tumors, but not all, presented three different histologic subtypes, being most of the times, one of them predominant among others (>70%): (a) myxoid melanoma (characterized by deposits of neutral and acidic mucin stained with Periodic Acid Schiff -PAS- and Alcian blue), (b) dermal spindle melanoma and (c) melanoma with nerve sheath differentiation (neural melanoma) (Figure 10). Even though in the literature is not frequent the histologic melanoma classification of the animal tumors, the most common subtype reported in *Braf*<sup>V600E</sup>-induced melanoma murine model corresponded to myxoid melanoma (75).



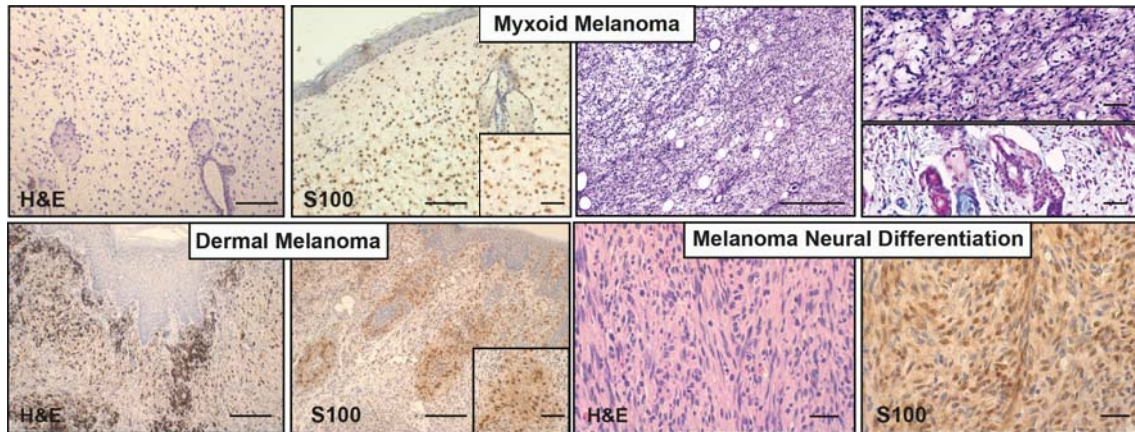


**Figure 10: Development of different melanoma subtypes in B/L/UV model.** Representative images of different subtypes of melanoma observed in B/L/UV model: (a) myxoid (Top), (b) dermal (left bottom), and (c) neural (right bottom). This figure shows the hematoxylin and eosin (H&E) staining and immunohistochemistry against the melanocyte marker -S100. PAS and alcian blue for mucin staining is showed for myxoid melanoma detection. Insets show a magnification of cells. Bars are 500µm and 50µm.

In order to better understand the histologic heterogeneity observed in the raised melanomas, we analyze the percentage of animals presenting tumors taking into consideration the predominant histology subtype, the genetic background of the mice, and the contribution of UVR (Figure 11).

The myxoid subtype, the most frequent in the B/L/UV model, was developed in all irradiated animals, independently of its genetic background. This data revealed the important correlation of this tumor subtype with UVR. On the other hand, spindle melanoma increased its penetrance when mice were UVB-irradiated and/or with the loss of *Lkb1*. Interestingly, tumors showing a homogenous neural phenotype increased their frequency with the loss of *Lkb1*, where UVR clearly increased its penetrance.

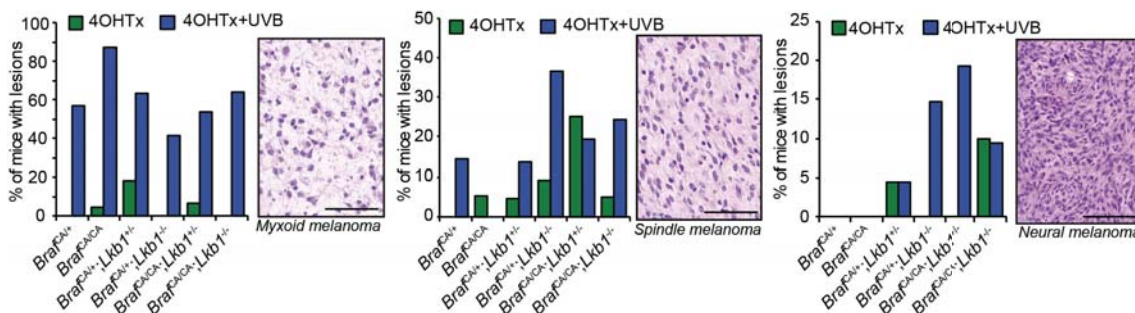


**Figure 11: Different melanoma subtypes could be associated to UVR and/or LKB1 loss.** Percentage of mice with lesions sorted within different melanoma subtypes: myxoid (left), spindle (center) and neural (right). Moreover, this data was classified according the genetic background of the mice and the UVR. Hematoxylin and eosin staining shows a representative histological example of the different melanoma subtypes. Scale bars are 500µm.

Since lack of *Lkb1* was associated to the incidence of a particular melanoma subtype, suggesting a differential cell origin, we investigated the possible differential expression of *Lkb1* among the murine melanocyte population. To this aim, we studied the LKB1 expression and localization by its co-immunofluorescence with the melanocyte marker, TRP2, in normal mice skin. LKB1 nuclear expression was limited to few hair follicle

melanocytes (Figure 12). It is known that melanoma can originate from melanocytes localized in the hair follicle (78). This data suggested a possible melanocyte dependent differential effect upon BRAF activation and concomitant loss of *Lkb1*, highlighting the connection between the restrained number of LKB1-positive cells and the overall low frequency of neural melanoma tumors.

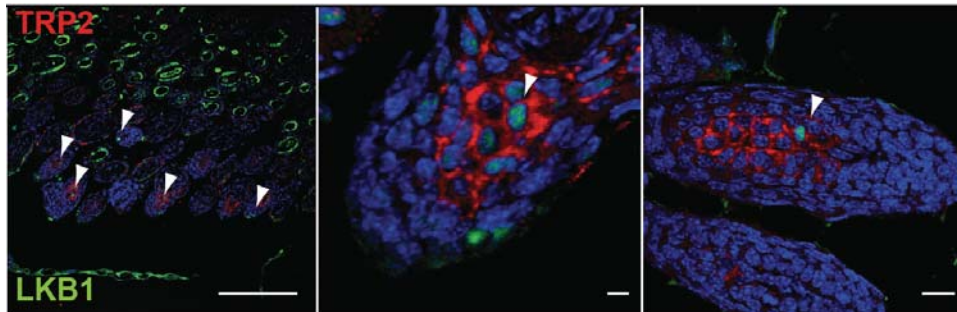


**Figure 12: Limited LKB1 expression in murine hair follicle melanocytes from B/L/UV model.** Immunofluorescence performed against the melanocyte marker TRP2 (red) and LKB1 (green) in neither non-irradiated nor induced B/L/UV mice. White arrowheads indicate the LKB1 positive melanocytes. White scale bars are 50 $\mu$ m, 500  $\mu$ m and 100  $\mu$ m.

Altogether, this data suggests that the genetic background of the melanocytes seems to influence the development of the different subtypes of melanoma. In our model, UVR increases frequency of all mentioned melanoma subtypes independently of the genetic context. Intriguingly, the frequency of neural-like melanomas appeared to be linked to the *Lkb1* tumor suppressor genetic dose. In this matter, LKB1 expression was heterogeneous and limited to few melanocytes within the hair follicle, suggesting a connection between this specific melanoma subtype and its cellular origin.

## 6. *Lkb1* loss increases the genetic instability favoring the melanoma histologic heterogeneity

The above results highlighted the different origin from the detected melanoma subtypes, pointing out the differential effect of UVR and the loss of *Lkb1* in melanoma development and progression. To further study the contributions of LKB1 to UVB-induced melanoma, we analyzed the number and percentage of tumor subtypes (tumor heterogeneity) according to the animal genotype and the influence of the environmental insult UVR.

Overall, the loss of *Lkb1* increased not only the number of all melanoma subtypes, but also tumor heterogeneity (Figure 13). *Lkb1* loss increased the percentage of the different histological melanomas, showing a clear cooperation with the *Braf*<sup>V600E</sup> genetic dose. As above described, myxoid-melanoma was the most common subtype in all the genetic backgrounds upon UVR. In the case of dermal-spindle melanoma, its incidence was promoted mainly by UVR, and in lesser extend by *Lkb1* loss. The neural-like melanoma showed again its clear *Lkb1* loss dependency and also the cooperation with UVR.

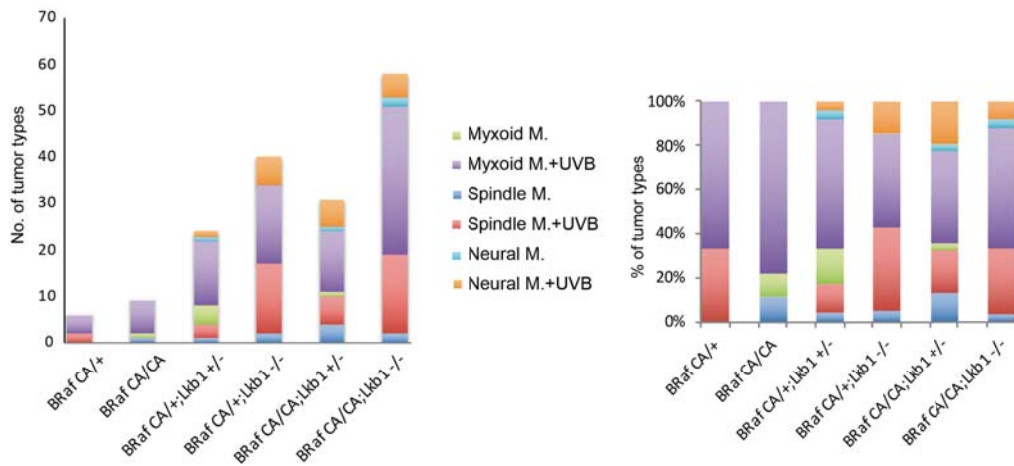


**Figure 13: *Lkb1* loss increases the genetic instability favoring the melanoma histological heterogeneity.** These graphs represent the number and percentages of the different melanoma subtypes classified within the different mice genetic background and the UVB-exposure.

Previous results from our group unveiled LKB1 as a UVB induced-DNA damage sensor (11,12), emphasizing its relevance in melanomagenesis and genetic stability. Thus, we investigated the contribution of *Lkb1* loss in the UVB-induced DNA damage repair. To address this question, we analyzed the UVB-induced DNA damage repair ratio of the genomic DNA obtained from the back skin of wild-type and *Tyr::CreER<sup>T2</sup>;Braf<sup>CA/CA</sup>;Lkb1<sup>-/-</sup>* mice (Figure 14). In order to study the DNA repair response, we performed a South-western with the genomic DNA at different time points after UVB irradiation to detect and quantify different UVB-induced DNA damage molecular lesions, such as: 6-4 phosphopproducts (6-4-pps), Dewar isomers and Cyclobutane Pyrimidine Dimers (CPDs).

As expected, not irradiated skin did not present any signal of DNA damage. Specific UVB-induced DNA damaged was detected in wild-type mice 20h after UVB irradiation that was significantly repaired one week after irradiation. However, animals harboring homozygous loss of *Lkb1* and *Braf<sup>V600E</sup>* mutation showed an impaired specific UVB-induced DNA damage repair at the same time point (Figure 14).

Thus, these results confirmed that lack of *Lkb1* impedes an appropriated UV-induced DNA damage repair, promoting genetic instability, tumor development and tumor heterogeneity.

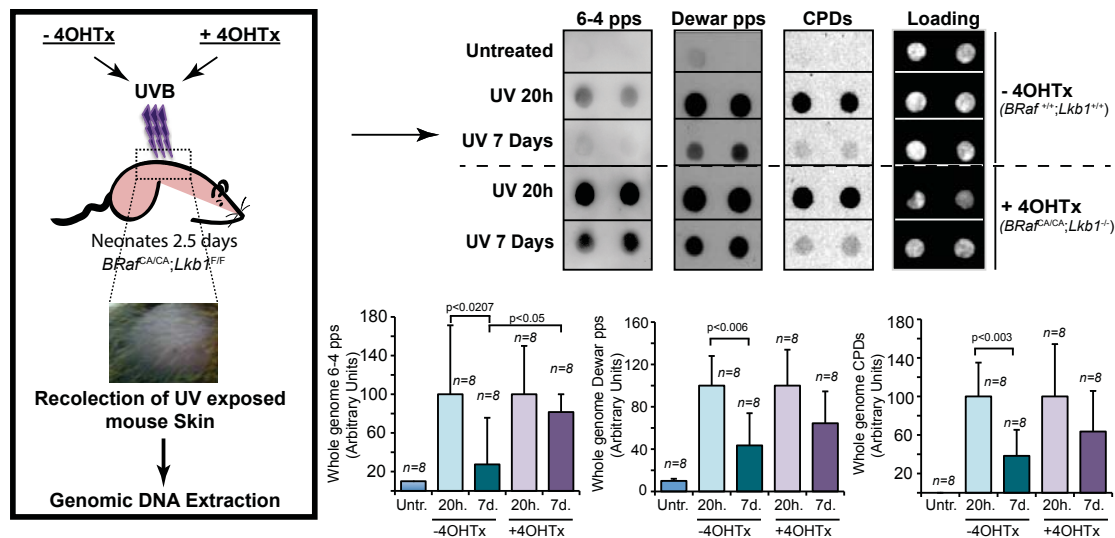


**Figure 14: Lack of *Lkb1* expression impeded the regular DNA-damage repair after UVB-radiation.** Workflow diagram for the genomic DNA extraction from mice back skin. South-Western from UVB-irradiated and non-irradiated mice at different post-exposition time points (20h and 7days). Blotting against DNA-damage antibodies: 6-4 phosphopproducts (6-4pps), Dewar and Cyclobutane Pyrimidine Dimers (CPDs). Graphs show the DNA-repair quantification under the different conditions studied (n = 8, per group). Error bars show mean  $\pm$  standard deviation.

## 7. Melanoma tumors showed both mTORC1 and mTORC2 signaling pathways activation

In a recent murine model (54), the concomitant loss of *Cdkn2a* and *Lkb1* in a *Braf*<sup>V600E</sup> context promoted nevi progression into melanoma. Through a Gene Set Enrichment Analysis (GSEA) of the Whole Exome Sequence (WES) data from tumors, the authors exposed that melanomagenesis was induced by the upregulation of the mTOR-signaling pathway. Specifically, the lack of *Lkb1* activates mTORC1, which had a central role in overcoming *Braf*<sup>V600E</sup>-induced senescence in melanocytes. However, they claimed that fully malignancy was achieved by the concomitant activation of mTORC2 through the loss of *Cdkn2a*. Consequently, we investigated the activation status of these pathways in tumors raised in the B/L/UV model.

In order to verify the activation of mTORC1 signaling pathway, we stained tumors against the phosphorylated forms of 4E-BP1 and S6K (Figure 15). Protein amounts of these mTORC1 downstream targets were increased in B/L/UV tumors. However, only the phospho-S6K had a significant increment that directly correlated with *Lkb1* genetic dose. To confirm the status of the mTORC2 signaling, we did an immunohistochemistry analysis of the phosphorylated AKT at Serine 473 (p-Ser473), a surrogate marker for mTORC2 activity (Figure 15). All tested lesions showed activation of mTORC2 signaling pathway.

Thus, *Lkb1* lack in the B/L/UV model contributed to melanocyte proliferation and malignant transformation through the direct activation of mTORC1. However, the activation of the mTORC2 activity, required for the fully malignant transformation of the melanocytes, was also achieved in all investigated tumors.



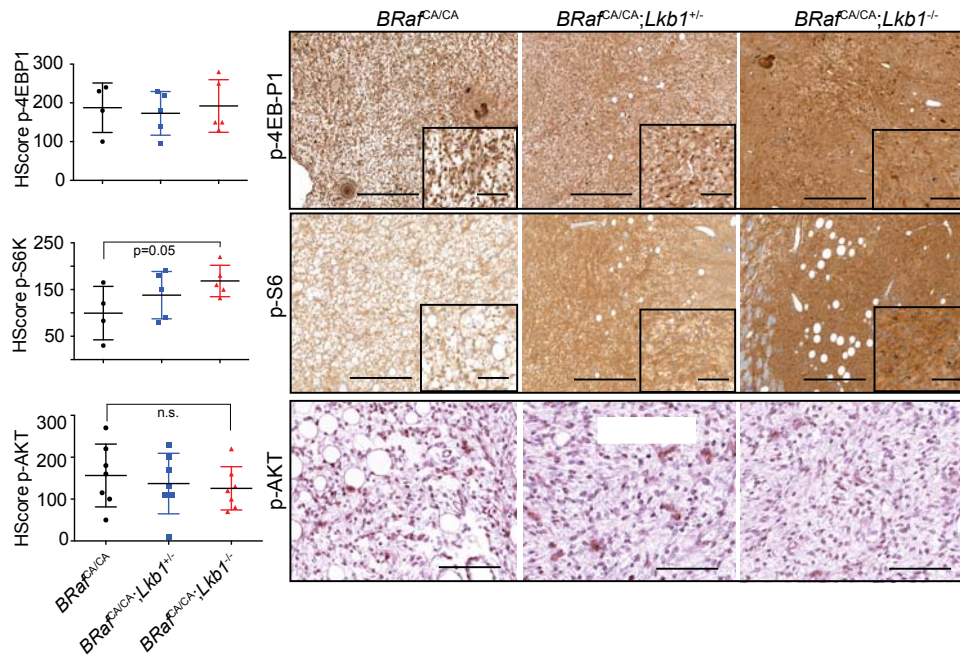


**Figure 15: B/L/UV melanomas were positive for mTORC1 and mTORC2 activated downstream substrates.** In the left, HScore quantification from the phospho-S6K, phospho-4E-BP1, and phospho-AKT (Ser473) in the B/L/UV tumors. At right, phospho-S6K, phospho-4E-BP1, and phospho-AKT (Ser473) immunohistochemistry panel with representative staining of tumors from the different genotypes (*Tyr::CreER<sup>T2</sup>;Braf<sup>CA/CA</sup>*, *Tyr::CreER<sup>T2</sup>;Braf<sup>CA/CA</sup>;Lkb1<sup>+/-</sup>*, and *Tyr::CreER<sup>T2</sup>;Braf<sup>CA/CA</sup>;Lkb1<sup>-/-</sup>*). Insets show a magnification of cells. Error bars shown mean  $\pm$  standard deviation. Scale bars are 500µm and 50µm.

## 8. An important percentage of human BRAF<sup>V600E</sup>-mutated cutaneous melanomas shows low or none levels of LKB1

Based on the above results, it is clear the relevant role of LKB1 in the B/L/UV melanomagenesis. For this reason, we wondered which was the status of *LKB1* in human *BRAF*-altered melanomas. To this aim, we analyzed the data available for skin cutaneous melanoma at The Cancer Genome Atlas (TCGA) database.

The data analysis revealed that *LKB1* (*STK11*) is primarily transcriptionally altered in 10% of human skin cutaneous melanoma, independently of the presence or absence of *BRAF* mutations (Figure 16A). Knowing the tumor suppressor nature of *LKB1*, it was expected to observe the inactivating mutations, truncating mutations or deletion of this gene. However, the most common *LKB1* genetic alteration was the mRNA up- or down-regulation. Thus, we first investigated the correlation between the promoter methylation (human methylome, HM450) and mRNA expression available at the TCGA database (Figure 16B). The analysis indicated that in human melanomas, *BRAF* was highly expressed, presenting low levels of promoter methylation. *LKB1* showed a most heterogeneous pattern, most samples presented a highly methylated promoter, independently of the mRNA expression amounts of this gene. Nevertheless, some samples, including *BRAF<sup>V600E</sup>* mutated samples, presented a clear negative correlation, showing a highly methylated *LKB1* promoter and lower amounts of mRNA expression (red circle, Figure 16B).



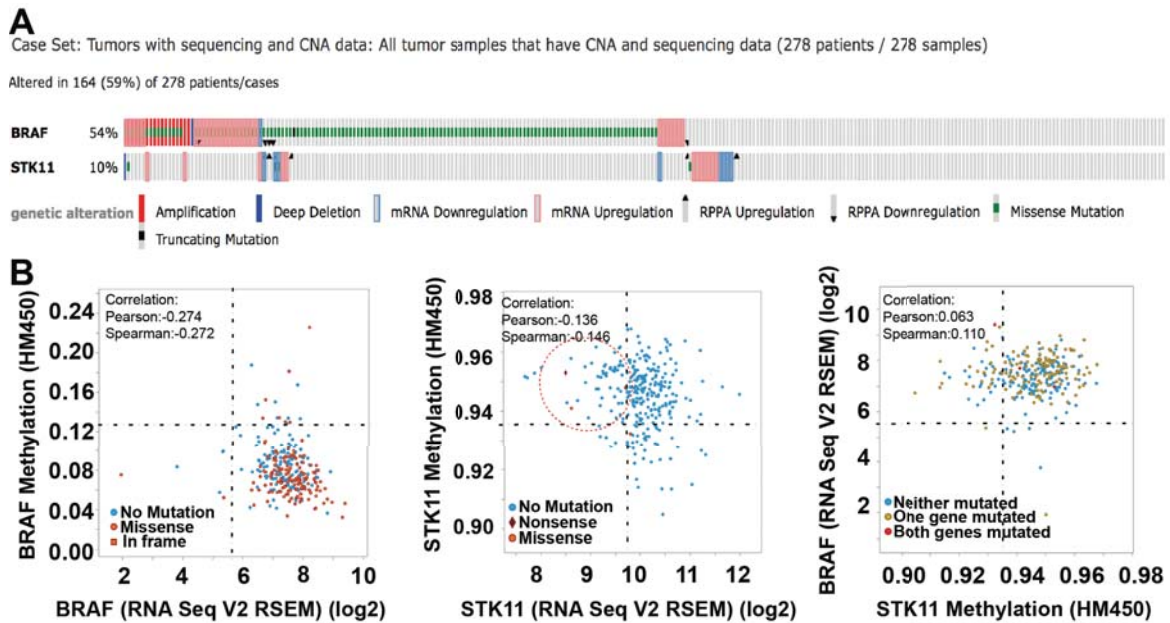
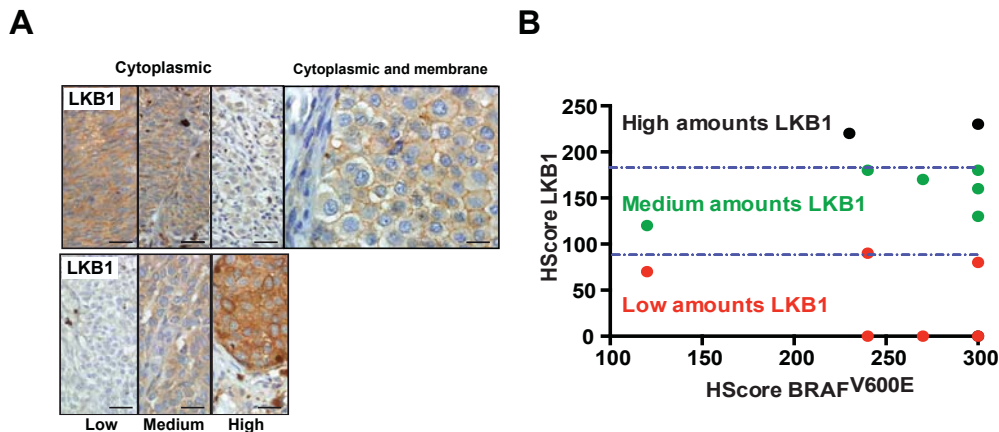


Figure 16: *BRAF* and *LKB1* transcriptional alteration in human cutaneous melanomas. (A) Representation of *BRAF* and *STK11* genetic alteration detected in skin cutaneous melanoma samples from TCGA provisional database ( $n = 276$  patients). This graph indicates the mutational percentage of the different genes, as well as the type of genetic alteration found in each patient for both genes (each bar is a patient) in this disease. (B) Expression profile for *BRAF* and *STK11* genes in skin cutaneous melanoma samples from TCGA provisional database. From left to right, representation of (a) *BRAF* methylation levels versus *BRAF* mRNA expression levels, (b) *STK11* methylation levels versus *STK11* mRNA expression levels, and (c) *BRAF* mRNA expression levels versus *STK11* methylation levels.

We next investigated the amounts of LKB1 protein present in human  $BRAF^{V600E}$  mutated tumors. To that end, we stained  $BRAF^{V600E}$ -mutated melanoma samples against LKB1 protein. We observed a heterogeneous LKB1 expression mainly located in the cytoplasm. However, melanomas having an epithelial phenotype also showed a clear staining of the cell membrane (Figure 17A). Interestingly, 42% of  $BRAF^{V600E}$  mutated human samples presented either low or none expression of LKB1 protein (Figure 17B).

Hence, these results highlighted the relevance of the B/L/UV model, mimicking the molecular status of *BRAF* and *LKB1* in a number of human melanomas.



**Figure 17: LKB1 has different expression levels in human BRAF<sup>V600E</sup>-mutated melanoma. (A)** Upper part, representative LKB1 immunohistochemistries show its different expression levels and its localization in BRAF<sup>V600E</sup>-mutated human melanomas. At the bottom, demonstrative LKB1 immunohistochemistries indicating low, medium and high LKB1 signal. **(B)** Graphic representation of LKB1 HScore values against the BRAF<sup>V600E</sup> HScore (high amounts, n = 2; medium amounts, n = 6; and low mounts, n = 6).

### 9. Differential prognosis of human BRAF and NRAS mutant melanomas depending on associated LKB1 genetic alterations

Knowing that a number of BRAF<sup>V600E</sup>-mutated melanomas has low or none levels of LKB1 protein, we next investigated the effect of this tumor suppressor genetic alterations in melanoma patient survival. To this aim, it was studied the Kaplan-Meier representation for disease/progression-free survival and overall survival in the human Skin Cutaneous Melanoma from the TCGA provisional data set. This data indicates that LKB1 genetic alterations increase melanoma recurrence (Figure 18A) and confer poor survival (Figure 18B) independently of any other genetic alterations.

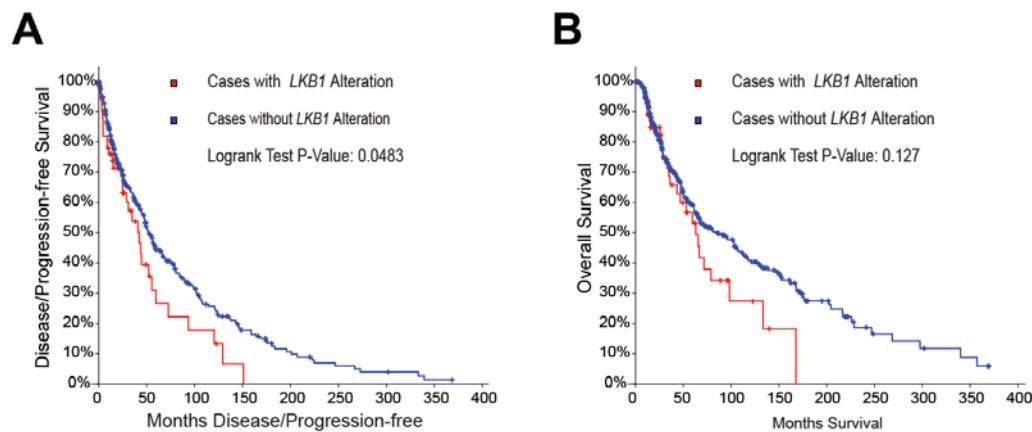


**Figure 18: Disease/progression-free- and overall-survival representation from the human skin cutaneous melanoma with and without LKB1 genetic alterations. (A)** Kaplan–Meier representation of the disease/progression free-survival from the skin cutaneous melanoma (TCGA, Provisional) data set. Representation of samples with altered LKB1. **(B)** Kaplan–Meier representation of the overall survival from the Skin Cutaneous Melanoma (TCGA, Provisional) data set. Representation of samples with altered LKB1. In each graph, it is represented 2 cohorts, which represent: patients where the query gene(s) is not altered (blue) and where the query gene(s) is altered (red).

### 10. LKB1 regulates *cMet* expression in mice and human melanoma cells, which has an effect *in vitro* cell proliferation

Additional information from parallel projects in our laboratory gave us the opportunity to find out proteins transcriptionally regulated by LKB1 upon UVR through the performance of LKB1 Chromatin Immunoprecipitation sequencing (ChIP-seq) in human lung cancer cell line reconstituted for the wildtype LKB1 expression. To further study the effect of *Lkb1* in tumor proliferation, we focused in the regulated proteins that could have an effect in this specific phenotype. Interestingly, the Hepatocyte Growth Factor (HGF)-receptor tyrosine kinase, *cMET*, appeared as one of the transcriptional targets of LKB1 (Appendix Figure 2). This receptor tyrosine kinase has been involved in

melanomagenesis before, and it is related with oncogenic mitogenic responses (75). Moreover, previous results from our group disclosed LKB1 as one of the downstream molecules responsive to HGF (84).

In order to corroborate this hypothesis, we analyzed the cMET protein levels in B/L/UV animal tumors (Figure 19). The loss of LKB1 correlated with a decrease in the levels of cMET. This effect was genetic dose dependent of LKB1, since *Tyr::CreER<sup>T2</sup>;Braf<sup>CA/CA</sup>;Lkb1<sup>+/-</sup>* tumors expressed higher amounts of cMET than *Tyr::CreER<sup>T2</sup>;Braf<sup>CA/CA</sup>;Lkb1<sup>-/-</sup>*.

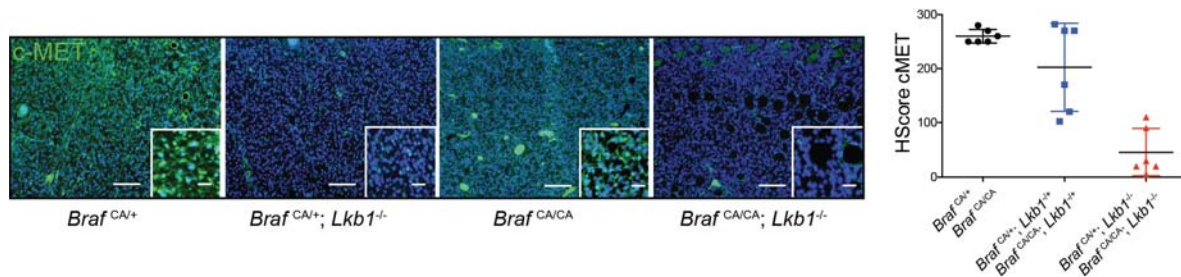


**Figure 19: Lack of *Lkb1* expression promotes depletion in cMET levels in B/L/UV tumors.** At the left, cMET immunofluorescence from *Tyr::CreER<sup>T2</sup>;Braf<sup>CA/+</sup>* (n = 6), *Tyr::CreER<sup>T2</sup>;Braf<sup>CA/+</sup>;Lkb1<sup>-/-</sup>* (n = 6), *Tyr::CreER<sup>T2</sup>;Braf<sup>CA/CA</sup>* (n = 6), and *Tyr::CreER<sup>T2</sup>;Braf<sup>CA/CA</sup>;Lkb1<sup>-/-</sup>* (n = 6) tumors. At the right, graphic representation of cMET HScore quantification classified according the genetic profile of the tumors. Insets show a magnification of cells. Error bars show mean  $\pm$  standard deviation. Scale bars are 500 $\mu$ m and 50 $\mu$ m.

To further confirm the possible transcriptional regulation of *cMET* by LKB1, we performed both, *in vitro* depletion and reconstitution experiments in human *BRAF<sup>V600E</sup>* melanoma cell lines. Depletion of LKB1 was performed in A375 melanoma cells. Stable infection of cells with a constitutive *LKB1* short hairpin (sh*LKB1*) resulted in 85% depletion of LKB1. On the other hand, G361 cells, null for LKB1, were infected with a doxycycline inducible expression vector for wildtype LKB1. As expected, LKB1 depletion was translated in a cMET decrease in A375 cell line (almost 90% of protein level reduction) (Figure 20A). Not all *BRAF<sup>V600E</sup>* cell lines shown this straightforward result when LKB1 was depleted, since the mutational genetic background of the cell lines could affect the gene regulation, including *cMET*. This was the case of the *BRAF<sup>V600E</sup>* mutated UACC903 cells, where LKB1 depletion does not regulate cMET expression (data not shown). On the other hand, LKB1 reconstitution of LKB1 in G361 cells promoted a slight increase of cMET levels (approximately 11% of expression increment) (Figure 20B). This specific cell line has probably developed unknown compensatory mechanisms to substitute the lack of the LKB1 for the transcriptional regulation of the *cMET*.

Then, we performed a proliferation assay to check the effect of LKB1 reconstitution or depletion in a *BRAF<sup>V600E</sup>* mutated context, with the absence or presence of the cMET ligand, HGF. Protein expression of LKB1 and cMET were compared by western blot in the parental and the stable cell lines generated.

In the case of the A375 cells, the expression of the sh*LKB1* had a reduction in proliferation independently of the HGF treatment. Moreover, treatment with HGF increased cell proliferation rate in parental cells, but not in A375-sh*LKB1* cell line, that lacks the cMET receptor (Figure 20A). Conversely, re-expression of *LKB1* in G361 cell line decreased the cell proliferation rate compared with the parental cells confirming the tumor suppressor role of *LKB1*. Both cell lines, parental and *LKB1*-transduced, increased their cell proliferation rate upon HGF triggering (Figure 20B).

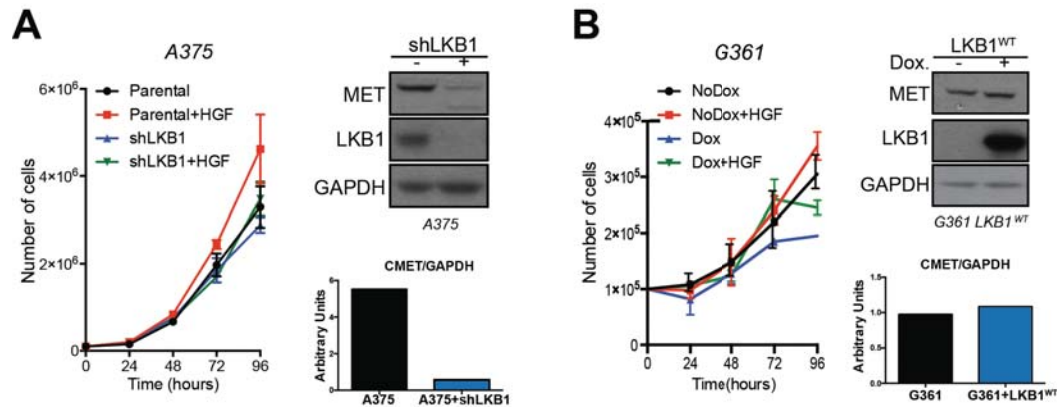


**Figure 20: LKB1 re-expression or depletion in *BRAF*<sup>V600E</sup>-melanoma cells regulates cMET levels and *in vivo* proliferation. (A) Growth curves from parental and LKB1-depleted A375 cell line. (B) Growth curves from parental and LKB1-reconstituted G361 cell line. LKB1 reconstitution assay was performed in the G361 cells by its infection with a doxycycline-inducible lentivirus for the expression of the wildtype *LKB1* form. The media from the doxycycline-induced (10µg/ml) and/or HGF-treated (40ng/ml) cell lines were changed every 2 days. Western blot to check the cMET, *LKB1* and GAPDH protein levels in: parental A375, A375 sh*LKB1*, parental G361, and G361 *LKB1*<sup>WT</sup>. Graph representation of the cMET levels normalized with GAPDH represented in arbitrary units.**

Next, we wondered whether *LKB1* transcriptional regulation of *cMET* was cell tissue-specific (Figure 21). To answer this question, we performed a reconstitution experiment using the A549 lung cell line *LKB1*-null. We observed a significant increment of *cMET* mRNA amounts 3 hours after the induction of *LKB1* expression by the addition of doxycycline. Together this data suggests that the *LKB1*-mediated transcriptional regulation of *cMET* is cell type dependent but is conserved in other tissues.

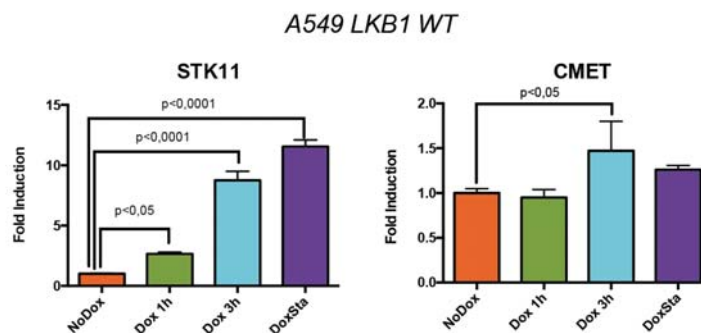


**Figure 21: LKB1 transcriptional regulation of *cMet* in A549 lung cells. *STK11* (*LKB1*) and *cMET* RT-PCR representation at different time points after doxycycline induction. This assay was performed in A549 cells reconstituted for the wildtype *LKB1*. RNA collection was performed in non-induced cells and induced cells (1h post induction, 3h post-induction and cells with stable induction (DoxSta). Error bars show mean + standard deviation.**



These results suggest that *Lkb1* loss might be related to the decrease of cMET amounts in the B/L/UV tumors, which could be responsible of the increment of the tumor onset. Although further investigation is guaranteed, LKB1-mediated transcriptional regulation was observed also in other tissues, as lung, emphasizing the role of LKB1 in the regulation of cMET protein levels.

### 11. Human melanoma analysis confirms the positive correlation between the LKB1 and cMET expression level

Next, we decided to study the correlation between LKB1 and cMET amounts in BRAF<sup>V600E</sup>-expressing human melanomas. Thus, we analyzed BRAF<sup>V600E</sup>, LKB1, and cMET expression in human melanoma samples obtained from the Vall d'Hebron Pathology Department (Figure 22A).

As exposed before human BRAF<sup>V600E</sup>-expressing tumors could present diverse LKB1 protein amounts. Interestingly, these tumors showed a positive correlation between LKB1 and cMET expression, independently of the BRAF mutational status (Figure 22A). Additionally, LKB1 staining revealed its cytoplasmic localization. In agreement with these results, analysis of LKB1 and cMET expression data from the data available in the TCGA showed a tendency for a positive correlation (*Pearson coefficient*,  $p=0.391$ ).

Altogether, this data reinforced the previous results suggesting the *cMET* transcriptional regulation by LKB1.

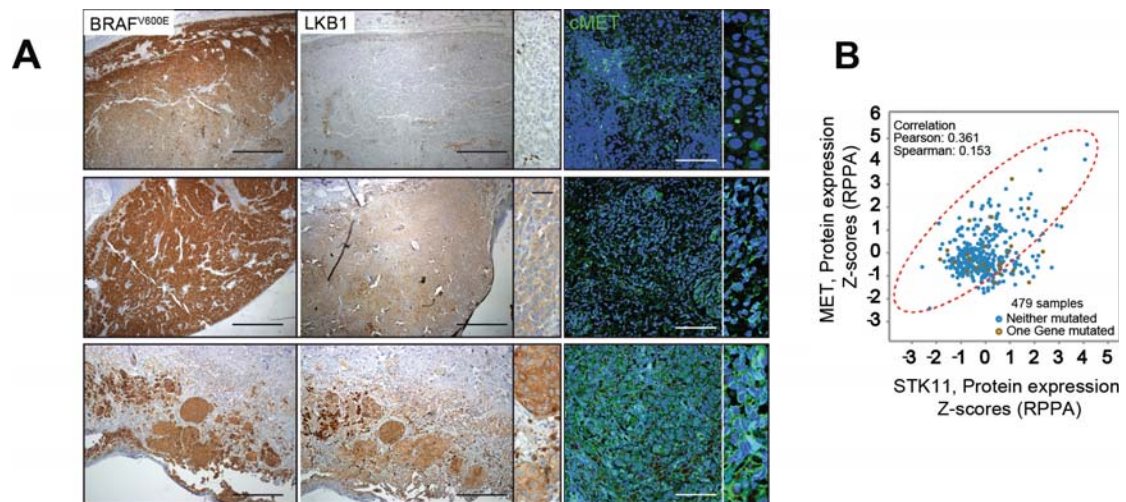


**Figure 22: cMET protein expression shows a positive correlation with the LKB1 levels in human melanoma tumors. (A)** Immunohistochemistry and immunofluorescence panel showing three different LKB1 expression levels, together with its correspondent levels of BRAF<sup>V600E</sup> and cMET. **(B)** Correlation between the cMET and LKB1 expression in human tumors. Blue dots indicates sample in which none LKB1 nor cMET present any mutation. The brown dots, at least one of these proteins are mutated. Data extracted from the Skin Cutaneous Melanoma (TCGA, Provisional) data set. Insets show a magnification of cells. Scale Bars, 500µm and 50µm.

### 12. Genetic profiling of mouse tumors unveils alterations in extracellular matrix interactions, neural differentiation and Rho-signaling pathways

To gain further insights about the mutations contributing to UV-induced melanomagenesis in our model we performed Whole Exome Sequencing (WES) in eight tumors (three spontaneous tumors and five UVB-induced tumors) with different genetic background (

Table 2). Despite the few tumors sequenced and knowing that this data does not offer statistically relevant results, we aimed to investigate the different genetic alterations and altered pathways present in these tumors upon UVR. Furthermore, only one non-irradiated *Braf*<sup>V600E</sup>-mutated tumor was observed in an old animal. The WES data from this animal model was used to study the contribution of UVR and *Lkb1*-depletion in a *Braf*<sup>V600E</sup>-mutated context.

**Table 2: General mice information from the Whole Exome-sequenced tumors.** Basic information from mice: animal ID, genotype, acronym and type of carcinogen.

Animal ID	Genotype	Acronym	Carcinogen
B12-225	<i>Tyr::CreER<sup>T2</sup>;Braf<sup>CA/+</sup></i>	B	Spontaneous
B12-226	<i>Tyr::CreER<sup>T2</sup>;Braf<sup>CA/+</sup>;Lkb1<sup>+/-</sup></i>	B/L	Spontaneous
B12-227	<i>Tyr::CreER<sup>T2</sup>;Braf<sup>CA/+</sup>;Lkb1<sup>+/-</sup></i>	B/L	Spontaneous
B12-213	<i>Tyr::CreER<sup>T2</sup>;Braf<sup>CA/+</sup></i>	B/UV	UVB
B12-214	<i>Tyr::CreER<sup>T2</sup>;Braf<sup>CA/+</sup></i>	B/UV	UVB
B12-218	<i>Tyr::CreER<sup>T2</sup>;Braf<sup>CA/+</sup></i>	B/UV	UVB
B12-223	<i>Tyr::CreER<sup>T2</sup>;Braf<sup>CA/+</sup>;Lkb1<sup>+/-</sup></i>	B/L/UV	UVB
B12-228	<i>Tyr::CreER<sup>T2</sup>;Braf<sup>CA/+</sup>;Lkb1<sup>+/-</sup></i>	B/L/UV	UVB

The whole exome sequencing analysis indicated the diverse genetic alterations found in the different animal genotypes with or without UVR-exposure (Table 3). Non-synonymous single nucleotide variants (SNVs) were the most common genomic alteration detected in all animal groups. The lack of *Lkb1* increased the proportion of stop gain alterations, while the exclusive presence of *Braf*<sup>V600E</sup> promoted the non-frameshift insertions.

**Table 3: Percentage of the different genetic alterations found in the B/L/UV model with the diverse genotypes with or without UVB-irradiation.** Percentage of frameshift deletions, non-frameshift insertions, non-synonymous single nucleotide variants, stop gain and stop loss found in the non-irradiated and irradiated *Tyr::CreER<sup>T2</sup>Braf<sup>CA</sup>* or *Tyr::CreER<sup>T2</sup>;Braf<sup>CA</sup>;Lkb1<sup>+/-</sup>* animals.

Mutation Type	<i>Braf<sup>CA/+</sup></i> +	<i>Braf<sup>CA/+</sup>;Lkb1<sup>+/-</sup></i>	<i>Braf<sup>CA/+</sup></i> + +UVB	<i>Braf<sup>CA/+</sup>;Lkb1<sup>+/-</sup></i> +UVB
Frameshift deletions	0,71	0,47	0,56	0,58
Non-frameshift insertions	1,06	0,24	1,27	0,00
Non-synonymous variants	95,41	95,04	95,91	94,02
Stop gain	2,83	4,26	2,26	5,21
Stop loss	0,00	0,00	0,00	0,19

As expected, the comparison between irradiated and non-irradiated mice tumors revealed the increment in the percentage of C to T transition, known as “UV-signature”, in the



UVB-exposed animals. *Lkb1*-depleted tumors increased  $\approx 6\%$  this nucleotide exchange, suggesting that *Lkb1* haploinsufficiency promoted the acquisition of UVB-induced genetic alterations (Figure 23).

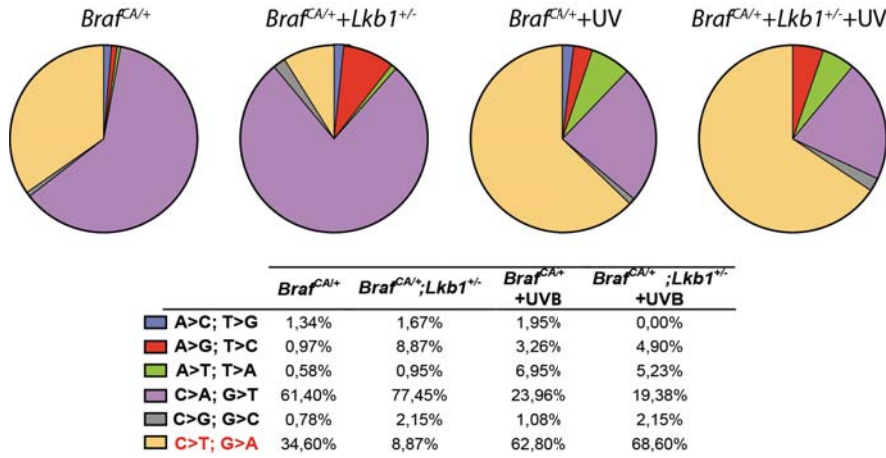


**Figure 23: UVR increased the “UV-signature” in the B/L/UV tumors, independently of their genetic background.** At the top, part of a whole graphs indicate the different transversion and transition modifications detected in the different tumors. At the lower part, corresponding percentages from the different nucleotides changes are shown in the table depending of the genotype of the animal. In the legend is highlighted in red the “UV-signature”.

Next, we analyzed which gene families were affected. To this aim, we used Broad Institute GSEA-MSigDB software that offers gene family classification of the mutated genes found in the different animal groups (Table 4). Analyzing irradiated and non-irradiated groups, mutated genes belonged to: oncogene, protein kinases, cell differentiation markers and transcription factors gene families. When we compared the irradiated and non-irradiated tumors from *Tyr::CreERT<sup>2</sup>;Braf<sup>CA/+</sup>;Lkb1<sup>+/-</sup>* animals, we observed that the UVR highly increased the percentage of altered genes in all affected families.

**Table 4: Percentage of affected gene families in the B/L/UV model.** Classification of the gene families found in the different non-irradiated and irradiated *Tyr::CreERT<sup>2</sup>;Braf<sup>CA/+</sup>* or *Tyr::CreERT<sup>2</sup>;Braf<sup>CA/+</sup>;Lkb1<sup>+/-</sup>* animals. The main families found were: tumor suppressors, oncogenes, protein kinases, cell differentiation markers, transcription markers, homeodomain proteins, cytokines and growth factors and translocated cancer genes. Analysis performed in GSEA-MSIGDB software. For detailed information see appendix tables from 1 to 4.

	<i>Tyr::CreERT<sup>2</sup>; Braf<sup>CA/+</sup></i>	<i>Tyr::CreERT<sup>2</sup>; Braf<sup>CA/+</sup> +UVB</i>	<i>Tyr::CreERT<sup>2</sup>; Braf<sup>CA/+</sup>;Lkb1<sup>+/-</sup></i>	<i>Tyr::CreERT<sup>2</sup>; Braf<sup>CA/+</sup>; Lkb1<sup>+/-</sup> +UVB</i>
Tumor Suppressor	0,0	0,8	0,2	0,4
Oncogenes	2,5	1,5	0,5	1,7
Protein kinases	4,5	3,8	1,2	6,1
Cell diff markers	1,5	3,1	1,0	3,0
Transcription factors	3,0	4,2	1,3	8,7
Homeodomain Proteins	0,0	0,4	0,1	0,9
Cytokine and growth factors	0,5	0,8	0,2	2,6
Translocated	2,5	1,9	0,6	1,3

Comparison of unique mutated genes between irradiated and non-irradiated *Tyr::CreER<sup>T2</sup>;Braf<sup>ΔA/+</sup>* tumors showed only 7 common genes between both groups (*Rps6ka6*, *Dnab8*, *Epha6*, *Ccdc22*, *Cilp*, *Col6a5*, and *Rims2*). These genes are related with the regulation of: synaptic vesicles, the MAPK signaling, and DNA damage signaling through p53, among other biological processes. To gain insight into the biological function of the irradiated and non-irradiated mutated genes in these melanomas, we used Kyoto Encyclopedia of Genes and Genomes (KEGG), Reactome and Biocarta databases from 2016. To focus in relevant biological processes, we considered those significantly affected ( $p$ -value $<0,05$ ), analyzing the unique mutated genes in both groups. The analysis of the 323 genes altered in the UVB-irradiated *Tyr::CreER<sup>T2</sup>;Braf<sup>ΔA/+</sup>* tumors were significantly associated with many cancer-related signaling pathways such as, extracellular matrix interactions, induction of hypoxia inducible factor gene expression and Rho-signaling, involved in cytoskeletal dynamics and cell movement and a surrogate marker for mTORC2 activity. Other relevant biological processes affected included focal adhesion and immune system regulation (Figure 24A).

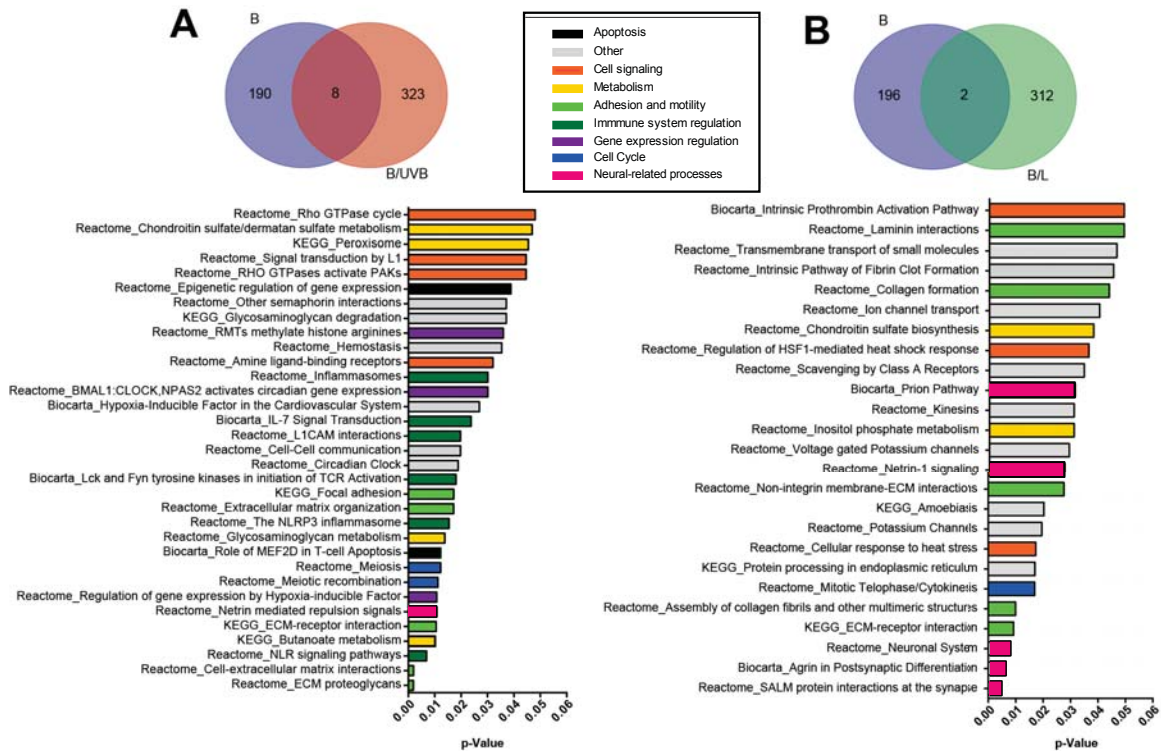


**Figure 24: UVB- and LKB1 loss-induced different mutations that affect diverse biological processes in *Braf<sup>ΔA/+</sup>*-context. (A) Venn diagram comparing non UVB-irradiated *Tyr::CreER<sup>T2</sup>;Braf<sup>ΔA/+</sup>* tumors (B) (blue, n = 1) and UVB-irradiated *Tyr::CreER<sup>T2</sup>;Braf<sup>ΔA/+</sup>* tumors (B/UV) (red, n = 3). In the lower part, there are the significant Homo sapiens pathways and biological processes affected by the 323 genes altered in UVB-irradiated tumors. (B) Venn diagram comparing non UVB-irradiated *Tyr::CreER<sup>T2</sup>;Braf<sup>ΔA/+</sup>* tumors (B) (blue, n = 1) and *Tyr::CreER<sup>T2</sup>;Braf<sup>ΔA/+</sup>;Lkb1<sup>+/-</sup>* tumors (B/L) (green, n = 2). At the bottom, there are the significant Homo sapiens pathways and biological processes affected by the 312 genes altered with *Lkb1*-loss. Biological processes classified in different groups by column color, see legend. For further detail of the Venn diagram genes see see **Appendix Figure 5** and **Appendix Figure 6**, respectively.**

Similar approach was performed between *Tyr::CreER<sup>T2</sup>;Braf<sup>ΔA/+</sup>* and *Tyr::CreER<sup>T2</sup>;Braf<sup>ΔA/+</sup>;Lkb1<sup>+/-</sup>*. This list comparison highlighted mutated genes and biological processes altered upon *Lkb1* haploinsufficiency. Interestingly, tumors lacking of one copy of *Lkb1* harbored similar number of mutations than tumors UVB-irradiated, suggesting the involvement of LKB1 in genetic instability. Both groups shared only 2 genes *Ehmt1* and *Lrig3*. While *Ehmt1* is a histone methyltransferase contributing to silencing of MYC- and E2F-responsive genes in G0 and regulating p53 activity (85), *Lrig3* has been involved in the control of Netrin-1, involved in axon guidance and regulation of apoptosis in tumorigenesis (Figure 24B). The biological processes significantly altered by the 312 genes altered with the *Lkb1* loss included: cell signaling, cell adhesion, and motility. This result is in agreement with previously published data, where cell polarity is one of the known biological functions of LKB1 (52). Interestingly, the most significant biological processes altered were related with the neuronal system. This result correlates with the increased frequency of neural melanoma observed in *Lkb1* deficient tumors. Moreover, Netrin-1 signaling, involved in mediating axonal guidance and survival preventing apoptosis of tumor cells, is also altered in this group, supporting the above results.

When we compared the set of genes expressed in the UVB-irradiated *Tyr::CreER<sup>T2</sup>;Braf<sup>ΔA/+</sup>* tumors versus the non-irradiated *Tyr::CreER<sup>T2</sup>;Braf<sup>ΔA/+</sup>;Lkb1<sup>+/-</sup>* tumors, we observed that UVR and lack of *Lkb1* expression targeted different genes and biological processes (Figure 24A,B). While UVR promoted the cancer-related biological processes, the lack of *Lkb1* induced neural-related processes. These two lists of genes share only 7 genes, which are involved in the focal adhesion (*Tbbs4*, *Csmd2*, *Fat4*, *Scn2a1*, *Lrp4*, *Ice2*, and *Cep350*) (Appendix Figure 3). The ECM-receptor interaction appeared as the unique common biological process shared between these two groups.

Next we investigated the genetic alterations targeted in the UVB-irradiated and non-irradiated *Tyr::CreER<sup>T2</sup>;Braf<sup>ΔA/+</sup>;Lkb1<sup>+/-</sup>* tumors (Figure 25A). This comparison revealed that there were 13 common genes (*Shroom2*, *Ip6k3*, *Phex*, *Mga*, *Itih2*, *Cic*, *Bcorl1*, *Csmd2*, *Kmt2d*, *Mlph*, *Plec*, *Evc2*, and *Cep350*). Interestingly, these genes were related significantly with the melanosome localization and the estrogen receptor signaling. To focus on the relevant UVB-altered biological process upon *Lkb1* haploinsufficiency, common processes shared between these two groups were subtracted. Again, the analysis showed that *Lkb1* lack promoted the neural-related processes upon UVB-exposure (Figure 25A).

Finally, we wondered whether UVB-targeted genes and pathways were similar in tumors either expressing *Lkb1* or lacking *Lkb1* expression, for this reason we compared data from both, irradiated *Tyr::CreER<sup>T2</sup>;Braf<sup>ΔA/+</sup>* and *Tyr::CreER<sup>T2</sup>;Braf<sup>ΔA/+</sup>;Lkb1<sup>+/-</sup>* tumors (Figure 25B). These groups shared 19 genes (*Cyp11b2*, *Capn8*, *Tnn*, *Dnab10*, *Csmd2*, *Hkdc1*, *Nos3*, *Pcdhb18*, *Clstn2*, *Ndst3*, *Ccdc185*, *Trpv4*, *Oosp3*, *Naip7*, *Flna*, *Magee1*, *Mnd1*, *Dnab1*, and *Cep350*). As common biological processes shared between both groups stood out the Rho-signaling and biological processes such as, axon guidance, extracellular matrix

organization and focal adhesion. In the 312 genes altered in the irradiated *Tyr::CreER<sup>T2</sup>;Braf<sup>C4/+</sup>* lesions, as mentioned before, it was affected cancer-related signaling pathways such as, inflammasome, hypoxia inducible factor gene expression and Rho-signaling. Focusing in the 316 genes altered in UVB-irradiated LKB1-haploinsufficient melanomas, we observed an enrichment in Rho-signaling pathway, as well as in cell adhesion and contractility, gene expression, cell division and proliferation biological processes, which were in agreement with previously reported data (49).

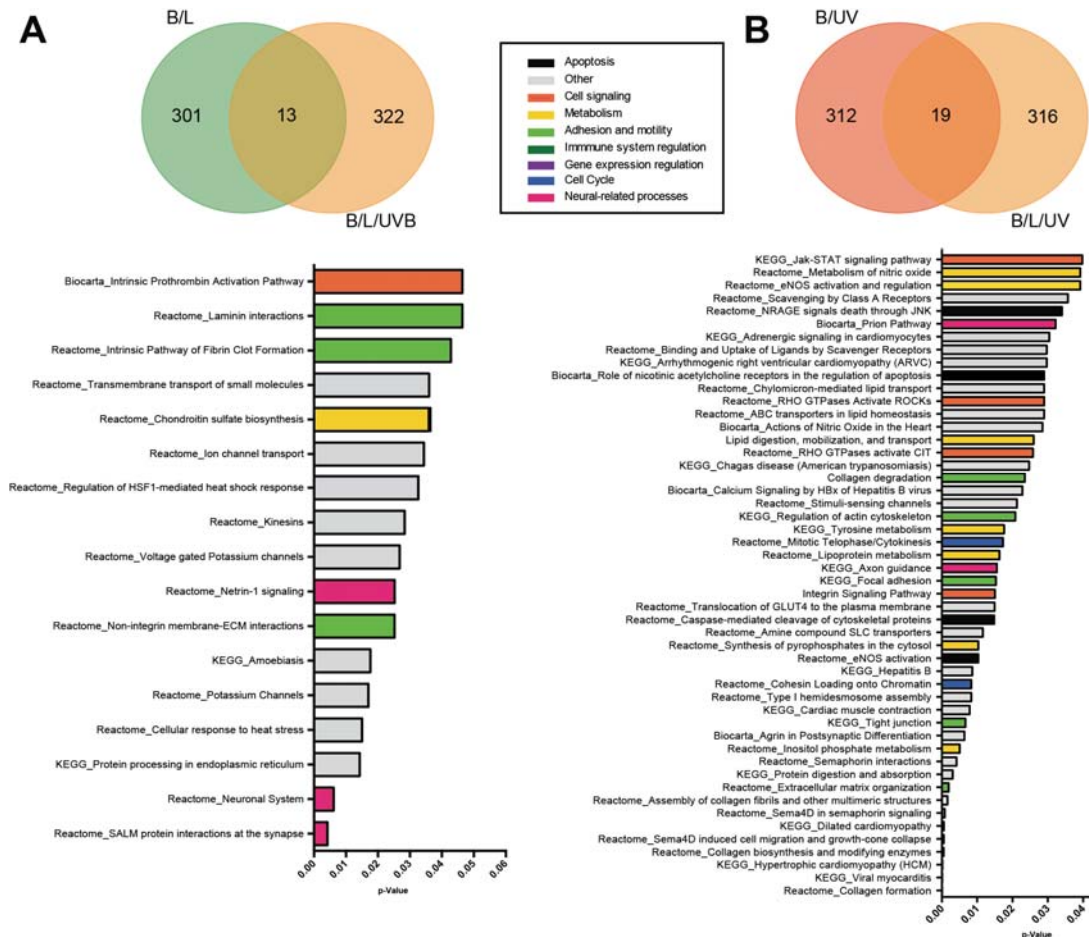


**Figure 25: Loss of *Lkb1* in the B/L/UV animal increased the number of mutation and altered different biological processes. (A)** Venn diagram comparing non UVB-irradiated and UVB-irradiated *Tyr::CreER<sup>T2</sup>;Braf<sup>C4/+</sup>;Lkb1<sup>+/-</sup>* tumors (B/L (green, n = 2) versus B/L/UV (orange, n = 2)). At the bottom, there are the significant Homo sapiens pathways affected by the 322 UVB-induced mutated genes. **(B)** Venn diagram comparing UVB-irradiated *Tyr::CreER<sup>T2</sup>;Braf<sup>C4/+</sup>* (B/UV) (red, n = 3) and *Tyr::CreER<sup>T2</sup>;Braf<sup>C4/+</sup>;Lkb1<sup>+/-</sup>* (B/L/UV) (orange, n = 2) lesions. In the lower part, there are the significant Homo sapiens pathways affected by 316 UVB-induced mutated genes. Biological processes classified in different groups by column color, see legend. For further detail of the Venn diagram genes see **Appendix Table 7** and **Appendix Table 8**, respectively.

Thus, the results showed that *Lkb1* haploinsufficiency promoted the selection of mutated genes affecting to biological pathways related with neural processes. This data correlates and provides evidence for the phenotypic characteristics observed in *Lkb1* deficient tumors. In this matter, Netrin-1 and Rho-signaling pathways appeared as significantly altered pathways in the B/L/UV animal model, stressing the relevant role of this pathways melanoma progression.



### 13. B/L/UV animal tumors harbor mutations found in similar animal models and the human disease

Recently, two different groups have generated two inducible animal models based on *Braf*<sup>V600E</sup> expression, describing relevant genetic alterations related with melanoma progression. The first study was generated by Dr. Marais' laboratory, using the previously described mouse model (from now on RM/B/UV model) (76). This group showed how UVR accelerates *Braf*<sup>V600E</sup>-nevi progression into melanoma cooperating with TP53. In this case, 2 months old animals were 4OHTx-treated to activate *Braf*<sup>V600E</sup> expression, which promotes naevogenesis. One, month later, animals were chronically irradiated for 6 additional months. This experimental design, in contrast with ours, was specifically designed to unveil genes involved in melanoma progression from nevi lesions harboring *Braf*<sup>V600E</sup> mutation upon intermittent chronic irradiation. Using the second animal model from Dr. Jenkins' laboratory, it was identified tumor suppressor genes that cooperate with *Braf*<sup>V600E</sup> in melanomagenesis. This is a mouse model inducible for *Braf*<sup>V600E</sup> and Sleeping Beauty transposon concomitant expression after birth (from now on B/SB model) (78).

In order to know which genes were relevant in melanoma progression in the B/L/UV model, we selected the mutated genes observed in more than one animal with a variant allele frequency  $\geq 20\%$ , a total of 65 genes were chosen (Table 5). Approximately, 28% of these set of genes had  $>50\%$  allele frequency in tumors (*Abca5*, *Abcc6*, *Abhd6*, *Acox2*, *Dbx1*, *Dhdb*, *Endou*, *Esp11*, *Fbn2*, *Fhit*, *Fuz*, *Krt82*, *Lmtk3*, *Pced1b*, *Top2b*, *Trerf1*, *Tsr1*, and *Vdr*) (Table 5). Then, this gene set was classified in respect to the type of sample, either: UV-irradiated or *Lkb1* deficient. To underscore the relevance of these genes in the human disease, we confirmed their mutational status at the provisional Human Skin Cutaneous Melanoma TCGA data set. Those genes, not genetically altered in the human disease, were discarded for further analysis (*Car6*, *Zfp641*, *Naip7*, and *Pramel6*). Remarkably,  $\approx 17\%$  of this gene collection was also found in the previously mentioned *Braf*<sup>V600E</sup>-mutated animal models (*Fhit*, *Flna*, *Grid2*, *Slc11a2*, *Top2b*, *Map3k1*, *Trerf1*, *Wdfy4*, *Zan*, *Cep350*, and *Flnb*).

**Table 5: More relevant genes altered in the B/L/UV model.** Genes altered in more than one B/L/UV animal and with  $\geq 20\%$  of variant allele frequency in the tumor. In this table is indicated: Gene ID, percentage of mutation in TCGA database, and its presence in the WES data from RM/B/UV and SB/B models. In red, it is represented the genes affected exclusively in UV-irradiated animals. In blue, it is depicted the genes affected exclusively in animals non-irradiated animals. In brown, it is shown the genes affected irradiated and non-irradiated animals. <sup>1</sup> Mutation found in  $\geq 50\%$  of variant allele frequency in the tumor. <sup>2</sup> Alterations of this gene does not overlap with BRAF alterations in human Skin Cutaneous Melanoma TCGA data set.

GENE ID	TCGA (%)	RM/B/UV	B/SB	GENE ID	TCGA (%)	RM/B/UV	B/SB
<i>Abca9</i> <sup>1</sup>	9			<i>Casr</i>	16		
<i>Abcc6</i> <sup>1</sup>	11			<i>Ccdc22</i>	0.7		

<i>Abhd6</i> <sup>1</sup>	2.1				<i>Cep350</i>	10	X	X
<i>Acox2</i> <sup>1</sup>	3				<i>Cilp</i>	8		
<i>Actr8</i>	1.7				<i>Ctnnap4</i>	14		
<i>Acvrl1</i>	5				<i>Col2a1</i>	14		
<i>Ambr2</i>	5				<i>Cpt1c</i>	6		
<i>Cers5</i>	2.1				<i>Dbx1</i> <sup>1</sup>	2.8		
<i>Csmdb2</i>	34				<i>Dbdb</i> <sup>1</sup>	1.4		
<i>Csrnp2</i>	1.4				<i>Endou</i> <sup>1</sup>	2.1		
<i>Dnab1</i>	77				<i>Evc2</i>	7		
<i>Dnab10</i>	24				<i>Flnb</i>	13		X
<i>Espl1</i> <sup>1</sup>	5				<i>Fn3k</i>	4		
<i>Fbn2</i> <sup>1</sup>	12				<i>Fuz</i> <sup>1</sup>	0.7		
<i>Fhit</i> <sup>1</sup>	2.4		X		<i>Hsd17b14</i>	1		
<i>Flna</i>	8	X		X	<i>Kif27</i>	4		
<i>Grid2</i>	19			X	<i>Lmtk3</i> <sup>1</sup>	6		
<i>Krt2</i>	6				<i>Mon1b</i>	2.4		
<i>Krt82</i> <sup>1</sup>	2.4				<i>Nudt7</i>	1.7		
<i>Letmd1</i>	1				<i>Pced1b</i> <sup>1</sup>	11		
<i>Magee1</i>	6				<i>Pla2r1</i>	9		
<i>Pcdhb18</i> <sup>2</sup>	0.7				<i>Rpap3</i>	3		
<i>Slc11a2</i>	1		X		<i>Scaf1</i>	6		
<i>Sntn</i>	2.1				<i>Senp1</i>	4		
<i>Top2b</i> <sup>1</sup>	4			X	<i>Slc38a1</i>	7		
<i>Adamts18</i>	17				<i>Srpx</i>	2.1		
<i>Eml3</i>	2.4				<i>Tbcd</i>	6		
<i>Map3k1</i>	2.1	X		X	<i>Thrb</i>	7		
<i>Trerf1</i> <sup>1</sup>	14			X	<i>Tmbim4</i>	1.7		
<i>Wdfy4</i>	1.7	X			<i>Tsr1</i> <sup>1</sup>	1.7		
<i>Zan</i>	18	X		X	<i>Vdr</i> <sup>1</sup>	2.8		
<i>Abca5</i>	7							

The independent study of each gene from cited selection revealed its implications in important biological processes disturbed in cancer and in melanoma in particular. Around 12% of these genes are related with DNA-processing (*Scaf1*, *Tsr1*, *Vdr*, *Rpap3*, *Thrb*, *Actr8*, *Top2b*, and *Trerf1*), or lipid metabolism (*Abca9*, *Abhd6*, *Acox2*, *Cers5*, *Abca5*, *Casr*, and *Cpt1c*). Apoptosis is another relevant cancer-associated process represented with a  $\approx 8\%$  of these gene set (*Csrnp2*, *Espl1*, *Senp1*, *Tmbim4* and *Fhit*). Near 5% of genes were related with the MAPK- (*Map3k1*, *Pla2r1*, and *Srpx*), TGF $\beta$ - (*Acvrl1*, *Ambr2*, and *Cilp*) and p53- (*Letmd1*, *Magee1*, and *Fhit*) signaling pathways. In lesser extend other signaling pathways were represented in this gene selection as PKC-AKT-FOXO3 pathway (*Lmtk3*) and NF $\kappa$ B signaling (*Ccdc22*). As expected due to the important role of *Lkb1* in polarization, the cytoskeleton organization and cell motility were also heavily represented in this gene set with almost 20% of the total genes (*Pcdhb18*, *Ctnnap4*, *Fbn2*, *Dnab1*, *Dnab10*, *Zan*, *Krt2*, *Sntn*, *Flna*, *Eml3*, *Col2a1*, *Cep350*, and *Flnb*) (Table 5).

Interestingly, some of the mutated genes from this collection presented the same point mutations detected in human melanomas (Appendix Table 10). These mutations affected to *Grid2* and *Thrb* genes; specifically, the mutations were GRID2<sup>E852K</sup>, GRID2<sup>G735R</sup>, THRB<sup>E203K</sup>, and THRB<sup>E217K</sup>. On the other hand, same point mutations from this gene set were found in other human cancer studies, such as EVC2<sup>R697C</sup> in liver hepatocellular



carcinoma, MAP3K1<sup>P484S</sup> in glioblastoma multiforme, and PCDHB18<sup>D595N</sup> lung adenocarcinoma (Appendix Table 10). This data reinforce further the relevance of the B/L/UV model in the recapitulation of the human disease.

To further explore the potential interaction network among genes from Table 5, we searched for its functional protein association networks. To this aim, we used the online STRING (Search Tool for the Retrieval of Interacting Genes/Proteins) biological database of known and predicted protein-protein interaction. Approximately 34% of these selected genes shown interaction between them (Figure 26). These results suggested that our model enriches for mutations affecting functionally interacting proteins.

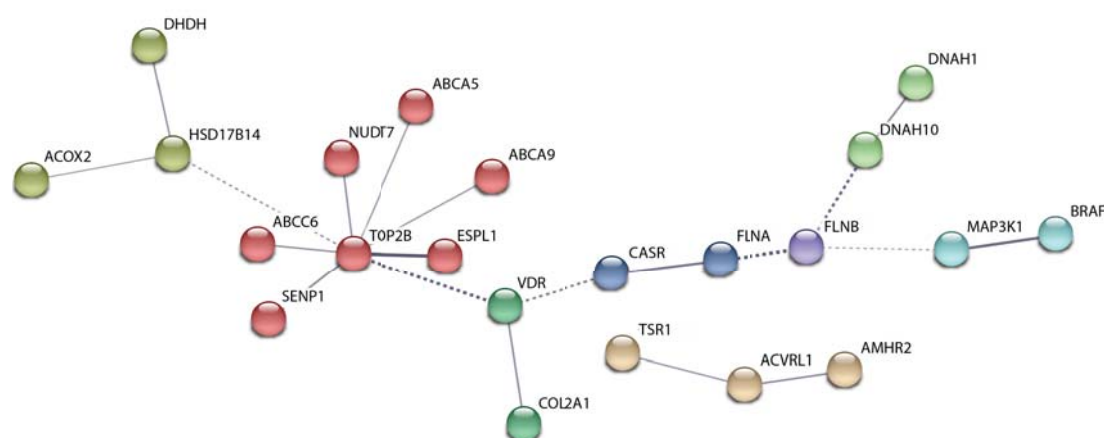


**Figure 26: Functional network from the most relevant B/L/UV genes.** Graphic interaction representation of genes from Table 5 using all active interaction sources available at STRING with a minimum required confidence of 0.4. The edge thickness indicates the confidence from the interactions, the thickest represent 0.9 confidence and the medium 0.7. Discontinuous lines indicate the cluster binding. Genes were clustered following the MCL clustering system.

In addition to this, recent publications, showed that telomerase promoter mutations have been found in  $\approx 75\%$  of BRAF-mutated melanoma subtype (76). We sequenced the *Tert* promoter region of all tumor samples, however, we did not find any mutation in this specific genomic region (data not shown). Nevertheless, mutations in the *Nfix1* gene, a transcriptional repressor that regulates *TERT* promoter (86), were found with 41.27% allele frequency in a single animal. On the other hand, WNT and JNK pathways have been related to melanomagenesis (87). In our model, a single animal harbored mutations in the *MDFI* gene with 40% of allele frequency, which is involved in the axis regulation of both signaling pathways.

Altogether, our data highlights a network of deregulated pathways that contribute to melanomagenesis in the B/L/UV animal model, which appear to have an effect also in the progression of the human disease.

#### 14. MAPK-, TNF $\alpha$ , NF $\kappa$ B, and p38-signaling pathways are key in *Braf*<sup>V600E</sup>-mediated melanoma progression

Since WES data from RM/B/UV and B/SB animal models were available, we compared them with our own results to extract the most relevant biological requirements for melanoma progression (Figure 27). The comparison between the three different animal models elucidated the common genes, revealing key *Braf*<sup>V600E</sup>-mediated biological processes involved in melanomagenesis. These 7 shared genes were: *Syne1*, *Flna*, *Cep350*, *Zan*, *Csmd3*, *Map3k1*, and *Dmd*. Through WikiPath2016 analysis, it was observed that they are involved significantly in MAPK-, TNF $\alpha$ , NF $\kappa$ B, and p38-signaling pathways.

Interestingly when we compared our list of unique mutated genes with the ones from the B/SB model, we found 85 common genes ( $\approx 7.5\%$ ), which we classified into different families using the GSEA-MSigDB database. The most relevant were: transcription factors (*Elf1*, *Ep300*, *Epas1*, *Ncoa1*, *Smarcc1*, *Tsc22d2*, *Tulp4*, and *Zfx*), protein kinases (*Braf*, *Epha6*, *Map3k1*, *Mark2*, *Mkl1*, and *Trpm7*), translocated cancer genes (*Braf*, *Ep300*, *Lpp*, *Ncoa1*, and *Nsd1*), and oncogenes (*Braf*, *Lpp*, *Ncoa1*, *Nsd1*, and *Ptpn11*). However, the tumor suppressor family, the most frequent in the B/SB animal model, we only shared 2 genes (*Ep300* and *Tet*). A possible explanation for the reduced number of tumor suppressor genes could be that GSEA-MSigDB dataset is limited to 82 genes. Through an analysis of these common genes with the B/SB in the WikiPath2016, we could conclude that they are significantly involved in the TNF $\alpha$ , NF $\kappa$ B, EGF/EGFR, and MAPK-signaling pathway.

Then, we compared our list of unique mutated genes with published genes altered in the RM/B/UV animal model (only 31 genes) (35), it was remarkable that 11 out of the 31 published genes (35%) were also mutated in our model. This common gene set comprises: *Cep350*, *Csmd3*, *Dmd*, *Flna*, *Map3k1*, *Obscn*, *Pclo*, *Syne1*, *Ttn*, *Wdfy4*, and *Zan*, which were involved also in MAPK, TNF $\alpha$ , NF $\kappa$ B and p38-signaling pathways.

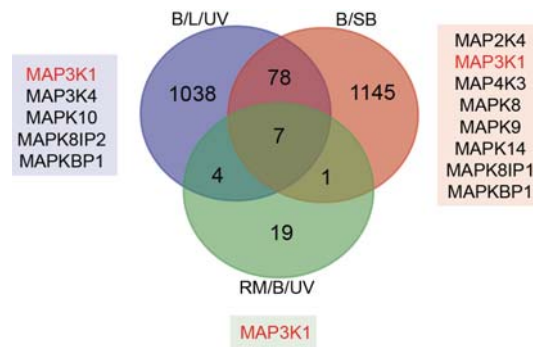


**Figure 27: WES gene comparison from B/L/UV, B/SB, and RM/B/UV models.** All unique mutations found in our B/L/UV animal model (1,127 total mutations, blue). B/SB correspond with all the common transposon internal sites (1,231 total mutations, red). RM/B/UV resemble all published genes altered in the Richard Marais' model (31 total mutations, green). In the boxes SAPK/JNK genes altered in each animal model. To see common genes shared between the different animal models see **Appendix Table 9**.

As stated in the literature, the MAPK signaling is composed of three major groups: the extracellular regulated kinases (ERKs), the c-Jun N-terminal kinases (JNKs), and the p38 MAPKs (78). In melanoma, all three axes are mutated. Interestingly, we found that several components of the SAPK/JNK signaling pathways were altered at different levels of the pathway in all three animal models (Figure 27). This suggested a relation between the MAPK-signaling pathways ( $BRAF^{V600E}$ ) and the SAPK/JNK pathway.

Collectively, these results suggested that SAPK/JNK signaling pathway should be further evaluated in human melanoma. To that end, all the components of this pathway were analyzed in the provisional human Skin Cutaneous Melanoma TCGA data set (n = 287 patients) (Figure 28). The analysis showed that in human melanoma there were clear transcriptional alterations in several components of the SAPK/JNK pathway, independently of BRAF mutational status. A more detailed analysis of this data showed that the mutational pattern affects at different levels of the pathway. Thus, integration of the alteration frequencies of the different component of the SAPK/JNK pathway showed that more than 50% of human melanomas harbor genetic alterations in one or more members of this pathway.

Indeed, *MAPK14* mRNA, that encodes for p38 $\alpha$ , was mainly upregulated in 35% of the human samples. This high percentage reveals that this protein might play an important role in MAPK-driven melanomagenesis. On the other hand, some components of the stress pathway seemed to exhibit an mRNA downregulation landscape. That was the case for *MAP3K7*, *MAP2K4*, *MAP2K7*, *MAPK8* and *MAPK9* genes, which were altered in the 23%, 26%, 19%, 16%, and 28% of human samples, respectively (TCGA database).

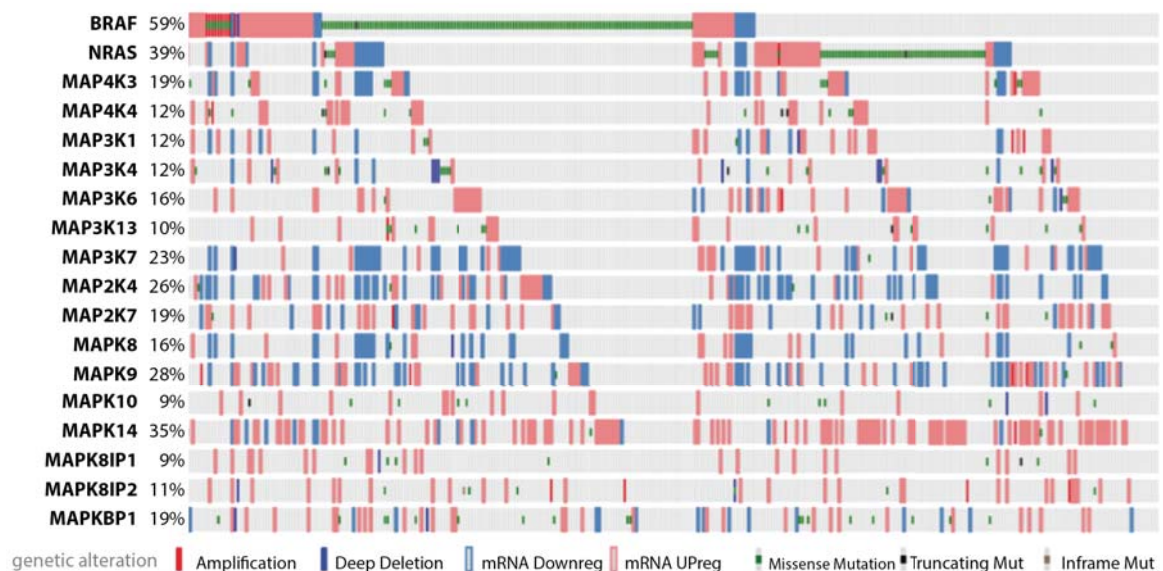


**Figure 28: Mutational status of the SAPK/JNK pathway components in human Skin Cutaneous Melanoma (TCGA, provisional) data set.** Data obtained from the cBioPortal in which it could be seen the genomic alterations detected in 287 human Skin Cutaneous melanomas. Percentage of genetic alterations found for the following genes: *BRAF*, *NRAS*, *MAP4K3*, *MAP4K1*, *MAP3K4*, *MAP3K6*,

*MAP3K13*, *MAP3K7*, *MAP2K4*, *MAP2K7*, *MAPK8*, *MAPK9*, *MAPK10*, *MAPK14*, *MAPK8IP1*, *MAPK8IP2*, and *MAPKBP1*. The genetic alterations detected are: amplification, deep deletion, mRNA downregulation, mRNA upregulation, missense mutation, truncating mutation, and in frame mutation.

Next, we investigated whether the protein amount status of the SAPK/JNK pathway components in human melanoma correlated with the mRNA expression data. To this aim, we mined the data available in The Human Protein Atlas database (Figure 29). As expected, MAPK14 protein level experimented an increase if compared with normal tissue, which correlated with the mRNA amplification presented in the TCGA database. Also, MAP3K7, MAP2K4, and MAPK9 protein data correlated with the genomic alteration information, showing a decrease in protein level in melanoma. The only exception was the MAPK8, where 55% of samples showed a slight increase in the protein staining, while showing a global mRNA downregulation in the TCGA dataset.

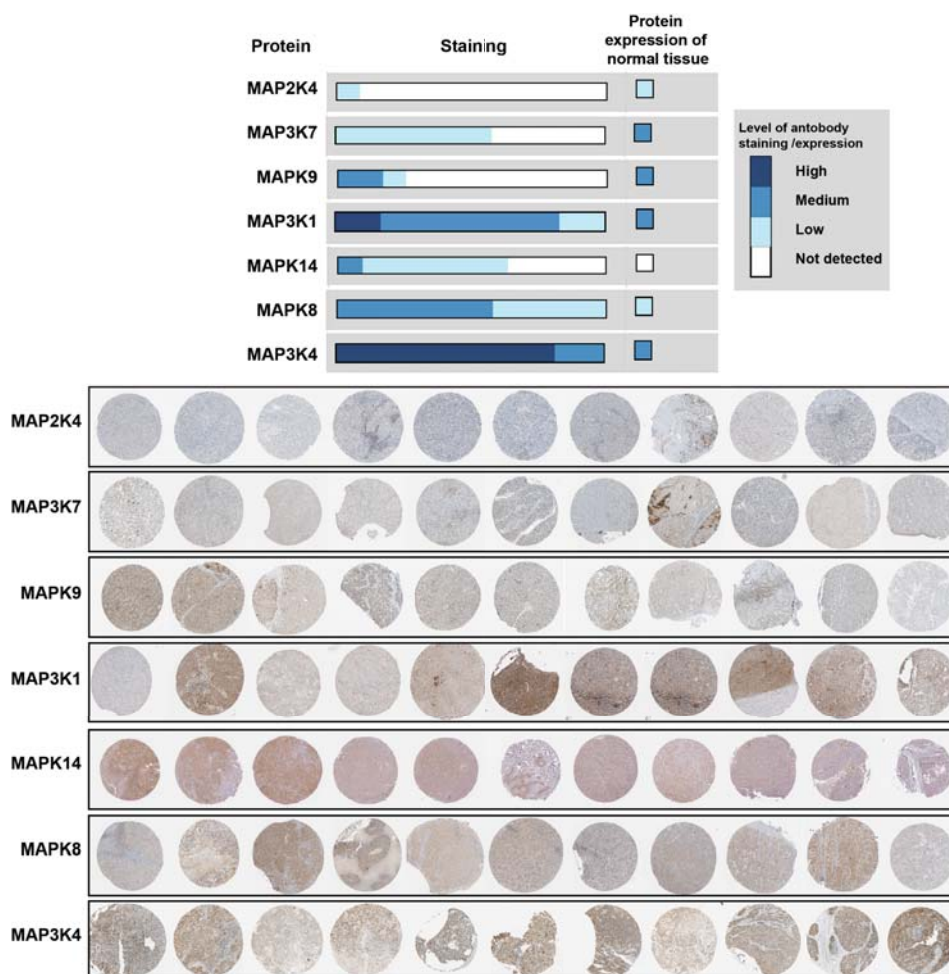


**Figure 29: Protein expression of SAPK/JNK pathway components in human melanoma samples.** This data was extracted from The Human Protein Atlas database Upper panel, graphic representation of the SAPK/JNK components that indicates the levels of protein detected in human melanomas and normal tissue. Lower panel, immunohistochemistry compilation from melanoma samples stained for: MAPK8 (CAB004463 antibody clone), MAPK9, MAPK14 (CAB040578 antibody clone), MAP2K4, MAP3K1, MAP3K4, and the MAP3K7.

Thus, the comparative analysis of B/L/UV-altered genes together with the data from B/SB and RM/B/UV mouse models has emphasized an important connection between



the MAPK- and SAPK/JNK-signaling pathways in melanomagenesis. Moreover, the study of human stress-activated pathway components status revealed that they are also altered at genomic and protein level in the human pathogenesis. Altogether, these results strength the data derived from our B/L/UV model that recapitulates important biological features observed in similar melanoma mouse models and the human disease.

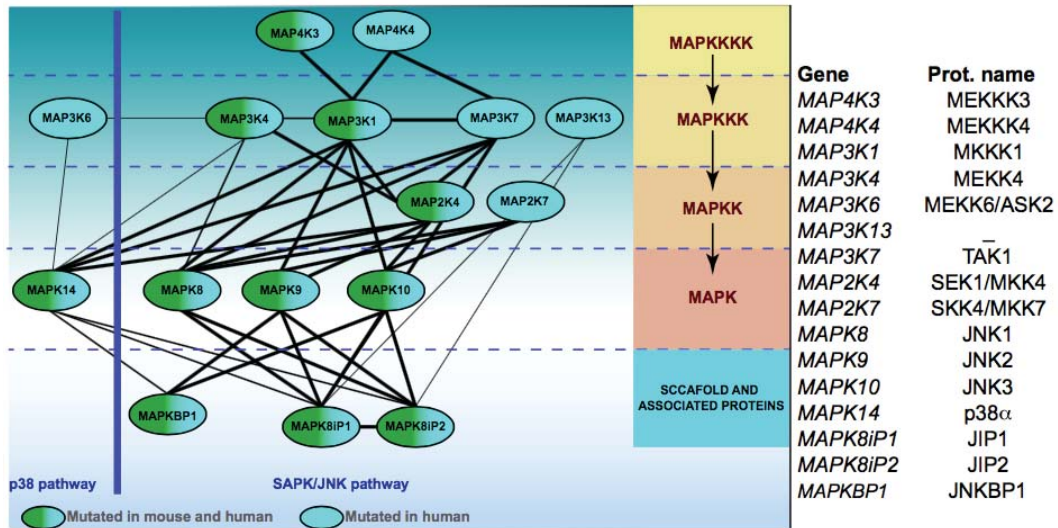


**Figure 30: Components of the p38- and SAPK/JNK-signaling pathway harbor mutation in the human and mice melanomas.** In the left side, it is represented the canonical structure of the signaling pathways, including the scaffold and the associated proteins. Extracellular stimuli activate the MAP3K through cell surface receptors and intracellular mediators (not shown). The signal is transduced to MAP2K and MAPK. Activated MAPKs phosphorylate various substrate proteins including transcription factors, resulting in regulation of a variety of cellular activities including cell proliferation, differentiation, migration, inflammatory responses, and death. In the right side, there is a compilation of the gene ID and their pertinent protein name of the different signaling pathway components. Interactions are shown with black lines, which thickness is proportional to the connection relevance. Blue-green components depict mutated protein in human and mouse, while the blue ones are only found altered in human.

### 15. Downregulation of SAPK/JNK signaling pathway components modified the *in vivo* proliferation rates in BRAF<sup>V600E</sup> human melanoma cells

Since all data suggest the importance of SAPK/JNK in the melanoma progression, we studied the effect of the downregulation of different components of this pathway. The component selection was based on: (a) presence of alteration in human and mice melanomas, (b) high percentage of alteration in the human disease, and (c) selection of components located at different levels of the pathway. The components that shared all these prerequisites were: MAPK8, MAPK9, MAPK14, MAP2K4, MAP3K1, MAP3K4, and MAP3K7. For this reason, human BRAF<sup>V600E</sup> mutant cell lines (A375 and UACC903) were infected with shRNAs against the mRNAs from the mentioned proteins, which downregulation was confirmed by RT-PCR (Appendix Figure 5-10). Unfortunately, the down-regulation achieved for the different components was not optimal for all components in the different cell lines. For this reason, the data from A375-shMAP3K1, A375-shMAP3K7, UACC903-shMAP2K4, UACC903-shMAP3K1, and UACC903-shMAP3K7 were discarded for this preliminary analysis.

The performance of proliferation curves with the different cell lines generated indicated that SAPK/JNK signaling pathway alterations conferred different proliferation properties (Figure 31A). As positive control, selected cells were infected against sh*BRAF*, which decrease the proliferation rate independently of all studied cell line.

The downregulation of the mentioned SAPK/JNK pathway components showed a cell line-dependent response. These results could be due to the different genetic background of each parental cell line, which could promote different basal expression levels of the downregulated genes and the existence of different compensatory mechanisms (Figure 31B). In the A375 cells, depletion of *MAP2K4* and *MAP3K4* is translated into an increment of the cell proliferation rate. In the same cellular context, downregulation of *MAPK8* and *MAPK9* reduces this phenotypic feature. In the UACC903 cells line, its transduction with sh*MAPK9* increase the cellular proliferation, the opposite effect observed in the A375. The loss of all other SAPK/JNK pathway components diminished cell-doubling rate including sh*MAP3K4* that increases the proliferation rate in A375 cell line.

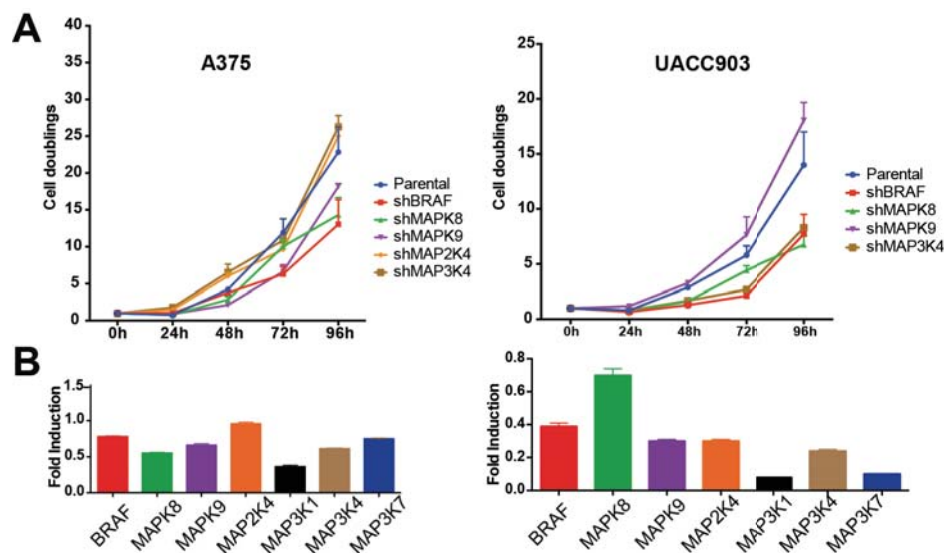


**Figure 31: Proliferation rates of BRAFV600E-mutated cell lines are affected by the downregulation of different SAPK/JNK signaling pathway components. (A)** Proliferation curves from A375 and UACC903 cells infected with shRNAs against the following genes: *MAPK8*, *MAPK9*, *MAP2K4*, *MAP3K1*, *MAP3K4*, and *MAP3K7*. **(B)** Representation of the normal transcriptional levels of the different SAPK/JNK components in A375 and UACC903 cell lines obtained by RT-PCR. Error bars shown mean  $\pm$  standard deviation.

Thus downregulation of the studied SAPK/JNK signaling pathway components might offer different proliferation advantages depending on the genetic profile of the human BRAF<sup>V600E</sup>-mutated melanoma cells.

#### 16. Combined study of the different *Braf*<sup>V600E</sup>-induced mouse with the TCGA data confirmed that B/L/UV animal model recapitulates human melanoma genetic alterations

Trying to unveil the relevant genes involved in the human disease, we compared the unique alterations registered in the three different animal models (RM/B/UV, B/SB and



B/L/UV) with the human melanoma gene alteration data available, extracted from The Cancer Genome Atlas (TCGA) Research Network.

Interestingly, it was estimated that approximately 226 genes were shared between the three different animal models and the melanoma TCGA provisional dataset. The use of the data available from the different animal models increased the statistical significance and biological relevance of this analysis since it reflected the data from 157 mice melanomas WES. The fact that the data from the different animal models targeted almost 20% of human melanoma mutated genes reflected the robustness from the data previously presented (Figure 32A), which allow us to understand better the human melanomagenesis.

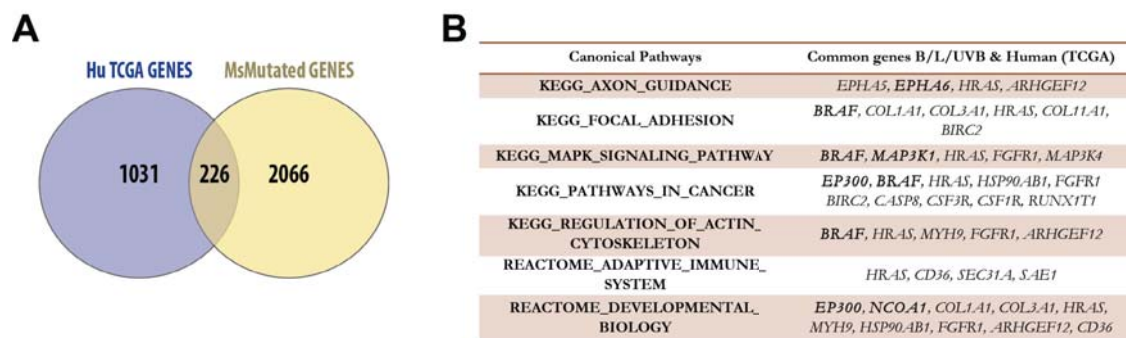


**Figure 32: *Braf*<sup>V600E</sup>-induced animal mouse models recapitulate human melanoma genetic alterations. (A)** Venn diagram representing the mutated genes found in human Skin Cutaneous Melanoma (TCGA, provisional) data set (blue, Hu TCGA genes, n = 1257) with the unique mutations found in RM/B/UV (from WES of 75 tumors), B/SB (from WES of 77 tumors) and B/L/UV (from WES of 8 tumors) melanoma lesions (yellow, MsMutated genes, n = 2292). **(B)** Table representing the canonical pathways and the common genes from each group altered in both B/L/UV and TCGA. In bold genes shared between B/L/U, B/SB and TCGA human data.

If we compared the different GSEA analysis shared between our animal model and B/SB mice together with the TCGA data, we were able to highlight the relevant biological processes altered in the melanoma progression. Those canonical pathways were: axon guidance, focal adhesion, MAPK signaling pathway, cancer signaling pathways, regulation of actin cytoskeleton, adaptive immune system and developmental biology. To know the relevant genes involved in the human disease, we studied the common genes altered in our animal model and the human TCGA data (Figure 32B). As expected, *BRAF* figured out as one of the common genes altered in different biological processes as: focal adhesion, MAPK signaling pathway, cancer-related pathways and regulation of actin cytoskeleton. Interestingly, SAPK/JNK signaling components, *MAP3K1* and *MAP3K4*, stood out as a relevant common component in the MAPK signaling canonical pathway. On the other hand, *EP300*, a histone acetyltransferase that regulates transcription via chromatin remodeling, appeared as an important gene altered in the cancer-related pathways and in developmental biology. Remarkably, this protein has an important role in the increment of the transcriptional activity of TP53 through acetylation and attenuation of SIRT2 (34), which suggest the indirect involvement of the p53-signaling pathway in the B/L/UV-induced melanomagenesis. Another protein is the *NCOA1* a nuclear receptor coactivator that directly binds nuclear receptors and

stimulates the transcriptional activities in a hormone-dependent manner, previously involved in the induction of Breast Cancer Metastasis (88).

Together this data, we have demonstrated that B/L/UV animal model recapitulates genetic alterations of the human disease. For this reason, this system constitutes a robust tool to understand better the human melanoma disease, which is essential to find new preventive and therapeutic tools.

# **DISCUSSION**

Understanding the molecular mechanisms related with melanomagenesis is critical to prevent and design novel therapeutic approaches against this lethal disease. Epidemiologic studies suggest that genetic alterations and environmental-factors are associated with melanoma development and progression. In this study, we investigated the cooperation between the neonatal activation of *Braf*<sup>V600E</sup>, the environmental insult, UVR, and the loss of the tumor suppressor, *Lkb1*. To that end, we generated the 4OHTx-induced conditional activated B/L/UV mouse model and study the effect of the UVR in the melanoma development in *Braf*<sup>V600E</sup>-context with and without the presence of *Lkb1*.

To mimic the early acquisition of *BRAF*<sup>V600E</sup> mutation in life in human, mice were treated with 4OHTx at 2.5-days old, leading to the physiological expression of *Braf*<sup>V600E</sup>. As expected, this genetic alteration promoted an initial melanocyte hyperproliferation, but it was not sufficient to induce melanoma. The *BRAF*<sup>V600E</sup> expression induced oncogene-induced senescence (OIS) avoiding the malignant melanocyte transformation. These results correlated with several publications, which claimed that *Braf*<sup>V600E</sup> expression in melanocytes promotes an initial proliferation followed by a growth arrest and OIS, inducing naevogenesis (89). In human, expression of *BRAF*<sup>V600E</sup> in normal melanocytes is characterized by the induction of both, p16<sup>INK4A</sup> expression and senescence-associated phenotypes (i.e.: high  $\beta$ -Galactosidase activity) contributing to cell growth arrest (74,75,77). All together indicates that *Braf*<sup>V600E</sup> early activation is a driver mutation that induces melanocyte hyperproliferation, but requires the acquisition of additional alterations to prevent senescence and progress into malignant melanoma.

As cited before, one of the most accepted model of human melanomagenesis is the Clark's model (15), which describes a linear histologic and morphologic changes from the benign lesions -nevi- to the malignant metastatic melanoma. In this model, the melanoma progression is promoted by the acquisition of different mutations that contributes to the malignant transformation of the melanocytes. Specifically, *BRAF*<sup>V600E</sup> mutation is present in 80% of nevi and 50% of malignant melanoma. Interestingly, only 20% of these malignant melanomas derive from the progression of nevi, meaning that 30% of *BRAF*<sup>V600E</sup>-mutated malignant melanomas have an uncertain origin (10). Retrospective epidemiological data indicates that 80% of cutaneous malignant melanoma is linked to UVR, particularly intermittent exposure during childhood (75). This data indicates that neonatal UVR has an important role in the acquisition of additional mutations acquired early on life that cooperate with *BRAF*<sup>V600E</sup>, promoting the development of malignant melanoma without progressing from nevi. Although the UVR-induced molecular mechanisms involved in melanomagenesis remains unclear, this environmental factor has strong genotoxic effects that induce DNA damage (72,90). Specifically, UVR promotes C>T transitions in the genome sequence, generating a landscape of punctual mutations known as "UV-signature" (78,91). Moreover, several studies has shown that UVR accelerates melanoma progression in different animal models harboring common genetic alterations in this disease (91).

In order to study the direct cooperation between *Braf*<sup>V600E</sup> and the UVR early in life, *Braf*<sup>V600E</sup>-expressing neonate mice were UVB-irradiated the day after the oncogene induction (postnatal day 3.5). Clearly, a single suberythral UVB-exposure was able to induce melanoma development, bypassing the nevus formation. Our experimental design, where the UVR is performed just after the *Braf*<sup>V600E</sup> activation, allows melanocytes to acquire the genetic alterations contributing to prevent OIS and promote the direct malignant transformation. All UVB-irradiated B/L/UV mice presented a mutational landscape with predominant C>T transitions (more than 50%), which correlates with other irradiated melanoma models (78,92).

In previous publication (RM/B/UV), UVR was not required to induce melanomagenesis in *Braf*<sup>V600E</sup>-context (78,93). In this experimental design, *Braf*<sup>V600E</sup> expression was activated in 2 months old mice, and one month after, when mice presented nevi, they were chronically UV-irradiated. Remarkably, this animal model was reported to develop melanoma in  $\approx 70\%$  of mice at a medium latency of  $\approx 12.6$  months by the exclusive *Braf*<sup>V600E</sup> induction (78). This data contrasted from ours, where exclusively 4OHTx-activated animals were not able to develop melanoma, with an exception of a single old animal. In addition, it is tempting to speculate that in RM/B/UV model, the lag time between the oncogene induction and the UVR eliminates the direct effect of this environmental carcinogen over the *Braf*<sup>V600E</sup>-induced mutation. Altogether, this data strengthens our animal model and experimental design in which *Braf*<sup>V600E</sup> expression does not promotes spontaneous melanomas, recapitulating better the human disease.

Despite the relevance of UVR in the mammalian cutaneous melanoma development (77,78), little is known about its molecular effect in melanocytes. Previous work suggested that UVR could accelerate epidermal hyperplasia and cutaneous inflammation (20). It is known that induces the migration of follicular melanocyte stem cells (MCSCs) to the interfollicular dermis (IFE) (16). Our results proved that UVR prevents *Braf*<sup>V600E</sup>-induced senescence. OIS was observed *in vivo* and *in vitro* in non-irradiated *Braf*<sup>V600E</sup>-induced melanocytes. However, a single dose of UVB-irradiation significantly reduced the expression of senescence markers increasing the expression of the proliferation markers, such as Ki67. Hence, these results prove the cooperation of neonatal acquisition of *BRAF*<sup>V600E</sup> mutation and UVR in melanoma development and progression, confirming further the role of this environmental factor in melanomagenesis early in life.

Previous results from our group reveal that: (a) *BRAF*<sup>V600E</sup> suppress the energy metabolism sensor function of LKB1 (12), and (b) that LKB1 has an important role as UVB-induced DNA damage response (52). These results anticipate an important role of this protein in human melanomagenesis. A major finding in our animal model was to observe *in vivo* cooperation of *Braf*<sup>V600E</sup> and *Lkb1* loss, promoting melanomagenesis and abrogating *Braf*<sup>V600E</sup>-induced senescence even in the absence of UVR. This result correlated with other studies, where the fully malignant progression of *Braf*<sup>V600E</sup>-

melanocytes was achieved by the loss of other tumor suppressors such as: *p53* (54), *Cdkn2a* (22, 71), or *Pten* (74). In a recent publication, it has also been reported that loss of *Lkb1* allowed melanocytes escape *Braf*<sup>V600E</sup>-induced senescence through the activation of mTORC1, but failed to reach full transformation (74). The latter was achieved through the concomitant activation of mTORC2 pathway with the further loss of *Cdkn2a*. In our model, *Lkb1* loss induced directly mTORC1 activity leading to tumor formation. However, tumors also presented activation of mTORC2 pathway, confirming the previous results and suggesting that both signaling pathways are required for malignant transformation. How the activation of mTORC2 is achieved in these lesions is unknown and it will need further investigations. Due the role of LKB1 in genomic integrity and that most of these tumors appeared in eight-months old animals, it is likely that loss of *Lkb1* in BRAF<sup>V600E</sup> mutated proliferating cells would increase the chance for mutations to occur and affect this key signaling pathway, leading to fully transformation.

In this study, we show that *Lkb1* loss in the B/L/UV animal model increases tumor onset, genetic instability and tumor heterogeneity. Genetic instability increment was clearly promoted by the lack of the DNA damage sensor function of LKB1. In line with this data, lack of *Lkb1* was linked also with an increment in the number of tumor per animal. Our results indicate that irradiated B/L/UV mice induced DNA photo-lesions accumulation, inducing genetic instability and melanomagenesis, which matches with previous results from different groups (75). Remarkably, the lack of this kinase function alone in a *Braf*<sup>V600E</sup>-context promotes the same magnitude of tumor mutational burden as UVR, indicating the importance of this tumor suppressor in the genetic integrity. Altogether, the genetic instability and the high tumor mutational burden would contribute to the enrichment of the different melanoma subtypes when this kinase is missing. The histological analysis of the B/L/UV tumors revealed three different melanoma subtypes: myxoid, spindle and neural. This data exposed the importance of the genetic background of the melanocytes and the effect of the UVR in the tumor histological complexity. Clearly, UVR cooperates increasing the penetrance of all three melanomas, but especially with the development of myxoid melanomas. Interestingly, *Lkb1* loss enriched the neural subtype. In this matter, another article revealed the role of the *Lkb1* loss in the promotion of genetic instability in mice with KRAS<sup>G12D</sup>-mutated pancreatic cells (54,70,95,96). Specifically, in this study, *Lkb1* lack promoted the serine–glycine–one carbon (SGOC) network, which increased DNA methylation affecting the transcriptional response. Then, one noteworthy question would be to investigate (a) whether the DNA methylation landscape of *Lkb1* deficient melanomas is altered in the B/L/UV tumors and (b) which is the contribution of the serine–glycine–one carbon (SGOC) network in the melanocyte malignant transformation.

Trying to understand the increment in the B/L/UV tumor onset, a parallel project in our laboratory revealed that LKB1 indirectly regulates the *cMET* transcriptional expression. In human, *cMET*, the HGF receptor tyrosine kinase, is expressed on epithelial cells and melanocytes; however, its autocrine activation or increased expression has been



described in melanoma progression and metastasis (97). In engineered mice models, constitutive and ubiquitous HGF expression establishes an autocrine loop with cMET, leading to the epidermal melanocyte localization and proliferation (14). This kinase has been involved in the development and progression of cutaneous and metastatic melanomas upon UVR (5). Moreover, mutations in cMET are one important melanoma hallmark in the acquisition of Vemurafenib-resistance (72). The B/L/UV tumor characterization showed that cMET protein amounts positively correlated directly with LKB1 expression in a genetic dose-dependent manner independently of BRAF<sup>V600E</sup> background. Although these results granted a more exhaustive investigation about the mechanisms involved, the increment in the B/L/UV tumor lag time could be related with the loss of the cMET expression and its proliferative functions. In line with this, LKB1-mediated cMET transcriptional regulation was observed when this kinase was depleted in the A375 cells. In this specific cellular context, we observed that LKB1 depletion led to the downregulation of cMET, which promoted a decrease of the proliferation rate of cells, even in the presence of its ligand, HGF. Interestingly, this data correlates with the data obtained from the B/L/UV model, where we observed a proportional expression of LKB1 and cMET and an increment in the tumor onset. However, the direct correlation between cMET and LKB1 expression as well as the proliferative properties was not clear in other BRAF<sup>V600E</sup>-mutated melanoma cell lines, such as SkMel28 cells. These diverse responses after the downregulation of LKB1 expression, suggests the existence of different mechanisms involved in cMET transcriptional regulation and the participation of other RTKs or mechanisms contributing in the tumor proliferation. Nevertheless, the LKB1 expression in human melanomas samples showed a direct correlation between the LKB1 and cMET protein expression in melanoma that was independent of the BRAF<sup>V600E</sup> mutation. On the other hand, we also tested the LKB1 reconstitution in different BRAF<sup>V600E</sup>-mutated cell lines null for the expression of this kinase, such as the melanoma, G361, and lung, A549. Using this approach we could determine that LKB1 regulates the expression of cMET in different tissues in a cell type dependent manner. Altogether our results suggest a possible novel role for LKB1 in the regulation of the cell proliferation by modulating the amounts of RTKs such as cMET.

To better understand the effect of UVR and *Lkb1* loss in a *Braf*<sup>V600E</sup>-context we performed WES from irradiated and non-irradiated B/L/UV tumors. Our animal model revealed that UVB-targeted genes were related with many cancer-related biological processes related with the immune system, cell adhesion and motility. Interestingly, Rho-signaling, a key regulator of cell proliferation, cytoskeletal reorganization and cell migration (91,97), appears as one of the most significant altered transduction pathways in irradiated tumors. In human cancers, it is well known the regulation role of extracellular signal-regulated kinases (ERK) and PI3K pathway in Rho GTPases-mediated cell motility and migration (93,99). Moreover, human melanoma exome analysis identified the activating mutation of Rho family of small GTPases, RAC1<sup>P29S</sup>, as a recurrent UV-signature present in 9.2% of sun-exposed melanomas (100,101). Although our data

indicate a significant alteration of Rho GTPases components, we did not observed an increment in the metastasis rate. Further studies will be required with the B/L/UV model to assess the effect of Rho family in melanoma metastasis. Due to the high melanoma metastatic potential, Rho-pathway could have a therapeutic benefit to prevent or improve survival of those patients that currently lack an effective treatment.

A recent report demonstrates that melanoma originates from *Braf*<sup>V600E</sup> and *Pten*-null MCSCs upon stimulation by UVR (93). This event induces MCSCs activation and translocation via an inflammation-dependent process. Specifically in this study, melanomagenesis is promoted by the extrinsic stimulation with the chromatin-remodeling factor, *Hmga2*. In this regard, exclusively irradiated B/L/UV tumors promote significantly inflammasomes, which are responsible for the activation of inflammatory responses, specifically the NLRP3 inflammasome. Interestingly, a recent study exposed that NLRP3 inflammasome inhibition prevents metastasis of melanoma cells *in vivo* (12). All these data indicates unveil the potential therapeutic role of inflammatory processes in the B/L/UV melanomagenesis and metastasis.

Despite some publications reveals that melanoma progression from nevi requires p53- and BRAF-pathway interaction (102) or postulates *Tp53* as a direct UVR-target (94), we do not found this gene altered in our animal model, indicating that *TP53* mutation is not a requirement to overcome or prevent the *Braf*<sup>V600E</sup>-induced senescence. Interestingly, we have found some genes involved indirectly in the p53-pathway that were found exclusively in irradiated animals, such as: *Letmd1*, *Magee1*, and *Fhit*. Furthermore, we found the *Nfx1* gene, also related with the p53-signaling, mutated in one single irradiated *Braf*<sup>V600E</sup> animal with a high tumor variant allele frequency. All together, these data indicate that irradiated B/L/UV tumors do target the p53-signaling pathway, which supports the previously described relevance of this signaling pathway in melanomagenesis (78).

The WES sequencing data from *Lkb1*-null B/L/UV tumors stressed genes related with the synapsis interaction, neuronal development, and key signaling pathways involved in the nervous system development, as the Netrin-1 pathway. In this regard, several studies claim the important role of LKB1 phosphorylation in the axon/dendrite differentiation, a critical step in the neuronal development (78,94,103). These results contrast with the fact that tumors lacking this kinase presented a higher proportion of neural-like melanoma subtype. However, we can suppose that due to the lack of *Lkb1* function, it was selected those melanocytes that harbor mutations in neural-related genes in order to compensate this kinase loss.

As mentioned before, Netrin-1 signaling pathway, involved in mediating axonal guidance (104–107), emerged as a significant pathway that is significantly altered in irradiated and non-irradiated B/L/UV tumors that lack *Lkb1*. Excitingly, another *Braf*<sup>V600E</sup>-induced mouse model that express contemporaneously the Sleeping Beauty transposon (B/SB

animal model) point out this signaling pathway as a genetic driver of melanomagenesis (76). Specifically, this publication showed that components of this specific pathway were found as transposon common insertion sites in  $\approx 47\%$  of the 77 B/SB melanomas sequenced, and they are altered in  $>30\%$  of human melanomas of the Catalogue of Somatic Mutations in Cancer (COSMIC). Moreover, Krauthammer *et al.* highlighted the tumor suppressor DCC gene, the Netrin-1 receptor, found also in our animal model, as a gene with high mutation burden in sun-exposed human melanomas (76). Recent publications indicated that and 19% of human melanoma samples harbor deleterious mutations in this DCC gene (93). Thus, unveiling the role of Netrin-1 pathway and DCC gene in melanomagenesis would contribute to increase our knowledge in the molecular bases of this disease and/or the developing of novel therapeutic strategies.

Through whole exome sequencing of different tumors, we identified 65 genes that were relevant in the B/L/UV tumor progression. Gene ontology studies indicated that the biological processes regulated by this gene set were: DNA-processing, lipid metabolism, apoptosis, cytoskeleton organization, and cell motility. A recent study indicated that *Braf*<sup>V600E</sup>-mutated pigment-producing interfollicular melanocytes, prone to form melanomas, required a transcriptome reprogramming and loss of differentiation before dermal invasion (108). This reprogramming entails the alteration of 3 gene clusters based on: (a) melanocyte differentiation markers, (b) invasion and migration identity genes, and (c) lipid metabolism and EphrinA3 signaling. Interestingly, some of the most significant mutated genes identified in our model could be classified into some of these cited biological clusters. We can find  $\approx 9\%$  of genes involved in cell motility and invasion (*Cntnap4*, *Pcdhb18*, *Dnab1*, *Dnab10*, *Fbn2*, *Zan*, and *Kif27*) and  $\approx 12\%$  genes related with the lipid metabolism (*Abca5*, *Abca9*, *Abhd6*, *Acox2*, *Casr*, *Cep350*, *Cers5*, and *Cpt1c*). Additionally, some genes or family-related genes from each cluster were found mutated in individual mice tumors, such as the case of the melanocyte marker, *Dctn1*; the lipid metabolism-related gene, *Pof1b*; or *Lamb3*, *Itgb1* and *Itgb8* genes associated with the invasion/migration program.

Different reports highlight the important role of TGF $\beta$  and NF $\kappa$ B-signaling pathways in melanomagenesis (11). Interestingly, one of these studies claimed that mutant BRAF<sup>V600E</sup> is addicted to TGF $\beta$  signaling through RHOA, which confers human melanocytes proliferation and metastatic potential and participates in Vemurafenib-resistance (98,100,109,110). In addition to this, upregulation of NF $\kappa$ B signaling has been involved in melanoma progression and its increased metastatic potential (98). Our results show that these signaling pathways were also targeted in the B/L/UV model. Some of the most relevant mutated genes identified in the B/L/UV tumors are related with these signaling pathways (*Acvr11*, *Ambr2*, *Cilp*, and *Ccdc22*) ( $\approx 6\%$  of the 65 genes). Moreover, some genes from this collection presented the same point mutations detected in human melanomas (such as GRID2<sup>E852K</sup>, GRID2<sup>G735R</sup>, THRB<sup>E203K</sup>, and THRB<sup>E217K</sup>) as well as in other human cancers, reinforcing the relevance of the B/L/UV model.

The genetic comparison between our B/L/UV model with the data from B/SB and B/UV studies (110) allows us not only to confirm the robustness of our animal data, but also to find the 7 common altered genes that cooperate with *Braf*<sup>V600E</sup> in melanomagenesis. Of note, it is outstanding one common gene between the three models, *Cep350*. This gene encodes a centrosomal protein that recruits FOP-FGFR1 to centrosomes in myeloproliferative disease and has been implicated in the melanoma progression (76,78). In B/SB model, it was studied the tumor suppressor genes that cooperates with BRAF<sup>V600E</sup>-mutation in melanoma progression through the *Sleeping Beauty* transposon. Among the highest ranked genes targeted in this system were the *Cep350*, downregulation of which enhanced *in vivo* tumor formation of BRAF<sup>V600E</sup> -cells. Its relevance in the melanoma progression is confirmed by the human data, since it is mutated in 10% of samples from human Skin Cutaneous Melanoma from the TCGA provisional dataset. In our animal model, this specific gene was found mutated in more than one animal with a variant allele frequency  $\geq 20\%$ . All this data support the importance of *Cep350* in melanomagenesis, indicating that further studies should be performed in order to deep understand its role in this disease.

The signaling pathway gene ontology obtained from the interrogation of the common gene set observed in the different animal models, outlines MAPK, TNF $\alpha$ , and NF $\kappa$ B signaling pathways as the common altered networks in the three animal models. Special emphasis must be given to the MAPK pathway, composed by three different axes: (a) the extracellular regulated kinases (ERKs), (b) the c-Jun N-terminal kinases (JNKs), and (c) the p38 MAPKs. The genetic analysis of the whole exome sequencing data from B/L/UV, B/SB, and RM/B/UV animal models revealed that different components of this pathway were found mutated in murine *Braf*<sup>V600E</sup>-mutated tumors. Importantly, genetic alterations of components of the SAPK/JNK pathway was also found altered in human Skin Cutaneous Melanoma from the TCGA provisional dataset. Despite the increasing body of evidence linking the three axis of MAPK family in melanomagenesis, its precise role has not been described yet. Our results show that downregulation of some of the key components of this pathway (*MAPK8*, *MAPK9*, *MAPK14*, *MAP2K4*, *MAP3K1*, *MAP3K4*, and *MAP3K7*) in human *Braf*<sup>V600E</sup>-mutated melanoma contributes to melanoma proliferation in a cell type dependent manner. Recently, it has been described that there is a clear interplay among ERK, JNK, and p38 pathways (76). In human melanoma, it has been shown that rewired ERK upregulates JNK and activates c-Jun oncogene, which have an important oncogenic role in melanoma pathogenesis (35,111,112). Another report demonstrates that in human melanoma cells ERK-mediated over expression of  $\alpha$ V $\beta$ 3 integrin promotes the activation of p38 (35), that activates NF $\kappa$ B-signaling, promoting growth and migration (111). In response to some stimuli, including UVR, MKK4 (coded by the *MAP2K4* gene) activates JNK and p38. This data suggests that MKK4 is an integration point for both pathways in melanoma (34). For this reason, we would expect that transduction of sh*MAP2K4* in the different *Braf*<sup>V600E</sup>-cell lines, would induced a decrease in cell proliferation. However, this effect was observed exclusively in the SkMel28 and UACC903 cells, but not in the A375. This different

response could be context-specific due the different expression amounts of the different components in the SAPK/JNK and the existence of compensatory mechanisms. There is no doubt that further studies should be performed to study the role of the different components of the SAPK/JNK network, which its central role in melanoma would allow us to acquire a better understanding in molecular requirement for melanoma progression.

In summary, the B/L/UV animal model presented here is a robust system to study the melanoma pathogenesis. This animal model reveals the important role of UVR in preventing the *Braf*<sup>V600E</sup>-induced senescence, a requisite in melanoma progression in this specific mutational context. Moreover, a patent fact is the important role of *Lkb1* loss in *in vivo* melanoma induction, which has a relevant role in the tumor genetic instability, which favors the development of different melanoma subtypes. The B/L/UV tumors whole exome sequencing and its genetic analysis highlight the important role of Rho-, Netrin1- and SAPK/JNK-signaling pathway in melanomagenesis, which could open new therapeutical options for melanoma patients.

# CONCLUSIONS

1. *Braf*<sup>V600E</sup>-expression induces a transient abnormal proliferation of dermal melanocytes. Malignant transformation was limited by oncogene-induced senescence, which could be prevented by a single neonatal dose of UVB.
2. Loss of *Lkb1* overcomes *Braf*<sup>V600E</sup>-induced senescence, increasing melanoma incidence independently of UVB radiation. In addition, lack of this tumor suppressor increase: tumor onset, genomic instability and histologic heterogeneity.
3. Loss of the *cMet* transcriptional regulation by *Lkb1* could be responsible for increasing the B/L/UV tumor onset and for decreasing of cell proliferation in human melanoma cell lines.
4. Genetic background of the melanocytes might influence the development of the different melanoma subtypes.
5. The loss of LKB1 role in UVB-induced DNA damage repair increases genomic instability, tumor heterogeneity and tumor multiplicity.
6. Characterization of the genetic profile of UVB-irradiated tumors depicts Netrin-1 and Rho-signaling pathways as the main UVR-altered network. Exome sequence analysis of tumor lacking *Lkb1* reveals neuronal biological processes as the most significantly altered.
7. Correlation of the genetic data from B/L/UV animal with other *Braf*<sup>V600E</sup>-induced animal models highlights the relevant role of MAPK, TNF $\alpha$  NF $\kappa$ B, and SAPK/JNK-signaling pathways in melanomagenesis.
8. The global comparison of B/L/UV, RM/B/UV, and B/SB animal models with human melanoma indicates the robustness of our animal model mimicking human melanoma genetic alterations.



# **MATERIAL AND METHODS**

## 1. Constructs

### a. Plasmid Generation

pLenti-IRES-GFP plasmid were obtained from Stephan Tenbaum (VHIO, Barcelona, Spain). Human LKB1 sequence was subcloned from pCMV5-Flag-LKB1<sup>WT</sup> to get the pLenti-LKB1<sup>WT</sup>-IRES-GFP. All short hairpin RNA against the components of the SAPK/JNK pathway were purchased from Sigma (Sigma, Saint Louis, MO, USA). The backbone of these plasmids is the pLKO.1.

#### *i. Digestion and ligation procedures*

For the pCMV5-Flag-LKB1<sup>WT</sup> of and pLenti-LKB1-IRES-GFP digestion, 20µg of each plasmid was digested with MluI restriction enzyme and NEB 3.1 buffer (New England Biolabs, Massachusetts, United States) at 37°C for 2 hours. Then, 10µg of each plasmid were dephosphorylated using 1 unit of Alkaline Phosphatase Schrimp (SAP) (Roche, Basilea, Switzerland) per 1 pmol of phosphorylated DNA for every at 37°C for 1 hour. Consecutively, dephosphorylated backbones were checked by electrophoresis in 0,8% agarose gel. Each single band corresponding to either the insert or the vector was purified with the QIAquick® Gel Extraction Kit (Qiagen Mississauga, Ontario, USA).

For ligation reactions, the following dephosphorylated vector: dephosphorylated insert molar ratios were used: 1:1 and 1:3. Ligation was performed using T4 DNA Ligase (Roche) in a final volume of 30µL while mixed gently and incubated at 16°C over-night. The day after, DNA was purified following the Phenol/Chloroform Protocol following the manufacturer's indications.

#### *ii. Transformation in NEB® Stable Competent E. coli*

Transformation of NEB® Stable Competent *E.coli* (New England Biolabs) was performed following the manufacturer's indications. After the overnight culture of *E.coli*, plasmids were purified using the QuickClean II Plasmid Miniprep Kit (Thermo Scientific, Waltham, MA, USA) and checked by MluI enzymatic digestion.

## 2. Cell Culture

### a. Cell lines

All the cells used in this work were obtained from American Type Culture Collection (ATCC). HEK293T, A375, and A549 cells were grown in Dulbecco's Modified Eagle Medium (DMEM) (Biowest, Riverside, MO, USA). UACC903 cell lines were grown in Roswell Park Memorial Institute (RPMI) (Biowest). SkMel28 cell lines were grown in Eagle's Minimum Essential Medium (EMEM) (Biowest). All medium was supplemented with 10% Fetal Bovine Serum (FBS) (Biowest), 100U/mL Penicillin/100µg/mL Streptomycin (Thermo Scientific), and 1,5µg/mL Plasmocin (New England Biolabs) (Table 6).

Cells were maintained at 37°C and 5% of atmosphere CO<sub>2</sub> in Nuair incubator (Nuair, Doncaster, England). All cells were manipulated in type II laminar flow cabinet, Telstar Bio Ila (Telstar, Barcelona, Spain) with a High Efficiency Particulate Filter (HEPA) filter.

**Table 6: General cell line information.** Compilation of cell line information: tissue of origin, cell type, organism of origin, specific cell-cultured media and specifications about the gene profile. MM: Malignant Melanoma; HS: Homo sapiens

Name	Tissue	Disease	Cell Type	Organism	Media	Gene Information
HEK293T	Kidney		Epithelial	HS	DMEM	
A549	Lung	Carcinoma	Epithelial	HS	DMEM	Lack of LKB1 KRAS <sup>G12S</sup>
A375	Skin	MM	Epithelial	HS	DMEM	BRAF <sup>V600E</sup>
UACC903	Skin	MM	Epithelial	HS	RPMI	BRAF <sup>V600E</sup>
SkMel28	Skin	MM	Epithelial	HS	EMEM	BRAF <sup>V600E</sup>

### b. Cell quantification

Cell quantification was performed counting cells using the Neubauer Chamber (Celeromics, Valencia, Spain) following manufacturer's recommendations. To check the viability of the cells, it was performed the dye exclusion test with Trypan Blue (Thermo Scientific). This test is based in the fact that healthy viable does not absorb the dye, whereas dead cells with damaged cell membrane are permeable and become blue.

### c. Subculture Procedure

The following protocol describes a general procedure for dissociation of adherent mammalian cells in culture into individual cells. This is important for the routine cell culture passaging or cryopreservation. Trypsin is a serine protease that specifically cleaves at the carboxyl side of lysine and arginine residue. On the other hand, calcium-dependent adhesion molecules, like cadherins, determine cell-cell and cell-matrix interaction. For this reason is important, the role of disodium ethylenediaminetetraacetic acid (EDTA) to weaken the interactions by the chelation of the divalent cations.

Before starting, it is important to warm up to 37°C all the reagents that are going to be used. The first step consists in washing the plate with Phosphate-Buffered Saline (PBS) (Biowest). This would allow us to remove all the Ca<sup>2+</sup> and Mg<sup>2+</sup> present in the media, which can inhibit the trypsin. After discarding the PBS, 0.5% Trypsin-EDTA 1x (Gibco, Waltham, MA, USA) is added into the plate in a size-dependent manner. The plates are incubated at 37°C for 2-5 minutes rely on the cell line. Once, the cells are detached from the plate, complete media is added in a 2:1 (complete media: trypsin). This mixture can be collected into a 15mL-falcon to be centrifuged 5 minutes at 200g. The media would be discarded, and cell pellet could be subcultured adding complete fresh media. In order to seed out a specific cell number, cells could be quantified as explained above (Cell quantification).

#### d. Cryopreservation procedure

This method would allow us to keep a stock of viable cell lines during long period of time. Before starting, it is important to select the cell lines that gather important characteristics, as low passage number or no Mycoplasma contamination. The cryopreservation of cells lines avoids genetic and morphologic alterations of the cell lines characterized of their long culturing. The main basis of this procedure is the resuspension of the cells with a cryoprotector, as the Dimethyl Sulfoxide (DMSO) (Sigma). This reagent avoids the disruption of the membrane structure preserving the viability of the cells.

The cryopreservation method consist in the resuspension of a pellet of cells with 10% DMSO in Fetal Bovine Serum (FBS) at a final concentration of  $[1 \times 10^6 - 2 \times 10^6]$  cells/mL. Cells should be kept in cryotubes (Sigma). In order to reduce the temperature of the cells in a progressive way, the cells were disposed into Cryo 1°C Freezing Container (Thermo Scientific), before its storage to -80°C freezer. For longer conservation of the cells they could be stored in liquid Nitrogen.

### 3. Cell Generation

#### a. Lentiviral Particles Production and infection

pLenti-LKB1<sup>WT</sup>-IRES-GFP and the different pLKO.1 plasmids were used to generate lentiviral particles in HEK293T cells. To this aim these cells were transfected with our plasmid of interest and the second-generation lentiviral system, which is composed of: (a) the packaging plasmid, psPAX2 which contains the HIV gag, pol, rev, and tat, and (b) the envelope plasmid pMD2.G, that encode the VSV-G protein.

For the transfection, it was used poly-L-Lysine-precoated 10cm plates (Sarstedt, Nümbrecht, Germany) of HEK293T cells at 80-90% of confluence (usually one plate per construct). Previous transfection of the cells, the media was changed with media containing 10% of FBS-complement inactivated with 25µM Chloroquine. For the transfection reaction, it is important to keep the proportion of the lentiviral and the packaging plasmids (Table 7). The transfection reagent used was the Polyethylenimine (PEI) (Polyscience, Inc., Warrington, PA, USA) diluted in 150mM NaCl and with a final concentration of 200µg/mL. This mix should be incubated 15 minutes at room temperature prior its addition to cells. The transfection was performed overnight. The next day, the media was replaced with 2% of FBS-complement inactivated with 5mM Sodium Butyrate (Sigma). The virus-containing media was collected after 24h and 48h. In order to avoid any contamination of the HEK293T cells the media were centrifuged and the collected media filtrated with 0,45µm filters (Sarstedt). After this media can be used for infection of stored at -80°C.

**Table 7: Basic information of the HEK29T cells transfection.** In this table is indicated the quantity ( $\mu\text{g}$ ) of DNA used in the transfection mix and the proportion of final media and the transfection reagent. The transfection mix was composed by the DNA and  $200\mu\text{g}/\text{mL}$  PEI, diluted in  $150\text{mM}$  NaCl.

Plasmid ID	Quantity ( $\mu\text{g}$ )	Transfection Mix (mL)	10cm-plate media (mL)
Plasmid of interest	25	1	9
pPAX2	18,75		
pPMD2.G	6,25		

For the infection of the desired cells, the parental lines were seeded 24 hours before the first virus collection in a 6-well plate (Sarsted). The viral supernatant was added in 2:3 ratio to the cells with  $8\mu\text{g}/\text{mL}$  of Polybrene (Sigma) for 8-16 hours. Then, media was discarded and appropriated fresh media was added to allow the recovery of cells.

Cells infected with the pLKO.1 plasmid were selected with Puromycin (Sigma) when they were recovered from the infection.

#### b. Cell Sorting

Once the pLenti-LKB1<sup>WT</sup>-IRES-GFP infected cells recover, it was induced with  $10\mu\text{g}/\text{mL}$  Doxycycline (Sigma) for 48 hours, and sorted at the High Technology Unit from VHIR to select the infected cells (green cells). Cells were resuspended at  $5 \times 10^6$  cells/mL in 10% FBS in PBS and kept on ice. Prior sorting, cells were filtrated with  $30\mu\text{m}$  filter (Sysmex, Barcelona, Spain). Green-cells were sorted in a High speed FacsAria Digital Cell Sorter (BD Biosciences, San Jose, Ca, USA). Parental cell lines were used as negative control to set fluorescence thresholds in the sorter.

### 4. Protein analysis techniques

#### a. Cell Lysis

Whole-cell extracts were prepared by washing the cell monolayers twice in cold PBS. Plates were scraped after the addition of RadioImmunoPrecipitation Assay buffer (RIPA) supplemented with phosphatase- and protease-inhibitor (Millipore, Billerica, CA, USA) on ice. Protein extracts were incubated 20 minutes on ice to complete the cells lysis. After that, samples were centrifuged at  $20,000\text{g}$  for 20 minutes. Supernatants containing proteins were transferred to a new tube and pellets were discarded.

#### b. Protein Quantification

Protein extracts were quantified using pierce BCA Protein Assay Kit (Thermo Fisher). This method is based on the fact that proteins reduce  $\text{Cu}^{2+}$  to  $\text{Cu}^{1+}$  in an alkaline media. Bicinchoninic Acid (BCA) binds to  $\text{Cu}^{1+}$  and makes a soluble compound with a maximum absorbance at  $562\text{nm}$ .

Protein concentration was calculated compared to a protein standard, result from a serial dilution of known Bovine Serum Albumin (BSA) standard concentrations (Sigma).

Protein quantification was performed in a 96-well plate (Sarsted). The increasing concentrations of the standard were: 0, 200, 400, 800, 1200, 1600 and 2000 $\mu$ g/mL. For the standard 5 $\mu$ L of each concentration was dissolved in 200 $\mu$ L of BCA, and 2 $\mu$ L of the samples were also dissolved in 200 $\mu$ L of BCA. It was let at 37°C for 30 minutes in a protected from light. The absorbance was measured at 562nm in the Epoch Spectrophotometer (BioTek, Winooski, VT, USA).

The desired amount of protein was suspended in a protein Laemli loading buffer buffer and denatured at 95°C for 10 minutes. The concentration of protein could vary between [30-80]  $\mu$ g of protein. Samples could be kept at -20°C.

### c. Western Blot

Samples were resolved in 10 or 12% acrylamide gels depending on the size of the protein of interest. Electrophoresis was performed at 120V for 60-90 minutes. Proteins were transferred at 110V for 90 minutes to an Immobilon-P Vinilide Polifluorur (PVDF) membrane (Millipore), previously activated 1 minute with methanol (Sigma) and rehydrated with transfer buffer. Both electrophoresis and transfer were performed using BioRad equipments (Bio-Rad Laboratories, Inc., Hercules, CA, USA).

Membranes were blocked with 5% non-fat dry milk (SCBT, Inc., Santa Cruz, CA, USA) dissolved in Tris-Buffered Saline (TBS) buffer with 0.1% Tween (Sigma) for 1 hour at room temperature. After rinsed the membrane with TBS-T, membranes were incubated with the desired primary antibody and secondary horseradish peroxidase-conjugated antibodies at the optimized concentrations and conditions (

Table 8).

The antibody binding was visualized using the ECL detection system (GE Healthcare, Chalfont St Giles, UK). Membranes were developed exposing them to Fuji Medical X-Ray Films (TDI, Madrid, Spain) in the automatic film processor Curix 60 (AGFA, Mortsel, Belgium). Different exposure times of the films were used to ensure that bands were not saturated. Quantification of the films was performed by densitometry using ImageJ software (NIH, Bethesda, MD, USA).

**Table 8: General information of the antibodies.** Antibody Information recompilation In this table it is recompiled all the information of the antibodies used in this work. WB: Western Blot; IF: Immunofluorescence, IP: Immunoprecipitation; IHC: Immunohistochemistry; RT: Room Temperature. Rb: rabbit; Ms: mouse; Sh: sheep.

Antibody	Isotype	Application	Dilution	Conditions	Commercial brand	Commercial Reference
<b>LKB1</b> (Ley37D/G6)	Ms	WB	1:1,000	O/N 4°C	SCBT	sc-32245
<b>LKB1</b> (27D10)	Rb	IP	2 $\mu$ g/IP	O/N 4°C	SCBT	sc-3050
<b>CPD</b> (clone KTM53)	Ms	WB	1:500	O/N 4°C	Kamiya Biomedical Company	MC-062
<b>Dewar</b>	Ms	WB	1:500	O/N 4°C	Cosmo Bio	CAC-NM-DND-003



<b>6-4pps (64M-5)</b>	Ms	WB	1:500	O/N 4 °C	Cosmo Bio	CAC-NM-DND-002
<b>cMET (H190)</b>	Rb	WB	1:1,000	O/N 4 °C	SCBT	Sc-8307
<b>GAPDH</b>	Rb	WB	1:5,000	1h RT	Trevigen	2275-PC-100
<b>ECL Mouse IgG</b>	Sh	WB	1:10,000	1h RT	GE Healthcare	NA-9310
<b>ECL Rabbit IgG</b>	Sh	WB	1:10,000	1h RT	GE Healthcare	NA-9340

#### d. Immunofluorescence protocol

Tumor tissue were fixed overnight in 4% Paraformaldehyde (Sigma). Next day, they were changed to 70% ethanol (Sigma). For later immunohistochemistry staining, samples were included in paraffin-embedded blocks and cut into 4µm sections in a microtome (Thermo Scientific Microm HM355S microtome). Slides were mounted on crystal slides (Thermo Scientific). Several consecutive sections were performed for the different immunostaining and routinely, hematoxylin and eosin staining. In skin sections and βGalactosidase Whole assay, Neutral Red staining was performed to check the skin orientation and the blue precipitate observation.

##### *i. Specific immunohistochemistry*

Formalin-fixed paraffin-embedded tumor samples were subjected to immunocytochemistry according to the manufacturer's antibody protocol. Immunostaining was performed on 4µm sections from formalin-fixed paraffin-embedded tissues. Staining was performed either manually or on an automated immunostainer Beckmarck XT (Ventana Medical Systems, Tucson, AZ, USA). Antibodies were visualized by the UltraView Universal DAB detection Kit (Ventana Medical Systems).

The patient samples used in this Project were provided by the Tumor Bank of the Vall d'Hebron University Hospital Biobank with appropriate ethical approval (supported by the Xarxa de Bancs de Tumors de Catalunya sponsored by Pla Director d'Oncologia de Catalunya (XBTC); supported by the RETICS de Biobancos (ISCIII).

All immunohistochemistry cases were evaluated independently by an expert dermatopathologist and one trained Molecular Biologist blinded for patient groups, taking into account the percentage of positive cells and intensity of the staining, which was assessed semiquantitatively. Final results were obtained utilizing the average of the two values. Whenever a major discrepancy was observed between both observers, the cases were discussed using a multi-headed microscope.

##### *ii. Specific immunofluorescence*

Paraffin sections were incubated at 56°C overnight. Then it was proceed to the deparaffination and rehydration of the samples in a fume hood. The deparaffination of

the samples was performed with two incubations in Xylol 100% for 10 minutes at room temperature, followed by the ethanol rehydration chain (100%, 96% and 70% of Ethanol) 5 minutes per wash. Samples were incubated for 10 minutes in water, previous antigen retrieval step.

Most paraffin-fixed tissue requires an antigen retrieval step before immuno-staining can proceed. This is due to the formation of methylene bridges during fixation, which cross-link proteins and therefore mask antigenic sites. The two methods of antigen retrieval are heat-mediated (also know as heat-induced epitope retrieval, or HIER) and enzymatic. In this protocol it was used the HIER procedure. In order to perform this it was used a citrate commercial solution from Dako (Agilent, Santa Clara, CA, USA). The pH selected was 6 or 9 (dependent of the antibody requirements (Table 9)). Before adding the samples, the retrieval buffer was warmed up to 95°C in a water bath. Samples were incubated for 20 minutes at 95°C. After this time, sections were kept at room temperature to cool down. Then each section was permeabilized with TBS1x, 0.2% Triton X-100 for 7 minutes at room temperature. Then it was performed the 1 hour blocking at room temperature in TBS1x, 1% BSA (Sigma), 10% Goat Serum (Gibco).

The primary antibody incubation was performed overnight at 4°C in a wet chamber. The antibody was diluted at a previous optimize concentration in TBS1x, 1% BSA (Table 9). The next day, after temper samples at room temperature, 2 washes were performed for 5 minutes in wash buffer (TBS1x, 0.025% Triton X-100). Later, sections were incubated with the fluorescent secondary antibody (Table 10) and Hoescht (final concentration 1µg/mL) diluted TBS1x, 0.025% Triton X-100 in a wet and dark chamber at room temperature. Afterwards, 3 washes were performed for 5 minutes at room temperature with wash buffer. Finally, after the elimination of the wash buffer excess slides were mounted with VECTASHIELD Antifade Mounting Media (VECTOR Laboratories, Burlingame, CA, USA). Images were taken using Nikon Eclipse TE2000-S microscope (Nikon, Tokyo, Japan).

**Table 9: Primary Antibodies for immunofluorescence:** Recompilation of the antibodies and its optimized conditions used in the immunofluorescence technique. In this table is shown the optimized condition for the dilution and retrieval conditions. Rb: rabbit; Ms: mouse.

Antibody	Isotype	Dilution	Retrieval pH	Biological marker	Commercial brand	Commercial Reference
<b>LKB1</b> (D60C5F10)	Rb	1:250	6	-	CST	# 13031
<b>PEP1</b>	Rb	1:1,000	9	Melanocyte	Homemade	
<b>TRP2</b> (E10)	Ms	1:50	9	Melanocyte	SCBT	sc-166716
<b>p16</b> (1E12E10)	Ms	1:200	6	Senescence	Thermo Scientific	MA5-17142
<b>Ki67</b>	Rb	1:100	9-6	Proliferation	Abcam	Ab16667
<b>MET</b> (H190)	Rb	1:50	6	Proliferation	SCBT	sc-8307
<b>Cre</b>	Rb	1:100	6	-	Novus Biological	NB100-

**Table 10: Secondary Fluorescence Antibodies:** Recompilation of the secondary antibodies and its optimized conditions used in the immunofluorescence technique.

Antibody	Host	Color	Dilution	Commercial brand	Commercial Reference
Alexa Fluor 488 Mouse	Go	Green	1:200	Invitrogen	A32723
Alexa Fluor 594 Mouse	Go	Red	1:200	Invitrogen	A11032
Alexa Fluor 488 Rabbit	Go	Green	1:200	Invitrogen	A11034
Alexa Fluor 594 Rabbit	Go	Red	1:200	Invitrogen	R37121

### *iii. Chromogenic assay for Whole Skin $\beta$ -Galactosidase activity*

Whole back skin of the animal was collected without fat. Then the tissue was fixed for 30 minutes with 2% Paraformaldehyde (Sigma) and 0.2% Glutaraldehyde (Sigma) diluted in PBS. Tissue was rinsed 2 times for 15 minutes in PBS. Sample staining was performed for 12-16 hours with fresh X-gal staining solution (Table 11) at 37°C in the dark (avoid CO<sub>2</sub> incubator). Skin should be washed 2 times in PBS for 5 minutes each. Half of the tissue was conserved in 50% ethanol and embedded in paraffin blocks. Sections of 4 $\mu$ m of thickness were obtained from the paraffin-embedded tissues (Thermo Scientific Microm HM355S microtome). The other half of the skin was flash freeze in liquid Nitrogen and embedded in OCT (VWR chemicals, Radnor, PA, USA) in a Tissue-Tek Cryomold. Section of 4 $\mu$ m were mounted onto Super-frost Plus Adhesion slides (Thermo Scientific) and routinely stained with Nuclear Fast Red for 5 minutes, washed 2 times with 1x PBS and mounted with DPX solution (Sigma). Images were taken using Nikon Eclipse TE2000-S microscope (Nikon, Tokyo, Japan).

**Table 11: Recipe of  $\beta$ -Gal Staining Solution recipe.** In this table is indicated the reagents and the final concentration used in the solution. This solution should be prepared freshly.

Reagent	Final concentration
Citric Acid/Na-Phosphate Buffer	40mM
Potassium Hexacyano-ferrate (III) Solution	5mM
Potassium Hexacyano-ferrate (II) Solution	5mM
NaCl	150mM
MgCl <sub>2</sub>	2mM
X-gal Solution (diluted in N, N-dimethylformamide) (Sigma)	1mg/mL

## 5. RNA analysis techniques

### a. RNA isolation

RNA from cell lines was isolated using the Direct-Zol RNA kit (ZymoResearch Corp., Irvine CA USA) according to the manufacturer's recommendations. Each condition was performed in triplicates in order to obtain a consistent statistically data.

## b. RNA quantification and quality control

Amount of all RNA were assessed by spectrometry measurements with Nanodrop (Nanodrop Co., Wilmington, DE, USA). An idea of the quality of the sample could be predicted by the  $A_{260/A280}$  and  $A_{260/A230}$  ratio values. While 260/280 ratio will give the purity of our samples against proteins, the 260/230 shows the existence of other contaminants derived from the extraction procedure. In RNA both should stand around 2.

To confirm the integrity of the RNA samples it was performed a Bioanalyzer 2100 RNA 6000 Nano Chip (Agilent), which checks RNA quality, including assignment of the RNA Integrity Number (RIN). Only samples with a RIN value >9 were used to perform the qRT-PCR.

## c. Quantitative-Reverse Transcriptase Polymerase Chain Reaction (qRT-PCR)

Around 200ng of RNA per sample was used to obtain the cDNA using SuperScript III First-Strand Synthesis System for RT-PCR (Invitrogen, Carlsbad, CA, USA). Quantitative PCR analysis was performed using the SYBR Green PCR Master Mix Kit (Applied Biosystems Inc., Foster City, CA, USA) and the ABI Prism 7900HT Fast Real-Time PCR System (Applied Biosystems Inc.). Primers used are shown in

Table 12.

The measurements were calculated applying the  $\Delta\Delta C_t$  methods using SDS 2.3 Software (Applied Biosystems, Inc.). Values were normalized versus housekeeping gene TATA-binding protein gene (TBP) and human Peptidyl-prolyl cis-trans isomerase A (HPPIA).

Table 12: RT-PCR primers information table

Primer ID	FWR/REV	Sequence
<i>TBP</i>	FWR	CGGCTGTTTAACTTCGCTC
<i>TBP</i>	REV	CACACGCCAAGAAACAGTGA
<i>hPPIA</i>	FWR	CAGAGGCAGGAAAAGCAA
<i>hPPIA</i>	REV	AACCGCAACAGATGTCTC
<i>MAPK8</i>	FWR	CACAGTCCTGAAACGATATCA
<i>MAPK8</i>	REV	CAAGAATGGCATCATAAGCTG
<i>MAPK9</i>	FWR	TTGCATCATGGGAGAGCT
<i>MAPK9</i>	REV	TCCCAGCTGCTCAATAAC
<i>MAP2K4</i>	FWR	CCCTGGAGAGTAATGTGAAG
<i>MAP2K4</i>	REV	GAACCTGAAATGGGAAGGTGC
<i>MAP3K1</i>	FWR	CCAGGAGTAAGGAGAAAAAG
<i>MAP3K1</i>	REV	CCAGGAGTAAGGAGAAAAAG
<i>MAP3K4</i>	FWR	GCATTGGTAAAGAACGATC
<i>MAP3K4</i>	REV	CACATGGGATCTGGAAATTCAG
<i>MAP3K7</i>	FWR	CCAACCTCAGAAAAGCCA
<i>MAP3K7</i>	REV	GTGTAAGATAAGCCATTGGG
<i>BRAF</i>	FWR	GGCTCTCGGTTATAAGATGG

<i>BRAF</i>	REV	CCATGTCCCCGTTGAA
<i>cMET</i>	FWR	GCATGAAGCAGGAGGAA
<i>cMET</i>	REV	AGGGAAGGAGTGGTACAA
<i>STK11</i>	FWR	TCTACACTCAGGACTTCACG
<i>STK11</i>	REV	GTTTCATACACACGGCCTT

## 6. DNA analysis techniques

### a. Whole Exome Sequencing (WES)

Whole Exome Sequencing performance and analysis were performed by the Genomic Facility from VHIO. Briefly DNA genomic libraries were prepared from Fresh normal and tumor and FFPE-tumor DNA, followed by capture of the exome (SureSelect XT Human All Exon v5, Agilent). Libraries were sequenced in a HiSeq2000 (Illumina) instrument, 2X100, to a mean coverage of 100X. Reads were aligned, and somatic variants detected by comparison to the normal sample (VarScan2).

### b. Global genomic DNA repair assay

Back skin of *Try::CreER<sup>T2</sup>;BRaf<sup>fA/CA</sup>;Lkb1<sup>F/F</sup>* neonates of 2.5 days were collected after 20 hours and 7 days post-UVB irradiation. In order to check the LKB1 role in the DNA repair, it was included 4OHTx- and non-treated animals. No irradiated control animals were also included as negative controls. Genomic DNA was isolated using Genomic DNA was isolated using the DNeasy kit (Qiagen Mississauga, Ontario, USA). DNA was resuspended in 0.5M NaOH and 10mM EDTA Buffer. Approximately, 100ng of DNA was denatured after boiling for 10 minutes. Ice-cold ammonium acetate was added to a final concentration of 1M. Denatured DNA was spotted onto a nitrocellulose membrane pre-wetted with 6×SSC using a slot-blot apparatus (Bio-Dot SF, Bio-Rad). The filter was baked at 80°C for 2 hours and incubated with the primary and secondary antibody as explained before (Table 9). Bound antibody was detected by ECL plus (Amersham), and quantified by autoradiography. The membrane was re-probed with radiolabeled mouse genomic DNA with Ethidium Bromide (Sigma) to quantify the amount of the sample DNA per slot. The antibody signal was normalized to the amount of DNA per lane, and the rate of lesion removal was calculated and graphed.

## 7. Proliferation Assay

In order to perform this experiment, a known number of cells were seeded under the different condition studied. The same initial number of cells was seeded by duplicate in the 6-well format plate (Sarsted). Cell quantification was performed at 24, 48, 72 and 96 hours after the initial seeding. The media and standard deviation of the two values were calculated in order to obtain the value of each time point.

## 8. In vivo assay

All of the mice were cared for and maintained in accordance with animal welfare regulations under an approved protocol by the Institutional Animal Care and Use

Committee of Vall d'Hebron Research Institute (VHIR) and the Biomedical Research Park of Barcelona (Prbb).

### c. Transgenic mice

*Braf*<sup>C<sub>A</sub>/C<sub>A</sub></sup> strain has been previously described (73). *Tyr::CreER*<sup>T2</sup>;*Lkb1*<sup>F/F</sup> mice were obtained from Marcus Bosenberg (Yale University, New Haven, USA). Original *Tyr::CreER*<sup>T2</sup> mice were from Lynda Chin (Dana Farber, Boston, USA). We crossed the *Tyr::CreER*<sup>T2</sup>;*Lkb1*<sup>F/F</sup> strain with *Braf*<sup>C<sub>A</sub>/C<sub>A</sub></sup> mice and generated their mendelian-offspring in a mixed genetic background. At postnatal day 2.5, mice were topically treated once with 100µl (100mg/mL) of 4OHTx in acetone (Sigma). Both sexes were used for experiments.

### d. UV irradiation

A bank of six Phillips F40 UV lamps was used. The Spectral Power Distribution and UV monitoring regimens have been described previously (73). Neonatal mice were irradiated in single wells of a 6-well tissue culture plate (Sarsted) without the lid, placed 20cm beneath the bank of sunlamps. The exposure time was 35 minutes for a total dose of 6.24 kJ/m<sup>2</sup> UVB (280–320 nm), 3.31 kJ/m<sup>2</sup> UVA (320–400 nm), 0,03 kJ/m<sup>2</sup> UVC (280 nm), and 5.04 kJ/m<sup>2</sup> of visible radiation (400–800 nm). Exposed mice exhibited skin reddening and occasional superficial desquamation; no UV-associated neonatal mortality was noted. Data for time to tumor development was analyzed by Kaplan-Meier survival analysis.

## 9. Melanocyte isolation

The protocol was adapted from (72). The skin was removed from one or two days old pups and sterilized by immersion into 70% ethanol (Sigma) for 10 seconds followed by six washes in warm PBS, approximately 30 seconds per wash. The skin was treated with 0.25% trypsin-EDTA (Invitrogen) for maximum 1.5 hours at 37°C in a CO<sub>2</sub> incubator. The epidermis was separated from the dermis using sterile forceps and incubated for 15 minutes in 0.25% Trypsin-EDTA. The epidermis was then finely minced using a sterile scalpel and transferred to a 60cm cell culture plate. Melanocyte culture media consisted of DMEM:F12 (Biowest), 5%FBS (Biowest), 584mg/L L-Glutamine (Thermo Scientific), 200pM Cholera Toxin (Sigma), 200nM phorbol esters (TPA) (Sigma), 10U/ml penicillin and 10µg/ml streptomycin (Gibco). It is important to prepare this media fresh, as TPA is labile and it should not be warmed too many times. *In vitro* recombination was induced with 0.25µM 4OHT in DMSO.



**SUPPLEMENTARY  
INFORMATION**

## 1. Abbreviations

4-OHTx: 4-hydroxytamoxifen	IF: Immunofluorescence
4EBP1: Translation repressor protein	IHC: Immunohistochemistry
4E-BP1	IFE: Interfollicular epidermis
6-4pps: 6-4 phosphoproducts	IFE: interfollicular epidermis
A: Adenosine	INK4A: Inhibitor of cyclin-dependent kinase 4A
AKT (also PKB): Protein kinase B	IP: Immunoprecipitation
AMPK: AMP-activated protein kinase	IR: ionizing radiation
ARF: Alternative Reading Frame	LKB1: Liver Kinase B1
ATM: ataxia telangiectasia mutated kinase	LOH: Loss of heterozygosity
ATR: ATM- and rad3-related kinase	LSL: LoxP-stop-LoxP
bFGF: basic fibroblast growth factor	MAPK: mitogen-activated protein kinase
BRCA1: Breast cancer 1	MC1R: melanocortin 1 receptor
BSA: bovine serum albumin	MCSCs: Melanocyte Stem Cells
cAMP: Cyclic adenosine monophosphate	MEK: Mitogen-activated protein kinase
CBS: cystathionine-beta-synthase	MET: tyrosine-protein kinase Met
CDK4: Cyclin-dependent kinase 4	MITF: Microphthalmia-associated transcription factor
CDKN2A: Cyclin-dependent kinase inhibitor 2A	Mo25: armadillo repeat-containing mouse protein 25
cDNA: complementary DNA	mTOR: Mammalian target of rapamycin
CPDs: Ciclobutane Pyrimidine Dimers	MUP: Melanoma of unknown primary
CRD: C-terminal regulatory domain	NER: Nucleotide excision repair
CREB: cAMP response element-binding	NF1: Neurofibromin 1
DMSO: Dimethyl sulfoxide	NLS: Nuclear localizing sequence
DNA-PK: DNA-dependent protein kinase	NRD: N-terminal regulatory domain
DNA-PK: DNA-dependent protein kinase	NSCLC: Non-small cell lung cancer
DNA: deoxyribonucleic acid	OCT: Optimal cutting temperature compound
DPX: Distyrene Plasticizer Xylene	OIS: Oncogene-Induced senescence
E: Glutamic Acid	PBS: Phosphate-buffered saline
EDTA: Ethylenediaminetetraacetic acid	PI3K: Phosphoinositide 3-kinase
ERK1/2: extracellular signal-regulated kinases	PIP <sub>3</sub> : Phosphatidylinositol (3,4,5)-trisphosphate
FAMM: Familial Atypical Mole-Melanoma	PJS: Peutz-Jeghers syndrome
FBS: Fetal bovine serum	PTEN: Phosphatase and tensin homolog
GPCRs: G-protein coupled receptors	qRT-PCR: quantitative polymerase chain reaction
HDR: Homology directed DNA repair	RGP: Radial growth phase
HGF: Hepatocyte Growth Factor	RIN: RNA Integrity Number
HPPIA: human peptidyl-prolyl cis-trans isomerase A	

RNA: ribonucleic acid  
ROS: reactive oxygen species  
RPPA: Reverse phase protein array  
RSK: Ribosomal s6 kinase  
RTK: Receptor tyrosine kinase  
S6K: p70 S6 kinase  
SA- $\beta$ gal: Senescence-associated  $\beta$ -galactosidase  
SASP: Senescence-associated secretory phenotype  
SCBT: Santa Cruz Biotechnology  
Ser: Serine  
SF: Scattered Factor  
STK11 (also LKB1): Serine threonine kinase 11  
STRAD: STE20-related adaptor  
T: Thymine  
TBP: TATA-Box Binding Protein  
TBS-T: Tris-Buffered Saline Buffer with 0.1% Tween  
TBS: Tris-Buffered Saline Buffer  
TCGA: The Cancer Genome Atlas  
TERT: Telomerase reverse transcriptase  
Thr: Threonine  
TSC1/2: Tuberous sclerosis proteins 1/2  
UAT: High Technology Unit  
UV: Ultraviolet  
UVR: Ultraviolet Radiation  
V: Valine  
VGP: Vertical growth phase  
VHIR: Vall d'Hebron Research Institute  
WHO: World Health Organization  
 $\alpha$ MSH: Melanocyte-stimulating hormone

## 2. Buffer Recipe Compilation

### RIPA

50mM Hepes pH 7.4, 150mM NaCl, 1.5mM MgCl<sub>2</sub>, 10% glycerol, 4mM EDTA, 1% Triton X-100, 0.1% SDS, 1% Deoxycholate.

### Laemli buffer (protein loading buffer)

60 mM Tris-HCl (pH 6.8), 2% SDS, 10% Glycerol, 5% β-mercaptoethanol, 0.01% Bromophenol Blue.

### Staining solution

40 mM citric acid/Na phosphate buffer, 5 mM K<sub>4</sub>[Fe(CN)<sub>6</sub>] · 3H<sub>2</sub>O, 5 mM K<sub>3</sub>[Fe(CN)<sub>6</sub>], 150 mM sodium chloride, 2 mM magnesium chloride and 1 mg/ml X-gal in distilled water. Note: This solution must be prepared freshly

### 6x DNA Loading Buffer

0.25% Bromophenol blue, 0.25% Xylene Cyanol 30% Glycerol

### 50x TAE (1L)

242g Tris-base, 57.1ml Acetic acid, 100ml 0.5M sodium EDTA

### LB-Ampicillin agar

35g/L LB-Agar. Autoclave and cool down to 55°C. Add Ampicillin to a final concentration of 50µg/ml. Pour into 100 mm dishes

### LB medium

20g/L LB. Autoclave

### Resolving gel (10% acrylamide – 10ml)

4ml H<sub>2</sub>O, 3.3ml 30% Acrylamide, 2.5ml 1.5M Tris (pH 8.8), 0.1ml 10% SDS, 0.1ml 10% Amonium persulfate, 0.004ml TEMED

### Resolving gel (12% acrylamide – 10ml)

3.3ml H<sub>2</sub>O, 4ml 30% Acrylamide, 2.5ml 1.5M Tris (pH 8.8), 0.1ml 10% SDS, 0.1ml 10% Amonium persulfate, 0.004ml TEMED

### Stacking gel (5 ml)

3.4ml H<sub>2</sub>O, 0.83ml 30% Acrylamide, 0.63ml 1.0M Tris (pH 6.8), 0.05ml 10% SDS, 0.05ml 10% Amonium persulfate, 0.005ml TEMED

### 10x Tris-Glycine buffer (1L)

144g Glycine, 30g Tris-HCl, pH 8.3

### 10x TBS buffer (Tris- Buffered Saline) (1L)

160g NaCl, 4g KCl, 150g Tris-HCl, pH 8.0

### 1x TBS-0.1%Tween (1L) (WB washing Buffer)

10% 10x TBS; 0.1% Tween 20

### Running buffer

1% 10% SDS, 10% 10x Tris-Glycine (pH 8.3)

### Transfer buffer

10% 10x Tris-Glycine (pH 8.3), 20% Methanol

### Crystal Violet staining solution

0.5% Crystal Violet, 25% methanol in water

### Permeabilization Buffer (IF)

TBS1x, 0.2% Triton X-100

### Primary antibody buffer (IF)

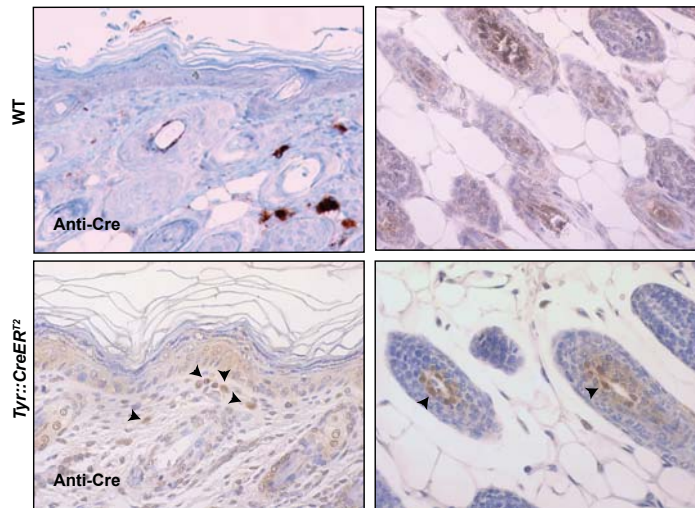
TBS1x, 1% BSA

### Blocking Buffer Solution (IF)

TBS1x, 1% BSA, 10% Goat Serum

### Wash buffer (IF)

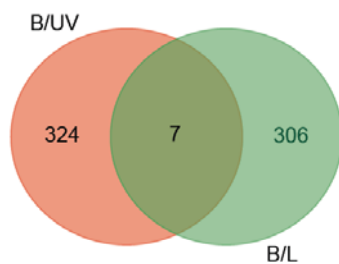
TBS1x, 0.025% Triton X-100



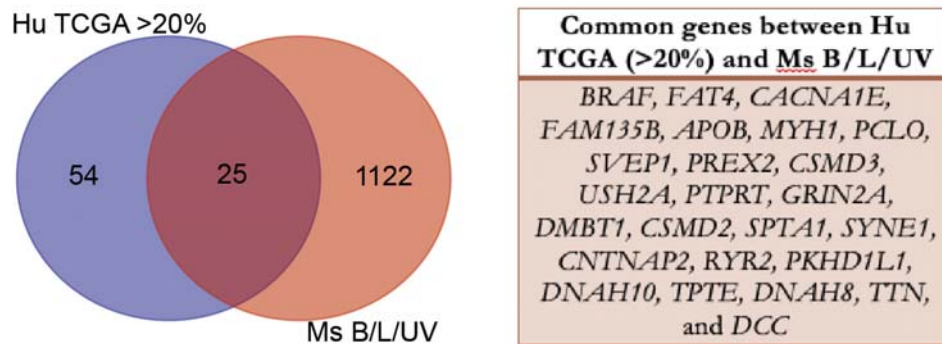
Appendix Figure 1: Tyrosinase Cre expressing cells in B/L/UV animal model. Cre immunohistochemistry to check its expression in wildtype or Tyr::CreER<sup>T2</sup> mice back skin.



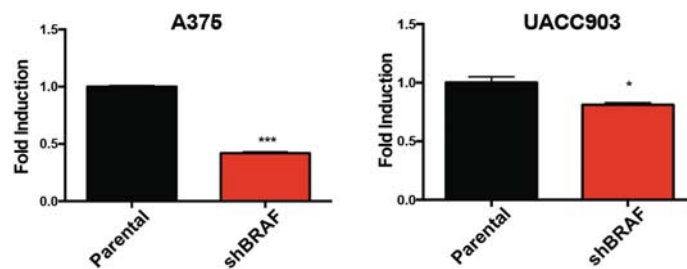
Appendix Figure 2: LKB1 reorganization in the *cMET* promoter upon UVR in A549-LKB1<sup>WT</sup> cells. LKB1-ChIP experiment A549-LKB1<sup>WT</sup> cells after 30 minutes of UVR. Red rectangle highlights the *cMET* promoter site.



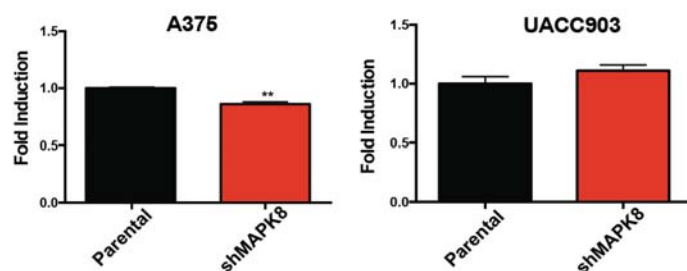
Appendix Figure 3: UVB- and LKB1 loss-induced different mutations that affect diverse biological processes in *Braf*<sup>V600E</sup>-context. Venn diagram comparing irradiated Tyr::CreER<sup>T2</sup>; *Braf*<sup>C4/+</sup> tumors (B/UV) (red, n = 3) and Tyr::CreER<sup>T2</sup>; *Braf*<sup>C4/+</sup>; *Lkb1*<sup>+/-</sup> (B/UV) (green, n = 2).



Appendix Figure 4: Comparison between human mutated TCGA Skin Cutaneous Melanoma dataset genes with >20% of frequency of alteration and the B/L/UV animal model mutated genes. At the left, comparison between genes with >20% frequency of alteration found in human TCGA Skin Cutaneous Melanoma dataset (Blue, n = 79), and unique genes altered in the B/L/UV mouse model (Red, n = 1,147). At the right, list of the 25 common genes between both groups.

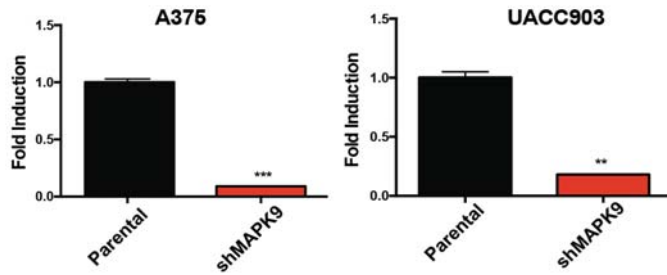


Appendix Figure 5: *BRAF* mRNA expression in parental ad *shBRAF*-transduced *BRAF<sup>V600E</sup>*-mutated human cell lines. RT-PCR representation of *BRAF* mRNA levels in different *BRAF<sup>V600E</sup>* cell lines. From left to right, it is represented the A375 and UACC903. Parental cell lines are represented in black and *shBRAF*-transduced cells in red. \* P-value ≤ 0.05; \*\* P-value ≤ 0.01; and \*\*\* P-value ≤ 0.001.

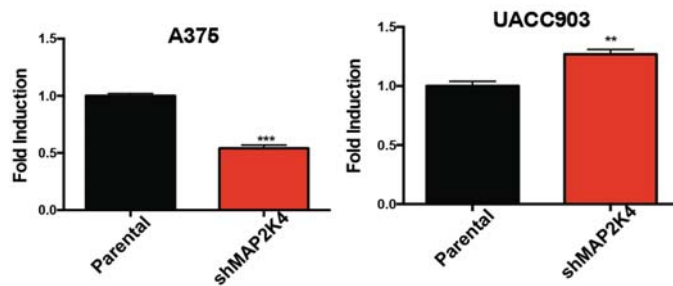


Appendix Figure 6: *MAPK8* mRNA expression in parental ad *shMAPK8*-transduced *BRAF<sup>V600E</sup>*-mutated human cell lines. RT-PCR representation of *MAPK8* mRNA levels in different *BRAF<sup>V600E</sup>* cell lines. From left to right, it is represented the A375 and UACC903. Parental cell lines are represented in black and *shMAPK8*-transduced cells in red. \* P-value ≤ 0.05; \*\* P-value ≤ 0.01; and \*\*\* P-value ≤ 0.001.

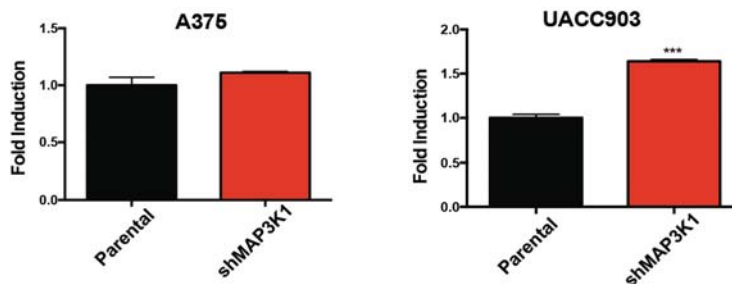




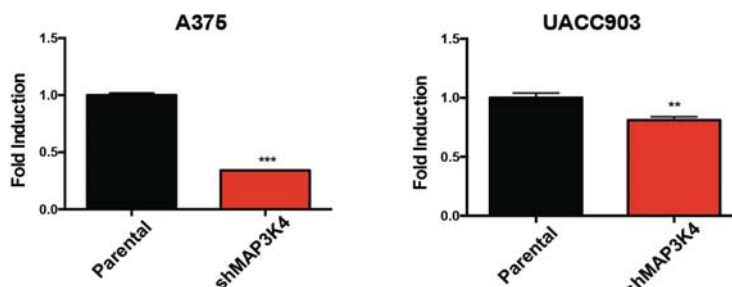
Appendix Figure 7: *MAPK9* mRNA expression in parental ad *shMAPK9*-transduced *BRAF<sup>V600E</sup>*-mutated human cell lines. RT-PCR representation of *MAPK9* mRNA levels in different *BRAF<sup>V600E</sup>* cell lines. From left to right, it is represented the A375 and UACC903. Parental cell lines are represented in black and *shMAPK9*-transduced cells in red. \* P-value $\leq$ 0.05; \*\* P-value $\leq$ 0.01; and \*\*\* P-value $\leq$ 0.001.



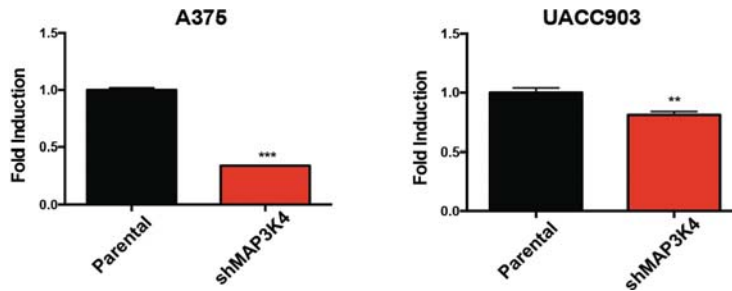
Appendix Figure 8: *MAP2K4* mRNA expression in parental ad *shMAP2K4*-transduced *BRAF<sup>V600E</sup>*-mutated human cell lines. RT-PCR representation of *MAP2K4* mRNA levels in different *BRAF<sup>V600E</sup>* cell lines. From left to right, it is represented the A375 and UACC903. Parental cell lines are represented in black and *shMAP2K4*-transduced cells in red. \* P-value $\leq$ 0.05; \*\* P-value $\leq$ 0.01; and \*\*\* P-value $\leq$ 0.001.



Appendix Figure 9: *MAP3K1* mRNA expression in parental ad *shMAP3K1*-transduced *BRAF<sup>V600E</sup>*-mutated human cell lines. RT-PCR representation of *MAP3K1* mRNA levels in different *BRAF<sup>V600E</sup>* cell lines. From left to right, it is represented the A375 and UACC903. Parental cell lines are represented in black and *shMAP3K1*-transduced cells in red. \* P-value $\leq$ 0.05; \*\* P-value $\leq$ 0.01; and \*\*\* P-value $\leq$ 0.001.



Appendix Figure 10: *MAP3K4* mRNA expression in parental ad *shMAP3K4*-transduced *BRAF<sup>V600E</sup>*-mutated human cell lines. RT-PCR representation of *MAP3K4* mRNA levels in different *BRAF<sup>V600E</sup>* cell lines. From left to right, it is represented the A375 and UACC903. Parental cell lines are represented in black and *shMAP3K4*-transduced cells in red. \* P-value $\leq$ 0.05; \*\* P-value $\leq$ 0.01; and \*\*\* P-value $\leq$ 0.001.



Appendix Figure 11: *MAP3K7* mRNA expression in parental and *shMAP3K7*-transduced *BRAF<sup>V600E</sup>*-mutated human cell lines. RT-PCR representation of *MAP3K7* mRNA levels in different *BRAF<sup>V600E</sup>* cell lines. From left to right, it is represented the A375 and UACC903. Parental cell lines are represented in black and *shMAP3K7*-transduced cells in red. \* P-value $\leq$ 0.05; \*\* P-value $\leq$ 0.01; and \*\*\* P-value $\leq$ 0.001.

Appendix Table 1: Gene family classification of the genes found in the different non-irradiated *Tyr::CreER<sup>T2</sup>;Braf<sup>Ca/+</sup>* animals. Classification of the gene in the different gene families: oncogenes, protein kinases, cell differentiation markers, transcription factors, cytokine and growth factors, and translocated cancer genes from the different animal, with the global percentage of each family.

	B12-225	Total	Percentage
<b>Oncogenes</b>	<i>Ncoa1, Nr4a3, Nsd1, Prc, Stil</i>	5	2,5
<b>Protein kinases</b>	<i>Camkk2, Pba5, Ephab6, Map3k1, Mlkl, Mylk2, Nr4a3, Prkdc, Rps6ka6</i>	9	4,5
<b>Cell diff. markers</b>	<i>Cd36, Ceacam3, Cr2</i>	3	1,5
<b>Transcription factors</b>	<i>Ncoa1, R4a3, Sap30bp, Thrb, Btb25, Zdbbc1</i>	6	3,0
<b>Cytokine and growth factors</b>	<i>Tnfsf18</i>	1	0,5
<b>Translocated cancer genes</b>	<i>Ncoa1, Nr4a3, Nsd1, Prc, Stil</i>	5	2,5
<b>Total Genes altered</b>	201	201	

Appendix Table 2: Gene family classification of the genes found in the different irradiated *Tyr::CreER<sup>T2</sup>;Braf<sup>Ca/+</sup>* animals. Classification of the gene in the different gene families: tumor suppressor, oncogenes, protein kinases, cell differentiation markers, transcription factors, homeodomain proteins, cytokine and growth factors, translocated cancer genes from the different animal, with the global percentage of each family.

	B12-213	B12-214	B12-218	Total	Percentage
<b>Tumor Suppressor</b>		<i>EP300, Tet3</i>		2	0,76
<b>Oncogenes</b>		<i>Egfr1</i>	<i>Cars, Iksf1, Ptpn11</i>	4	1,53
<b>Protein kinases</b>	<i>Rps6ka6, Stradb</i>	<i>Bmpr1B Fgfr1, Csf1r, Ephab6, Map3k4, Trpm7, Trrap</i>	<i>Camkv</i>	10	3,82
<b>Cell diff. markers</b>	<i>Ptprc, Il2RB</i>	<i>Bmpr1B Fgfr1, Csf1r</i>	<i>Itga1, Il4r, Itga2b</i>	8	3,05

<b>Transcription factors</b>	<i>Runx1t1, Tbx15, St18, Epcas1</i>	<b>Npas2</b> , <i>Ep300, Zfx</i>	<i>Ikzf1, Pknox2, Barx2, Nfx1</i>	11	4,20
<b>Homeodomain Protein</b>			<i>Nanog</i>	1	0,38
<b>Cytokine and growth factors</b>			<i>Ltpb2, Sema6b</i>	2	0,76
<b>Translocated cancer genes</b>	<i>Runx1t1, Tet1</i>	<i>EP300, Fgfr1</i>	<i>Ikzf1</i>	5	1,91
<b>Total Genes altered</b>	66	106	90	262	

**Appendix Table 3: Gene family classification of the genes found in the different non-irradiated *Tyr::CreER<sup>T2</sup>;Braf<sup>CAJ/+</sup>;LKB1<sup>+/-</sup>* animals.** Classification of the gene in the different gene families: oncogenes, protein kinases, cell differentiation markers, transcription factors, homeodomain proteins, cytokine and growth factors, and translocated cancer genes from the different animal, with the global percentage of each family.

	B12-226	B12-227	Total	Percentage
<b>Oncogenes</b>	<i>Aspscr1, Cic, Col1a1, Myb, Pax5</i>	<i>Hsp90ab1</i>	6	1,9
<b>Protein kinases</b>	<i>Mark2, Plk1, Wnk3</i>		3	0,9
<b>Cell diff markers</b>	<i>Cd97</i>		1	0,3
<b>Transcription factors (TF)</b>	<i>Cic, Irf7, Lf15, Mga, Myb, Otud7b, Pax, Phf3, Rax, Rfx4, Tbx2, Tsc22d2, Tulp1, Tulp4</i>	<i>Hira, Hoxb7, Neurod6, Sox18</i>	18	5,6
<b>Homeodomain Protein</b>	<i>Pax5, Rax</i>	<i>Hoxb7</i>	3	0,9
<b>Cytokine and growth factors</b>	<i>Calcb</i>	<i>Gdf7, Scg2</i>	3	0,9
<b>Translocated cancer genes</b>	<i>Aspscr1, Cic, Col1a1, Myb, Pax5</i>	<i>Hsp90ab1</i>	6	1,9
	231	90	321	

**Appendix Table 4: Gene family classification of the genes found in the different irradiated *Tyr::CreER<sup>T2</sup>;Braf<sup>CAJ/+</sup>;LKB1<sup>+/-</sup>* animals.** Classification of the gene in the different gene families: tumor suppressor, oncogenes, protein kinases, cell differentiation markers, transcription factors, homeodomain proteins, cytokine and growth factors, translocated cancer genes from the different animal, with the global percentage of each family.

	B12-223	B12-228	Total	Percentage
<b>Tumor Suppressor</b>	<i>Tet2</i>		1	0,43
<b>Oncogenes</b>	<i>Cic, Arghgef12, Lpp</i>	<i>Hras</i>	4	1,73
<b>Protein kinases</b>	<i>Mast4, Wnk2, Ptk2b, Pak4, Peak1</i>	<i>Dapk1, Dyrk1b, Gucy2f, Mapk10, Obscn, Pdik11, Ror2, Slk, Ttn</i>	14	6,06
<b>Cell diff. markers</b>	<i>Ncam1, Tlr6, Itgae, Art1</i>	<i>Enpp3, Sema4d, Tnfsf8</i>	7	3,03
<b>Transcription factors</b>	<i>Triobp, Nanog, Cic, Prdm15, Fosh, Scml2</i>	<i>Arid3b, Atf6b, Egr4, Ldoc1, Mlxipl, Prdm1, Ring1, Scrt2, Six4, Snai3, Stat4, Tbr1, Zmym3, Znf318</i>	20	8,66
<b>Homeodomain Protein</b>	<i>Nanog</i>	<i>Six4</i>	2	0,87
<b>Cytokine and growth factors</b>	<i>Tg, Infb1</i>	<i>Bmp8b, Sema3f, Sema4d, Tnfsf8</i>	6	2,60
<b>Translocated cancer genes</b>	<i>Cic, Arghgef12, Lpp</i>		3	1,30
<b>Total Genes altered</b>	113	118	231	

Appendix Table 5: Venn diagram genes from the comparison between irradiated and non-irradiated *Tyr::Cre<sup>ER</sup>;Braf<sup>CA1</sup>* mice.

Animal group	Gene ID
Common (8 genes)	<i>Rps6ka6, Dnab8, EphA6, Ccdc22, Ehhp111, Cilp, Col6a5, Rims2</i>
<i>Tyr::CreER<sup>T2</sup>;Braf<sup>CA1</sup></i> (190 genes)	<i>1700017B05Rik, 1700125H20Rik, 2610034M16Rik, 4921504E06Rik, 4933402J07Rik, 5031439G07Rik, 6430573F11Rik, A1cf, Abca15, Abcc2, Abi2, Ache, Actg2, Actl9, Adamts9, Adamtsl2, Agr2, Aldh1b1, Ankle2, Ankrd26, Arap3, Arhgef5, Armc6, Atg9b, Bbmt, C1s2, Cacna1f, Cacnb2, Camkk2, Catsper1, Ccbr1, Cd36, Ceacam3, Cep5711, Cfb, Chil3, Clasp2, Clnk, Cntn1, Cntnap5c, Col4a3, Colq, Cpa5, Cr2, Csl, Cts8, Cul4b, Cyp2c68, D430041D05Rik, Dag1, Dcc, Dclre1a, Ddx54, Dnajc13, Dnajc14, Dock1, Dppa5a, Dsg1b, Ehmt1, Eml3, Epb4.1, EphA5, Epm2a, F830016B08Rik, Fam71e2, Fcnb, Fech, Fgg, Fnip2, Frmd3, Frmd5, Fsch, Gdapl11, Gna15, Golgb1, Gpr111, Gpr65, Grin2a, Grin3a, Hps5, Il12rb2, Il1r11, Inpp4b, Itgb8, Kcnab1Kcnj15, Kcnj6, Kif9, Kmo, Krt72, Lgals12, Lpl, Lrig3, Map3k1, Map7, Mapk8ip2, Mdfi, Mgat5b, Mlkl, Muc19, Mug2, Mybp1, Myb1, Mylk2, Myom2, Ncf4, Ncoa1, Neo1, Neurl3, Nme5, Npy2r, Nrep, Nsd1, Os9, Otud7a, Pab, Pcdhb4, Pcnxl3, Pde6c, Pkd1l2, Pklr, Pla2r1, Ppp1r42, Prmel5, Prmel6, Prcv, Prex2, Prkdc, Prss44, Ptchd1, Ptprq, Rab11fp4, Rab6b, Rasgrp3, Rbfox1, Rbm47, Rdb19, Rbpn1, Rimbp2, Rnpepl1, Safb2, Sap30bp, Scaper, Scd3, Sctr, Seb11, Serac1, Serpina3j, Sh3bp4, Shq1, Sipa1, Ski, Slc10a4, Slc15a3, Slc17a8, Slc18a1, Slc25a13, Slc25a2, Slc5a9, Slc9a3, Snaip, Stil, Stxbp5, Tas1r2, Tbc1d4, Tec, Thrb, Tmem8c, Tmprss11c, Tnfrsf18, Tpte, Trim34b, Tspan10, Ubr2, Unc79, Vmn1r194, Vmn1r225, Vmn1r87, Vmn2r1, Vmn2r101, Vmn2r25, Vmn2r57, Vwce, Wdfy4, Zan, Zbtb25, Zdbbc1, Zfp341, Zfp474, Zfp575</i>
<i>Tyr::CreER<sup>T2</sup>;Braf<sup>CA1</sup>+UV</i> (323 genes)	<i>1810046K07Rik, 2010106E10Rik, 2610528J11Rik, 3110007F17Rik, 3632451O06Rik, 3830406C13Rik, 4930519F16Rik, 4930578C19Rik, 4933430I17Rik, 5730559C18Rik, Abca8b, Abcc10, Abcc6, Abi3, Acsm5, Adam18, Adcy8, Adra1a, Afap1, Aldoart1, Amer1, Amer3, Aox4, Arhgef6, Armcx6, Arsb, Asnsd1, Atxn7l1, B3gat1, B4galnt4, Barx2, Birc2, Birc7, Bmpr1b, Bptf, C1rl, C2cd3, Caap1, Cacna1e, Camkv, Capn8, Cars, Catsperb, Ce2d2a, Ccdc108, Ccdc183, Ccdc185, Ccdc39, Cd209e, Cdr1, Cenpi, Cep350, Cfap57, Cfap74, Chil6, Cbrl2, Chst7, Ciapin1, Cib1, Cidec, Clstn2, Clta, Cmya5, Cntnap5a, Col10a1, Col12a1, Crb2, Crxos, Cryge, Csf1r, Csmid2, Csmid3, Cul7, Cyp11b2, Cyp2j9, Cyp4a30b, Cystm1, D15Ert621e, Dear1, Dfna5, Dfnb59, Dhx34, Diras2, Dkk1l, Dnab1, Dnab10, Dnmbp, Dnmt3a, Dock10, Dock3, Dock8, Dok7, Dupd1, E130308A19Rik, Ehhadh, Enox2, Ep300, Epas1, Errf1, Exd1, Fam154b, Fam171a2, Fat1, Fat4, Fbjf1, Fgfr1, Flna, Flnc, Fndc1, G6pd2, Gabbr2, Gal3st4, Galnt6, Galr2, Gnat1, Gpsm1, Hacl1, Hars2, Has1, Hgfc1, Herc3, Hid1, Hist1b2bb, Hkdc1, Hmgcll1, Hpse2, Htr1d, Ice2, Ifi202b, Ifi74, Ikbzf1, Il2rb, Il4ra, Iqgap2, Itga1, Itga2b, Kirrel3, Klhl14, Klra8, Kndc1, Krba1, Krcv1, Krt76, Kynu, Lcn6, Lctl, Lmnb1, Lnc1, LOC100504608, Lrba, Lrp4, Ltbp2, Ly6g6e, Macf1, Magee1, Magee2, Map3k4, Mbl1, Mefv, Mfap3l, Micalcl, Mnd1, Mocs3, Mpl, Mrgprx1, Msh4, Msh5, Mtmr14, Mup17, Myh3, Myh9, Myo16, Nagpa, Naip7, Nap112, Ndst3, Ndufs3, Nefm, Neto1, Nfxc1, Ninl, Nhrp4g, Nos3, Npas2, Nup210l, Nxp3, Oat, Oosp3, Osbpl5, Osbpl6, P2rx7, P4htm, Parp14, Pcdh11x, Pcdhb18, Pcdh1b, Pclo, Pde5a, Pdlim2, Piezo2, Pipox, Pkd1, Pkhd11l, Pknoc2, Pla2g2a, Plekha6, Pnck, Pnmal1, Poc5, Polg, Ppp4c, Prdx3, Prmt6, Psme1, Ptpn11, Ptpre, Ptptr, Prr14, Qrfpr, Rab44, Racgap1, Rai1, Rasa4, Rbbp8nl, Rbm26, Rbm41, Rbobb1, Rnf207, Rnfj2, Rnpep, Rpl18, Runx1t1, Scgb2b19, Scn2a1, Sdk1, Sema6b, Serpine1, Setx, Sfmbt1, Sh3bp1, Sh3kbp1, Shkbp1, Slc16a9, Slc22a21, Slc24a3, Slc35a5, Slc38a4, Slc38a5, Slc45a4, Slc9c1, Slfn8, Smcr8, Smand1, Snx21, Sobp, Sorbs2, Spag6, Spata31d1d, Spta1, Srsf9, St18, Stard13, Steap1, Stradb, Sult1e1, Supt6, Svopl, Syndig1l, Synpo, Taar6, Tanc1, Tas2r130, Tas2r139, Tas2r144, Tbx15, Tekt5, Tet1, Tet3, Thbs4, Tiam2, Tmprss7, Tnc, Tnfrsf3, Tnfrsf19, Tnn, Tns1, Trim69, Triml2, Trpm7, Trpv4, Trrap, Tic3, Tuba3a, Ubd1, Unc5a, Upb1, Upf1, Vmn1r22, Vmn1r5, Vmn2r109, Vmn2r113, Vmn2r124,</i>

<i>Vmn2r63, Vmn2r82, Vmn2r88, Vmn2r9, Vmn2r97, Vrtn, Vva5b2, Wdr43, Wdr75, Wdr77, Wisp3, Zap70, Zc2hc1b, Zcabc3, Zfp384, Zfp385b, Zfp763, Zfp764, Zfp831, Zfp961, Zjx</i>
---

Appendix Table 6: Venn diagram genes from the comparison between non-irradiated *Tyr::CreER<sup>T2</sup>;Braf<sup>CA/+</sup>* and non-irradiated *Tyr::CreER<sup>T2</sup>;Braf<sup>CA/+</sup>;Lkb1<sup>+/-</sup>* mice.

Animal group	Gene ID
<b>Common (2 genes)</b>	<i>Ehmt1, Lrig3</i>
<b><i>Tyr::CreER<sup>T2</sup>;Braf<sup>CA/+</sup></i> (196 genes)</b>	<i>1700017B05Rik, 1700125H20Rik, 2610034M16Rik, 4921504E06Rik, 4933402J07Rik, 5031439G07Rik, 6430573F11Rik, A1cf, Abca15, Abcc2, Abi2, Ache, Actg2, Actl9, Adams19, Adams12, Agr2, Aldh1b1, Ankle2, Ankrd26, Arap3, Arhgef5, Armc6, Atg9b, Bbmt, C1s2, Cacna1f, Cacnb2, Camkk2, Catsper1, Ccdc22, Ccbr1, Cd36, Ceacam3, Cep57l1, Cjfb, Chil3, Cilp, Clasp2, Clnk, Cntn1, Cntnap5c, Col4a3, Col6a5, Colq, Cpa5, Cr2, Csl, Cts8, Cul4b, Cyp2c68, D430041D05Rik, Dag1, Dcc, Dclre1a, Ddx54, Dnab8, Dnajc13, Dnajc14, Dock1, Dppa5a, Dsg1b, Ebbp11l, Eml3, Epb4.1, EphA5, EphA6, Epm2a, F830016B08Rik, Fam71e2, Fcnb, Fech, Fgg, Fnip2, Frmd3, Frmd5, Fscb, Gdap11l, Gna15, Golgb1, Gpr111, Gpr65, Grin2a, Grin3a, Hps5, Il12rb2, Il1rl1, Inpp4b, Itgb8, Kcnab1, Kenj15, Kcnj6, Kij9, Kmo, Krt72, Lgals12, Lpl, Map3k1, Map7, Mapk8ip2, Mdfi, Mgat5b, Mlkl, Muc19, Mug2, Myhpc1, Myh1, Mylk2, Myom2, Ncf4, Ncoa1, Neo1, Neur13, Nme5, Npy2r, Nrep, Nsd1, Os9, Otud7a, Pab, Pcdhb4, Pcnxl3, Pde6c, Pkd1l2, Pklr, Pla2r1, Ppp1r42, Pramel5, Pramel6, Prc, Prex2, Prkdc, Prss44, Ptchd1, Ptpnq, Rab11jfp4, Rab6b, Rasgrp3, Rbfox1, Rbm47, Rdb19, Rlhp1, Rimbp2, Rims2, Rnpep1l, Rps6ka6, Safb2, Sap30bp, Scaper, Sed3, Sctr, Seb1, Serac1, Serpina3j, Sh3bp4, Shq1, Sipa1, Ski, Slc10a4, Slc15a3, Slc17a8, Slc18a1, Slc25a13, Slc25a2, Slc5a9, Slc9a3, Snaip, Stil, Stxcp5, Tas1r2, Tbc1d4, Tec, Thrb, Tmem8c, Tmpnrs1c, Tnfrsf18, Tpte, Trim34b, Tspan10, Ubr2, Unc79, Vmn1r194, Vmn1r225, Vmn1r87, Vmn2r1, Vmn2r101, Vmn2r25, Vmn2r57, Vwce, Wdfy4, Zan, Zbtb25, Zdbbc1, Zfp341, Zfp474, Zfp575</i>
<b><i>Tyr::CreER<sup>T2</sup>;Braf<sup>CA/+</sup>;Lkb1<sup>+/-</sup></i> (312 genes)</b>	<i>1700013G24Rik, 1810030O07Rik, 2310022A10Rik, 2610028H24Rik, 27000097O09Rik, 4833423E24Rik, 4930402K13Rik, 4930503L19Rik, 4933413G19Rik, Aars2, Abca2, Abcf3, Abtb1, Actl6b, Actr2, Adar, AF529169, AI464131, Akap11, Aldh1l2, Alox15, Alox8, Ank2, Ankrd50, Apob, Arhgap31, Armcx3, Arpp21, Aspsr1, Atg3, Atp6ap1, Atp7b, Atp8b4, Bag2, Baiap2l2, Bbs4, Bco2, Bcor1l, C1qtnf4, Cacna1i, Calcb, Calr4, Camsap1, Camsap2, Car14, Ccdc114, Ccdc163, Ccdc33, Ccdc71, Cd97, Cdc42ep3, Cdhrl, Cep350, Cfap44, Chd7, Chtf18, Cic, Cldn14, Clec18a, Cntnap1, Col1a1, Col4a6, Col8a2, Crim1, Crocc, Crybb3, Crygd, Csgalnact2, Csm2, Cspg4, Ctnnd1, Ctnn, Cul9, Cxxc5, Cyp4a14, Dctd, Dcam1d2, Ddi1, Dgkd, Dip2c, Dkk2, Dlgap3, Dlgap4, Dmd, Dnab17, Dnajc2, Dnase1l1, Dnmt3b, Dtx3l, Dusp3, Elp5, Emp3, Eps8l3, Ergic3, Erlec1, Ero1l, Etfjd, Evc2, F8, Fam160b2, Fant1, Fasn, Fat4, Fbxo2, Fklp8, Fmn2, Fmn3, Folr4, Foxp4, Frem1, Fst, Ftl1, Fut1, Fzd2, Gabrr1, Gadd45gip1, Galnt7, Gent3, Gdf7, Glipr1, Glt25d1, Gm15800, Gm4922, Gprin, Gps1, Grasp, Grin2d, Grwd1, Hapln4, Hcn4, Hira, Hoxb7, Hs3st6, Hsd3b7, Hsp90ab1, Htt, Ice2, Ifnlr1, Igsf9b, Inpp1l, Ip6k3, Irf7, Itih2, Itpka, Kbtbd4, Kenb1, Kong2, Kenb7, Kenn3, Khgrp, Kij26b, Kij27, Kij5a, Klf15, Kmt2d, Kpna3, Krtap10-10, Krtap4-6, Lamb2, Lame3, Lancl2, Lman2, Lrfn2, Lrp3, Lrp4, Lrrc28, Mark2, Matn2, Mbd6, Mef2, Mcm5, Mettl21c, Mga, Mlf2, Mlph, Msln, Myb, Mychpap, Myb15, Myo10, Nbea, Nbeal2, Ndufaf7, Nes, Neurod6, Nipa1, Nlrc5, Nlrp12, Nol8, Npat, Nrn1, Ntn5, Ning2, Ntsr2, Nup155, Nup62-il4i1, Nwd2, Nxp4, Odf2, Otud7b, P4ha3, Paqr3, Parp8, Pax5, Pcdhgb1, Pcdhgc4, Pdlim3, Pds5b, Pdxd2, Pdxdk1, Pglyrp2, Phactr3, Pbc2, Phex, Phf3, Phldb1, Pigx, Pitpnm2, Pkdrej, Pkfp4, Pla2g15, Plec, Plekhh6, Plk1, Pof1b, Pole, Ppan, Prcp, Psmb8, Psmg1, Ptchd2, Ptpn13, Ptpnrd, Pzp, Rab5c, Rasgrp4, Rassf5, Rax, Rfx4, Rgl3, Rgmb, Rgs3, Rbg, Rin1, Rnf165, Rpl13a, Rusc1, Ryr3, Scara3, Sed2, Scg2, Scn2a1, Sec14l1, Sec31a, Shc4, Shroom2, Simc1, Slc10a6, Slc26a4, Slc6a1, Slc7a4, Slc8a2, Sox18, Spac1, Sphk2, Sybm, Syne2, Szl2, Tbc1d2, Tbx2, Tgfb3, Tgm3, Tlbs4, Tbsd4, Thtpa, Tm9sf2, Tmc5, Tmem72, Tns3, Treb, Tril, Trim66, Trim9, Tro, Tsc22d2, Ttc23l, Tti1, Tyhb2, Tubgp2, Tulp1, Tulp4, Unc13b, Unc5b, Upk1b, Ush2a, Usp11, Usp15, Usp34,</i>



*Usp38, Usp53, Vmn2r6, Vmn2r60, Vps13b, Vps13d, Wbp2nl, Wdr17, Wnk3, Wrap53, Zar1l, Zc3b12d, Zcabc16, Zfp703*

Appendix Table 7: Venn diagram genes from the comparison between non-irradiated and irradiated *Tyr::CreER<sup>T2</sup>;Braf<sup>CA/+</sup>;Lkb1<sup>+/-</sup>* mice.

Animal group	Gene ID
<b>Common (13 genes)</b>	<i>Bcor1l, Cep350, Cic, Csm2, Evc2, Ip6k3, Itih2, Kmt2d, Mga, Mlph, Phex, Plec, Shroom2</i>
<b><i>Tyr::CreER<sup>T2</sup>;Braf<sup>CA/+</sup>;Lkb1<sup>+/-</sup></i> (301 genes)</b>	<i>1700001C19Rik, 2610015P09Rik, 4921507P07Rik, 4931406B18Rik, 4933433C11Rik, Abca12, Abca6, Abeg3, Aess1, Afp, Abctf1, Aifm1, Aipl1, Akr1c12, Alb, Aldh1a3, Alox12e, Alpi, Ambra1, Aox1, Apha1, Appbp2, Arcn1, Arhgap27, Arhgef12, Arhgef7, Arid3b, Arid5a, Art1, Aspm, Atf6b, Bbox1, BC068157, Bmp8b, Bpifc, Bsn, Capn8, Carkd, Casp8, Cav1, Ccdc141, Ccdc158, Ccdc185, Ccdc64, Cd209f, Cdh20, Cdh7, Cenpf, Cep135, Cep290, Ces3a, Cgn, Chrbn1, Clea2, Clec4f, Clstn2, Cntnap2, Col11a1, Col23a1, Col25a1, Col3a1, Col5a1, Colect1, Cpa3, Cpel1, Crbr2, Csf3r, Csn1s2b, Cybr1, Cyp11b2, Cyp2d22, Cyp3a25, D10Bwg1379e, D930015E06Rik, Dap3, Dapk1, Dazl, Dbb, Dcn1, Ddx47, Dmbt1, Dmkn, Dnab1, Dnab10, Dolpp1, Dopey1, Dppa3, Dpysl3, Dyrc1b, Egflam, Egr4, Elfl1, Enah, Enam, Enpp3, Eyt3, F7, Fads1, Fam132b, Fam135b, Fam13c, Fam160a1, Fam186b, Fam24a, Fbxo4, Fbxv24, Flna, Fosb, Fpr3, Frem2, Frmpd1, Gas2l2, Gcfi2, Gen1l1, Ggyl1, Gpkon, Gpr149, Grap, Gria4, Grid2, Gucy2f, Hc, Hkdc1, Hnrnpu, Hnrnpu2, Hras, Hscb, Hsdl1, Ifnb1, Il23r, Inpp4a, Itgae, Kank1, Katnbl1, Kcnc2, Kcnt2, Kif14, Krtap11-1, Lama2, Lamb3, Ldoc1, Limk2, Lipc, Lpbn3, Lpp, Lrp1, Lypla1, Macc1, Magee1, Map1a, Mapk10, Mapkbp1, Mast4, Mep1a, Mlxipl, Mmp10, Mnd1, Mpeg1, Mrgrb2, Mrps36, Muc5b, Mug1, Mvk, Myb13, Myb6, Myb7, Myl12b, Myo5a, Mypn, N6amt1, Naip1, Naip7, Nanog, Ncam1, Neckap5, Neckap5l, Ndst3, Nbsl1, Nipbl, Nii1, Nos3, Nubpl, Nudt3, Nyap1, Obx1, Obscn, Oosp3, Otog, P4bb, Pabpc2, Pabpc4, Pak4, Pard3b, Pblid2, Pedba2, Pedbb18, Pedbb19, Pdik1, Peak1, Perm1, Phactr4, Pla2r1, Plaa, Pleb4, Ppfia2, Pram6l, Prb1, Prdm1, Prdm15, Prl3b1, Prl8a6, Pichd3, Ptk2b, Ptpn3, Pygm, Rad21, Raver1, Rcor1, Rps18, Rgs14, Ring1, Rnf145, Ror2, Rorb, Rpl11, Rplp0, Rsad1, Rsf1, Ryr2, Sae1, Scaf8, Scml2, Sort2, Sec24c, Sel1l, Sema3f, Sema4d, Serpina3k, Serpina7, Sgca, Sh3rf1, Sipa1l2, Six4, Slc14a2, Slc37a3, Slc38a10, Slc44a5, Slc6a18, Slc8a1, Slitrk4, Slk, Smad9, Smarcc1, Smg9, Snai3, Sorbs3, Spata31d1b, Sptbn4, Srp72, Stat4, Su2a, Svep1, Syap2, Syne1, Synj2, Synpo2, Syt12, Taar8b, Tarm1, Tars2, Tas2r117, Tax, Tbr1, Tdrd5, Tet2, Tfjp11, Tg, Thnsl1, Timm23, Tle1, Tlr12, Tlr6, Tmte3, Tnfrsf21, Tnfsf8, Tnn, Tpcn1, Trappc9, Trioip, Trpc5, Trpv4, Tspan10, Till11, Ttn, Uba7, Ugt2b38, Ubrf1bp1, Uqcrc2, Usp17le, Usp26, Vmn1r12, Vmn1r174, Vmn2r14, Vmn2r26, Vmn2r51, Vmn2r57, Vmn2r65, Vmn2r66, Vmn2r7, Vmn2r86, Wdr19, Wdr95, Wig, Wnk2, Xpo7, Zfp318, Zfp366, Zmym3, Znf512b, Zscan4d, Zsvim2, Zyx</i>
<b><i>Tyr::CreER<sup>T2</sup>;Braf<sup>CA/+</sup>;Lkb1<sup>+/-</sup></i> +UV (322 genes)</b>	<i>1700013G24Rik, 1810030O07Rik, 2310022A10Rik, 2610028H24Rik, 2700097O09Rik, 4833423E24Rik, 4930402K13Rik, 4930503L19Rik, 4933413G19Rik, Aars2, Abca2, Abcf3, Abtb1, Actl6b, Actrt2, Adar, AF529169, AI464131, Akap11, Aldb1l2, Alox15, Alox8, Ank2, Ankerd50, Apob, Arhgap31, Armcc3, Arpp21, Aspsr1, Atg3, Atp6ap1, Atp7b, Atp8b4, Bag2, Baiap2l2, Bbs4, Bco2, C1qtnf4, Cacna1i, Calcb, Calr4, Camsap1, Camsap2, Car14, Ccdc114, Ccdc163, Ccdc33, Cdc71, Cd97, Cdc42ep3, Cdb1, Cjap44, Cdh7, Cbtf18, Cldn14, Clec18a, Cntnap1, Col1a1, Col4a6, Col8a2, Crim1, Crocc, Crybb3, Crygd, Csgalnact2, Cspg4, Ctnd1, Citn, Cul9, Cxnc5, Cyp4a14, Dctd, Dcn1d2, Ddi1, Dgkd, Dip2c, Dkk2, Dlgap3, Dlgap4, Dmd, Dnab17, Dnajc2, Dnase1l1, Dnmt3b, Dtx3l, Dusp3, Ehmt1, Elp5, Emp3, Eps8l3, Ergic3, Erlec1, Ero1l, Etfidb, F8, Fam160b2, Fan1, Fasn, Fat4, Fbxo2, Fkbp8, Fmn2, Fmn3, Folr4, Foxp4, Frem1, Est, Fil1, Fut1, Fzd2, Gabrr1, Gadd45gip1, Galn7, Gcnt3, Gdf7, Glipr1, Glt25d1, Gm15800, Gm4922, Gprin1, Gps1, Grasp, Grin2d, Grvd1, Hapln4, Hon4, Hira, Hoxb7, Hs3st6, Hsd3b7, Hsp90ab1, Htt, Ice2, Ifnlr1, Igsf9b, Inpp1l, Irf7, Itpka, Kbtbd4, Kcnb1, Kcng2, Kcnh7, Kcnn3, Khsrp, Kif26b, Kif27, Kif5a, Klf15, Kpna3, Krtap10-10, Krtap4-6, Lamb2, Lamc3, Lancel2, Lman2, Lrjn2, Lrig3, Lrp3, Lrp4, Lrrc28, Mark2, Matn2, Mbd6, Mef2, Mem5, Mettl21c, Mlf2, Msln, Myb, Mycbp, Myb15, Myo10, Nbea, Nbeal2, Ndufaf7, Nes, Neurod6, Nipa1, Nlrc5, Nlrp12, Nol8, Npat, Nrn1, Ntn5, Ntng2, Ntsr2, Nup155, Nup62-il4i1, Nwd2, Nxp4, Odf2, Otud7b, P4ba3, Paqr3, Parp8, Pax5, Pcdhgb1, Pcdhgc4, Pdlim3, Pds5b, Pdza2, Pdzk1, Pglyrp2, Phactr3, Phc2, Phf3, Phldb1, Pixg, Pitpnm2, Pkdrej, Pkp4, Pla2g15, Plekhg6, Plk1, Pof1b, Pole, Ppan, Prcp, Psmb8, Psmg1, Pchd2, Ptpn13, Ptpnd, Pzp, Rab5c, Rasgrp4, Rassf5, Rax, Rfx4, Rgl3, Rgmb, Rgs3, Rhcg, Rin1, Rnf165, Rpl13a, Rusc1, Ryr3, Scar3, Scd2, Scg2, Scn2a1, Sec14l1, Sec31a, Shc4, Simc1, Slc10a6, Slc26a4, Slc6a1, Slc7a4, Slc8a2, Sox18, Spatc1,</i>

	<i>Sphk2, Sybu, Syne2, Szt2, Tbc1d2, Tbx2, Tgfb3, Tgm3, Thbs4, Thsd4, Thtpa, Tm9sf2, Tmc5, Tmem72, Tns3, Treb, Tril, Trim66, Trim9, Tro, Tsc22d2, Ttc23l, Tti1, Tyhb2, Tubgp2, Tulp1, Tulp4, Unc13b, Unc5b, Upk1b, Ush2a, Usp11, Usp15, Usp34, Usp38, Usp53, Vmn2r6, Vmn2r60, Vps13b, Vps13d, Wbp2nl, Wdr17, Wnk3, Wrap53, Zar1l, Zc3b12d, Zcchc16, Zfp703</i>
--	--

Appendix Table 8: Venn diagram genes from the comparison between irradiated *Tyr::CreER<sup>T2</sup>;Braf<sup>CA/+</sup>* and *Tyr::CreER<sup>T2</sup>;Braf<sup>CA/+</sup>;Lkb1<sup>+/-</sup>* mice.

Animal group	Gene ID
<b>Common (19 genes)</b>	<i>Capn8, Ccdc185, Cep350, Clstn2, Csm2, Cyp11b2, Dnab1, Dnab10, Flna, Hkdc1, Magee1, Mnd1, Naip7, Ndst3, Nos3, Oosp3, Pcdhb18, Tnn, Trpr4</i>
<b><i>Tyr::CreER<sup>T2</sup>;Braf<sup>CA/+</sup>+UV (312 genes)</i></b>	<i>1810046K07Rik, 2010106E10Rik, 2610528J11Rik, 3110007F17Rik, 3632451O06Rik, 3830406C13Rik, 4930519F16Rik, 4930578C19Rik, 4933430I17Rik, 5730559C18Rik, Abca8b, Abcc10, Abcc6, Abi3, Acsm5, Adam18, Adcy8, Adra1a, Afap1, Aldoart1, Amer1, Amer3, Aox4, Arhgef6, Armx6, Arsb, Asnsd1, Atxn7l1, B3gat1, B4galnt4, Barx2, Bir2, Bir7, Bmpr1b, Bptf, C1rl, C2cd3, Caap1, Cacna1e, Camkv, Cars, Catsperb, Cc2d2a, Ccdc108, Ccdc183, Ccdc22, Ccdc39, Cd209e, Cdr1, Cenpi, Cfap57, Cfap74, Chil6, Chrdl2, Chst7, Ciapin1, Cib1, Cidec, Cilp, Clta, Cmya5, Cntnap5a, Col10a1, Col12a1, Col6a5, Crb2, Crxos, Crygc, Csf1r, Csm2, Cul7, Cyp2j9, Cyp4a30b, Cystm1, D15Ert621e, Dear1, Dfna5, Dfnb59, Dhx34, Diras2, Dkk1l, Dnab8, Dnmhp, Dnmt3a, Dock10, Dock3, Dock8, Dok7, Dupd1, E130308A19Rik, Ebbp1l1, Ebbadb, Enox2, Ep300, Epas1, Eph6, Errfi1, Exd1, Fam154b, Fam171a2, Fat1, Fat4, Fbf1, Fgfr1, Flnc, Fndc1, G6pd2, Gabbr2, Gal3st4, Galnt6, Galr2, Gnat1, Gpsm1, Hacl1, Hars2, Has1, Hcfc1, Herc3, Hid1, Hist1b2fb, Hmgcll1, Hpse2, Htr1d, Ice2, Ifi202b, Ifi74, Ikc3l, Il2rb, Il4ra, Iqgap2, Itga1, Itga2b, Kirrel3, Klhl14, Klna8, Kndc1, Krba1, Krcl1, Krt76, Kynu, Lcn6, Lctf, Lmnb1, Lnx1, LOC100504608, Lrba, Lrp4, Libp2, Ljy6g6e, Macf1, Magee2, Map3k4, Mbl1, Mefj, Mfap3l, Micalc, Mocs3, Mpl, Mrp3r1, Msh4, Msh5, Mtmr14, Mup17, Myb3, Myb9, Myo16, Nappa, Nap1l2, Ndufs3, Nefm, Neto1, Nfx1, Ninl, Nlrp4g, Npas2, Nup210l, Nxp3b3, Oat, Osbp15, Osbp16, P2rx7, P4btm, Parp14, Pcdh11x, Pced1b, Pclo, Pde5a, Pdlim2, Piezo2, Pipox, Pkd1, Pkhd1l1, Pkenox2, Pla2g2a, Plekha6, Pnck, Pnmall1, Poc5, Polg, Ppp4c, Prdx3, Prmt6, Psme1, Ptfn11, Ptprc, Ptprt, Prr14, Qrfpr, Rab44, Racgap1, Rai1, Rasa4, Rbbp8nl, Rbm26, Rbm41, Rbobb1, Rims2, Rnf207, Rnfi2, Rnpep, Rpl18, Rps6ka6, Runx1t1, Scgb2b19, Scn2a1, Sdk1, Sema6b, Serpine1, Setx, Sfmbt1, Sh3bp1, Sh3kbp1, Shkbp1, Slc16a9, Slc22a21, Slc24a3, Slc35a5, Slc38a4, Slc38a5, Slc45a4, Slc9c1, Slfn8, Smer8, Smndc1, Snx21, Sobp, Sorbs2, Spag6, Spata31d1d, Spta1, Srsf9, St18, Stard13, Steap1, Stradb, Sult1e1, Supt6, Snopl, Syndig1l, Synpo, Taar6, Tanc1, Tas2r130, Tas2r139, Tas2r144, Tbx15, Tek5, Tet1, Tet3, Thbs4, Tiam2, Tmprss7, Tnc, Tnfai3, Tnfisf19, Tns1, Trim69, Triml2, Trpm7, Trrap, Ttc3, Tuba3a, Ubtd1, Unc5a, Upb1, Upf1, Vmn1r22, Vmn1r5, Vmn2r109, Vmn2r113, Vmn2r124, Vmn2r63, Vmn2r82, Vmn2r88, Vmn2r9, Vmn2r97, Vrtm, Vwa5b2, Wdr43, Wdr75, Wdr77, Wisp3, Zap70, Zc2bc1b, Zcchc3, Zfp384, Zfp385b, Zfp763, Zfp764, Zfp831, Zfp961, Zfx</i>
<b><i>Tyr::CreER<sup>T2</sup>;Braf<sup>CA/+</sup>;Lkb1<sup>+/-</sup>+UV (316 genes)</i></b>	<i>1700001C19Rik, 2610015P09Rik, 4921507P07Rik, 4931406B18Rik, 4933433C11Rik, Abca12, Abca6, Abcg3, Accs1, Afp, Abctf1, Aifm1, Aipl1, Akr1c12, Alb, Aldb1a3, Alox12e, Alpi, Ambra1, Aox1, Apba1, Appbp2, Arcn1, Arhgap27, Arhgef12, Arhgef7, Arid3b, Arid5a, Art1, Aspm, Atf6b, Bbox1, BC068157, Bcorl1, Bmp8b, Bpifc, Bsn, Carkd, Casp8, Cav1, Ccdc141, Ccdc158, Ccdc64, Cd209f, Cdh20, Cdh7, Cenpf, Cep135, Cep290, Ces3a, Cgn, Chrb1, Cic, Cka2, Clec4, Cntnap2, Col11a1, Col23a1, Col25a1, Col3a1, Col5a1, Colec12, Cpa3, Cpdl1, Crbr2, Csf3r, Csn1s2b, Cybr1, Cyp2d22, Cyp3a25, D10Bwg1379e, D930015E06Rik, Dap3, Dapke1, Dazl, Dbh, Dctn1, Ddx47, Dmbt1, Dmkn, Dolpp1, Dopey1, Dppa3, Dpysl3, Dyrk1b, Eglam, Egr4, Elf1, Enab, Enam, Enpp3, Eyt3, Evc2, F7, Fads1, Fam132b, Fam135b, Fam13c, Fam160a1, Fam186b, Fam24a, Fbxo4, Fbxw24, Fosb, Fpr3, Frem2, Frmpd1, Gas2l2, Gefc2, Gcn1l1, Gigyf1, Gpkov, Gpr149, Grap, Gria4, Grid2, Gucy2f, Hc, Hnrnpu, Hnrnpul2, Hras, Hscb, Hsd1l, Ifnb1,</i>

	<p><i>Il23r, Inpp4a, Ip6k3, Itgae, Itih2, Kank1, Katnb1l, Kcnc2, Kent2, Kif14, Kmt2d, Krtap11-1, Lama2, Lamb3, Ldoc1, Limk2, Lipc, Lphn3, Lpp, Lrp1, Lyp1a, Macc1, Map1a, Mapk10, Mapkbp1, Mast4, Mep1a, Mga, Mlph, Mlxipl, Mmp10, Mpeg1, Mrgrpb2, Mrps36, Muc5b, Mug1, Mvk, Myb13, Myb6, Myb7, Myl12b, Myo5a, Mypn, N6amt1, Naip1, Nanog, Ncam1, Nckap5, Nckap5l, Nhs1l, Nipbl, Nit1, Nubpl, Nudt3, Nyap1, Obox1, Obscn, Otog, P4bb, Pabpc2, Pabpc4, Pak4, Pard3b, Pblid2, Pcdha2, Pcdhb19, Pdik1l, Peak1, Perm1, Phactr4, Phex, Pla2r1, Plaa, Plcb4, Plec, Ppfa2, Pramel6, Prb1, Prdm1, Prdm15, Prl3b1, Prl8a6, Ptcdb3, Ptk2b, Ptpn3, Pygm, Rad21, Raver1, Rcor3, Resp18, Rgs14, Ring1, Rnf145, Ror2, Rorb, Rp11l, Rplp0, Rsad1, Rsf1, Ryr2, Sae1, Scaf8, Scml2, Sct2, Sec24c, Sel1l, Sema3f, Sema4d, Serpina3k, Serpina7, Sgca, Sh3rf1, Shroom2, Sipa1l2, Six4, Slc14a2, Slc37a3, Slc38a10, Slc44a5, Slc6a18, Slc8a1, Slitrk4, Slk, Smad9, Smarcc1, Smg9, Snai3, Sorbs3, Spata31d1b, Sptbn4, Srp72, Stat4, Sv2a, Svep1, Sycp2, Syne1, Synj2, Synpo2, Syt12, Taar8b, Tarm1, Tars2, Tas2r117, Taz, Tbr1, Tdrd5, Tet2, Tfjp11, Tg, Thnsl1, Timm23, Tle1, Tlr12, Tlr6, Tmtc3, Tnfrsf21, Tnfrsf8, Tpcn1, Trappc9, Triobb, Trpc5, Tspan10, Till11, Ttn, Uba7, Ugt2b38, Ubrf1bp1, Uqrc2, Usp17le, Usp26, Vmn1r12, Vmn1r174, Vmn2r14, Vmn2r26, Vmn2r51, Vmn2r57, Vmn2r65, Vmn2r66, Vmn2r7, Vmn2r86, Wdr19, Wdr95, Wiz, Wnk2, Xpo7, Zfp318, Zfp366, Zmym3, Znf512b, Zscan4d, Zswim2, Zyx</i></p>
--	--

**Appendix Table 9: Common genes between the different *Braf<sup>V600E</sup>*-induced animal model.** Table indicates the common genes between the B/L/UV, B/SB and RM/B/UV animal models.

Animal group	Gene ID
<b>Common (7 genes)</b>	<i>Syne1, Flna, Cep350, Zan, Csmc3, Map3k1, Dmd</i>
<b>B/L/UV and B/UV (4 genes)</b>	<i>Wdfy4, Ttn, Pclo, Obscn</i>
<b>B/L/UV and B/SB (79 genes)</b>	<p><i>Fam71e2 Tet2 Ehmt1 Macf1 Arap3 Ep300 Tns3 Parp8 Sdk1 Mark2 Apob Sema4d Nckap5 Ptpn11 Rsf1 Sel1l Vnce Nipbl Dear1 Fnip2 Dock10 Mapkbp1 Dip2c Grid2 Lphn3 Trpm7 Nsd1 Ptpn13 Ptprt Usp34 Smarcc1 Ndst3 Sipa1l2 Bmp8b Tulp4 Mfap3l D430041D05Rik Sec31a Tsc22d2 Appbp2 Cntnap5a Lrp1 Lpp Raver1 Mlkl Lmnb1 Atxn71l Cntnap2 Dock1 Sorbs2 Aldb1a3 Col5a1 Akap11 Mtmr14 Egflam Trerf1 Ush2a Mga Golgb1 Galr2 Hpse2 Ncoa1 Pkd1 EphA6 Zfx Myo10 Ggfy1 D930015E06Rik Thsd4 Sae1 Epas1 Dnmhp Inpp1l Elfl1 Mocs3 Fmnl3 Ptpnd Pblidb1 Nup155</i></p>
<b>B/UV and B/SB (1 gene)</b>	<i>Hydin</i>

**Appendix Table 10: List of B/L/UV syngeneic mutations in different human diseases.** In this table is represented the Gene ID, the mutation position in the mice genome, and the frequency of the mutation. At the right, it is represented the human data with the human Gene ID, the homologous position of the mutation in the human genome, and the studies where the syngeneic mutation has been found.

Mouse			Human		
GeneID	Mutations	Freq	GeneID	Position	Human studies// Found mutation
<i>Ache</i>	p.E323K	30,77%	<i>ACHE</i>	E323	TCGA-BS-A0UJ-01//Uterine (TCGA)//E323
<i>Abctf1</i>	p.R706C	20,45%	<i>AHCTF1</i>	R706	TCGA-BT-A20O-01//Bladder (TCGA)//R706H
<i>Alpi</i>	p.L220F	32,14%	<i>ALPI</i>	L219	MEL-Ma-Mel-114//Melanoma (Broad)//L219F
<i>Appbp2</i>	p.R549X	33,33%	<i>APPBP2</i>	R549	TCGA-BR-8363-01//Stomach (TCGA pub)//R549Q TCGA-ND-A4WC-01//Uterine CS (TCGA)//R549W
<i>Armc6</i>	p.R373W	32,93%	<i>ARMC6</i>	R406	TCGA-IB-7651-01//Pancreas (TCGA)//R406C TCGA-44-6777-01//Lung adeno (TCGA)//R406S
<i>Cacnb3</i>	p.R620Q		<i>CACNB2</i>	R625	TCGA-WB-A81W-01//PCPG (TCGA)//R625H
<i>Chd7</i>	p.A2919S	23,81%	<i>CHD7</i>	A2930	TCGA-AP-A0LT-01//Uterine (TCGA)//A2930V
<i>Clstn2</i>	p.L108F	20%	<i>CLSTN2</i>	L106	UACC_257//NCI-60//L106H
<i>Cttn</i>	p.G528V	20%	<i>CTTN</i>	G532	TCGA-CV-5444-01//Head & neck (TCGA pub)//G532V
<i>Dfnb59</i>	p.S127L	21,28%	<i>DFNB59</i>	S127	TCGA-GM-A2D9-01//Breast (TCGA)//S127*
<i>Evc2</i>	p.R697C	25%	<i>EVC2</i>	R787	H090156//Liver (AMC)//R787W
<i>Fcnb</i>	p.H285Y	23,08%	<i>FCN2</i>	H284	TCGA-13-1477-01//Ovarian (TCGA)//H284R
<i>Flna</i>	p.A1191V	21,05%	<i>FLNA</i>	A1191	TCGA-12-3650-01//GBM (TCGA)//A1191V
<i>Fpr3</i>	p.F292Y	37,29%	<i>FPR3</i>	F292	TCGA-HZ-A49I-01//Pancreas (TCGA)//F292fs TCGA-BR-6452-01//Stomach (TCGA)//F292fs
<i>Grid2</i>	p.G735R	20%	<i>GRID2</i>	G735	MEL-JWCI-14//Melanoma (Broad)//G735R
<i>Grid2</i>	p.E852K	25,64%	<i>GRID2</i>	E852	TCGA-D3-A51R-06//Melanoma (TCGA)//E852K
<i>Grin2a</i>	p.S280F	37,21%	<i>GRIN2A</i>	S280	MEL-Ma-Mel-102//Melanoma (Broad)//S280F
<i>Herc3</i>	p.R358S	21,74%	<i>HERC3</i>	R358	PD4205a //Breast (Sanger)// R358C TCGA-AA-3554-01// Colorectal (TCGA) //R358C TCGA-AP-A059-01//Uterine (TCGA) //A356S
<i>Itgae</i>	p.G612R	25%	<i>ITGAE</i>	G620	TCGA-FW-A3R5-06//Melanoma (TCGA)//G620R
<i>Kcnj15</i>	p.E176K		<i>KCNJ15</i>	E176	LUAD-QCHM7//Lung adeno (Broad)//E176K
<i>Kirrel3</i>	p.R371Q	25,42%	<i>KIRREL3</i>	R371	TCGA-IB-7651-01//Pancreas (TCGA)//R371W
<i>Map3k1</i>	p.P484S	28,57%	<i>MAP3K1</i>	P489	TCGA-06-0743-01 GBM//(TCGA 2013)//P489S
<i>Myom2</i>	p.G1359S	33,33%	<i>MYOM2</i>	G1359	YULAN//Melanoma (Yale)//G1359E
<i>Ncam1</i>	p.R165W	20%	<i>NCAM1</i>	R165	A165V CCLE NCIH2172_LUNG
<i>Ninl</i>	p.L263Q	21,62%	<i>NINL</i>	L262	587220//Colorectal (Genentech)//L262V

<i>Npas2</i>	p.S311L	33,33%	<i>NPAS2</i>	S311	TCGA-IB-7651-01//Pancreas (TCGA)//S311L
<i>Npy2r</i>	p.R241C	33,33%	<i>NPY2R</i>	R241	TCGA-FZ-5919-01//Pancreas (TCGA)//R241H
<i>Oat</i>	p.P417L	32%	<i>OAT</i>	P417	TCGA-AP-A0LD-01//Uterine (TCGA)//P417Q
<i>Pab</i>	p.E141K	40,54%	<i>PAH</i>	E141	HCT_15//NCI-60//E141D
<i>Pax5</i>	p.P363Q	20,59%	<i>PAX5</i>	P363	ESO-1427//Esophagus (Broad)//P363L
<i>Pcdhb18</i>	p.D595N	20,79%	<i>PCDHB18</i>	D542	TCGA-44-6147-01//Lung adeno (TCGA)//D542G
<i>Pkhd11</i>	p.Q862X	31,82%	<i>PKHD1L1</i>	Q862	TCGA-05-4398-01//Lung adeno (TCGA)//Q862H
<i>Plaa</i>	p.S119F	28,57%	<i>PLAA</i>	S119	TCGA-FW-A3R5-06//Melanoma (TCGA)//S119L
<i>Ptpn3</i>	p.S430F	27,38%	<i>PTPN3</i>	S430	pfg043T//Stomach (Pfizer UHK)//S430P
<i>Scaf8</i>	p.R512K	20,27%	<i>SCAF8</i>	R512	TCGA-CD-A487-01//Stomach (TCGA pub)//R512W
<i>Sema4d</i>	p.L322P	22,41%	<i>SEMA4D</i>	L322	587256//Colorectal (Genentech)//L322M
<i>Slc25a13</i>	p.R586C		<i>SLC25A13</i>	R585	TCGA-AX-A05Z-01//Uterine (TCGA)//R585C H061394//Liver (AMC)//R585C
<i>Slc35a5</i>	p.R404H	50%	<i>SLC35A5</i>	R391	TCGA-HU-A4GX-01//Stomach (TCGA pub)//R391* TCGA-B5-A0JZ-01//Uterine (TCGA)//R391Q
<i>Slc38a4</i>	p.G133E	20,69%	<i>SLC38A4</i>	G133	TCGA-BH-A18G-01//Breast (TCGA)//G133*
<i>Spag6</i>	p.R447W	25%	<i>SPAG6</i>	R447	TCGA-AA-3672-01//Colorectal (TCGA)//R447Q TCGA-AA-A010-01//Colorectal (TCGA)//R447* TCGA-BS-A0UV-01//Uterine (TCGA)//R447*
<i>St18</i>	p.P357S	25%	<i>ST18</i>	P359	LUAD-NYU259//Lung adeno (Broad)//P359A
<i>Stxbp5</i>	p.R595C	22,73%	<i>STXBP5</i>	R594	TCGA-BS-A0UV-01//Uterine (TCGA)//R594C
<i>Tars2</i>	p.R251W	25,35%	<i>TARS2</i>	R246	TCGA-EE-A2A1-06//Melanoma (TCGA)//R246W
<i>Tet1</i>	p.C1458S	25,58%	<i>TET1</i>	C1482	587286//Colorectal (Genentech)//C1482YN
<i>Thrb</i>	p.E203K	20%	<i>THRB</i>	E203	TCGA-EE-A181-06//Melanoma (TCGA)//E203K
<i>Thrb</i>	p.E217K		<i>THRB</i>	E217	TCGA-EE-A2GT-06//Melanoma (TCGA)//E217K TCGA-GF-A6C9-06//Melanoma (TCGA)//E217K
<i>Tle1</i>	p.P360S	21,74%	<i>TLE1</i>	P360 -- P361	HS746T_STOMACH//CCLE//P361H
<i>Unc13b</i>	p.R582L	20%	<i>UNC13B</i>	R570	TCGA-46-3765-01//Lung squ (TCGA pub)//R570L
<i>Unc5a</i>	p.S354F	24,07%	<i>UNC5A</i>	S298	TCGA-55-7727-01//Lung adeno (TCGA pub)//S298C

# **BIBLIOGRAPHY**



1. Douglas H, Robert W. The Hallmarks of Cancer. *Cell*. 2000;100:57–70.
2. Hanahan D, Weinberg RA. Hallmarks of cancer: the next generation. *Cell*. 2011;144(5):646–74.
3. Schadendorf D, Fisher DE, Garbe C, Gershenwald JE, Grob JJ, Halpern A, et al. Melanoma. *Nat Rev Dis Prim*. 2015;1(April):1–20.
4. Geller AC, Clapp RW, Sober AJ, Gonsalves L, Mueller L, Christiansen CL, et al. Melanoma epidemic: An analysis of six decades of data from the connecticut tumor registry. *J Clin Oncol*. 2013;31(33):4172–8.
5. Chin L. The genetics of malignant melanoma: lessons from mouse and man. *Nat Rev Cancer*. 2003;3(8):559–70.
6. Gray-Schopfer V, Wellbrock C, Marais R. Melanoma biology and new targeted therapy. *Nature*. 2007;445(7130):851–7.
7. Lo JA, Fisher DE. The melanoma revolution: From UV carcinogenesis to a new era in therapeutics. *Science (80- )*. 2014;346(6212):945–9.
8. Shain AH, Bastian BC. From melanocytes to melanomas. *Nat Rev Cancer*. 2016;16(6):345–58.
9. Lin JY, Fisher DE. Melanocyte biology and skin pigmentation. *Nature*. 2007;445(7130):843–50.
10. Bastian BC. The Molecular Pathology of Melanoma: An Integrated Taxonomy of Melanocytic Neoplasia. Vol. 9, *Annu. Rev. Pathol. Mech. Dis*. 2014. 239-271 p.
11. Köhler C, Nittner D, Rambow F, Radaelli E, Stanchi F, Vandamme N, et al. Mouse Cutaneous Melanoma Induced by Mutant BRAf Arises from Expansion and Dedifferentiation of Mature Pigmented Melanocytes. *Cell Stem Cell*. 2017;21(5):679–693.e6.
12. Moon H, Donahue LR, Choi E, Scumpia PO, Lowry WE, Grenier JK, et al. Melanocyte Stem Cell Activation and Translocation Initiate Cutaneous Melanoma in Response to UV Exposure. *Cell Stem Cell*. 2017;21(5):665–678.e6.
13. Shain AH, Yeh I, Kovalyshyn I, Sriharan A, Talevich E, Gagnon A, et al. The Genetic Evolution of Melanoma from Precursor Lesions. *N Engl J Med [Internet]*. 2015;373(20):1926–36. Available from: <http://www.nejm.org/doi/10.1056/NEJMoa1502583>
14. Chin L, Garraway L a, Fisher DE. Malignant melanoma : genetics and therapeutics in the genomic era Malignant melanoma : genetics and therapeutics in the genomic era. 2006;2149–82.
15. Michaloglou C, Vredeveld LCW, Soengas MS, Denoyelle C, Kulman T, van der Horst CMAM, et al. BRAFE600-associated senescence-like cell cycle arrest of human naevi. *Nature*. 2005;436(7051):720–4.
16. Elder DE. Melanoma progression. *Pathology*. 2016;48(2):147–54.
17. Werner-Klein M, Scheitler S, Hoffmann M, Hodak I, Dietz K, Lehnert P, et al. Genetic alterations driving metastatic colony formation are acquired outside of the primary tumour in melanoma. *Nat Commun*. 2018;9(1):595.
18. Wolber R, Schlenz K, Wakamatsu K, Smuda C, Nakanishi Y, Hearing VJ, et al. Pigmentation effects of solar-simulated radiation as compared with UVA and UVB radiation. *Pigment Cell Melanoma Res*. 2008;21(4):487–91.
19. Karran P, Brem R. Protein oxidation, UVA and human DNA repair. *DNA Repair (Amst) [Internet]*. 2016;44:178–85. Available from: <http://dx.doi.org/10.1016/j.dnarep.2016.05.024>
20. Fabo EC De, Noonan FP, Fears T, Merlino G. Ultraviolet B but not Ultraviolet A Radiation Initiates Melanoma Ultraviolet B but not Ultraviolet A Radiation Initiates Melanoma. 2004;6372–6.
21. Day C, Marchalik R, Merlino G, Michael H. Mouse models of UV-induced melanoma : genetics, pathology, and clinical relevance. *Lab Investig*. 2017;00:1–8.
22. Pho L, Grossman D, Leachman SA. Melanoma genetics: A review of genetic factors and clinical phenotypes in familial melanoma. *Curr Opin Oncol*. 2006;18(2):173–9.
23. Greene MH, Clark WH, Tucker MA, Kraemer KH, Elder DE, Fraser MC. High risk of malignant melanoma in melanoma-prone families with dysplastic nevi. *Ann Intern Med*. 1985;102(4):458–65.
24. Beauséjour CM, Krtolica A, Galimi F, Narita M, Lowe SW, Yaswen P, et al. Reversal of human cellular senescence: Roles of the p53 and p16 pathways. *EMBO J*. 2003;22(16):4212–22.
25. Goel VK, Ibrahim N, Jiang G, Singhal M, Fee S, Flotte T, et al. Melanocytic nevus-like hyperplasia and melanoma in transgenic BRAFV600E mice. *Oncogene*. 2009;28(23):2289–98.
26. Davies H, Bignell GR, Cox C, Stephens P, Edkins S, Clegg S, et al. Mutations of the BRAF gene in human cancer. *Nature*. 2002;417(6892):949–54.
27. Tsao H, Goel V, Wu H, Yang G, Haluska FG. Genetic Interaction between NRAS and BRAF Mutations and PTEN/MMAC1 Inactivation in Melanoma. *J Invest Dermatol*. 2004;122(2):337–41.
28. Stahl JM, Sharma A, Cheung M, Zimmerman M, Cheng JQ, Bosenberg MW, et al. Deregulated Akt3 Activity Promotes Development of Malignant Melanoma Deregulated Akt3 Activity Promotes Development of Malignant Melanoma. 2004;(12):7002–10.
29. Sharpless NE, Chin L. The INK4 $\alpha$ /ARF locus and melanoma. *Oncogene*. 2003;22(20):3092–8.

30. Straume OS, Akslen LAA. Alternation and prognostic significance of p16 and p53 protein expression in subgroup of cutaneous melanoma. *Int J Cancer*. 1997;539:535–9.
31. Guldberg P, Straten P, Ahrenkiel V, Seremet T, Kirkin AF, Zeuthen J. Somatic mutation of the Peutz-Jeghers syndrome gene, LKB1/STK11, in malignant melanoma. *Oncogene*. 1999;18(9):1777–80.
32. Kennedy C, Ter Huurne J, Berkhout M, Gruis N, Bastiaens M, Bergman W, et al. Melanocortin 1 receptor (MC1R) gene variants are associated with an increased risk for cutaneous melanoma which is largely independent of skin type and hair color. *J Invest Dermatol*. 2001;117(2):294–300.
33. Garraway LA, Widlund HR, Rubin MA, Getz G, Berger AJ, Ramaswamy S, et al. Integrative genomic analyses identify MITF as a lineage survival oncogene amplified in malignant melanoma. *Nature*. 2005;436(7047):117–22.
34. Lopez-Bergami P. The role of mitogen- and stress-activated protein kinase pathways in melanoma. *Pigment Cell Melanoma Res*. 2011;24(5):902–21.
35. Lopez-Bergami P, Huang C, Goydos JS, Yip D, Bar-Eli M, Herlyn M, et al. Rewired ERK-JNK Signaling Pathways in Melanoma. *Cancer Cell*. 2007;11(5):447–60.
36. Bennett DC. Genetics of melanoma progression: The rise and fall of cell senescence. *Pigment Cell Melanoma Res*. 2016;29(2):122–40.
37. Wellbrock C, Karasarides M, Marais R. The RAF proteins take centre stage. *Nat Rev Mol Cell Biol*. 2004;5(11):875–85.
38. Souroullas GP, Sharpless NE. mTOR signaling in melanoma: Oncogene-induced pseudo-senescence? *Cancer Cell*. 2015;27(1):3–5.
39. Vivanco I. Targeting molecular addictions in cancer. *Br J Cancer*. 2014;111(11):2033–8.
40. Keith T, Flaherty, M.D., Igor Puzanov, M.D., Kevin B. Kim, M.D., Antoni Ribas MD, Grant A. McArthur, M.B., B.S., Ph.D., Jeffrey A. Sosman, M.D., Peter J. O'Dwyer, M.D., Richard J. Lee, M.D., Ph.D., Joseph F. Grippo, Ph.D., Keith Nolop, M.D., and Paul B. Chapman MD, Abstract. Inhibition of Mutated, Activated BRAF in Metastatic Melanoma. *N Engl J Med*. 2005;353(10):977–87.
41. Wilhelm S, Carter C, Lynch M, Lowinger T, Dumas J, Smith RA, et al. Discovery and development of sorafenib: A multikinase inhibitor for treating cancer. *Nat Rev Drug Discov*. 2006;5(10):835–44.
42. Garbe C, Eigentler TK, Keilholz U, Hauschild A, Kirkwood JM. Systematic Review of Medical Treatment in Melanoma: Current Status and Future Prospects. *Oncologist*. 2011;16(1):5–24.
43. Fedorenko I V., Gibney GT, Sondak VK, Smalley KSM. Beyond BRAF: Where next for melanoma therapy? *Br J Cancer*. 2015;112(2):217–26.
44. Zhang C, Spevak W, Zhang Y, Burton EA, Ma Y, Habets G, et al. RAF inhibitors that evade paradoxical MAPK pathway activation. *Nature*. 2015;526(7574):583–6.
45. Menzies AM, Long G V. Systemic treatment for BRAF-mutant melanoma: Where do we go next? *Lancet Oncol*. 2014;15(9):371–81.
46. Davies MA. The Role of the PI3K-AKT Pathway in Melanoma. *Cancer J*. 2012;18(2):142–7.
47. Carnero A, Blanco-Aparicio C, Renner O, Link W, Leal JFM. The PTEN/PI3K/AKT signalling pathway in cancer, therapeutic implications. *Curr Cancer Drug Targets*. 2008;8(3):187–98.
48. Vredevelde LCW, Possik P a, Smit M a, Meissl K. Abrogation of BRAF V600E -induced senescence by PI3K pathway activation contributes to melanomagenesis. *Genes Dev*. 2012;26:1055–69.
49. Williams T, Brenman JE. LKB1 and AMPK in cell polarity and division. *Trends Cell Biol*. 2008;18(4):193–8.
50. Scott KD, Nath-Sain S, Agnew MD, Marignani PA. LKB1 catalytically deficient mutants enhance cyclin D1 expression. *Cancer Res*. 2007;67(12):5622–7.
51. Tiainen M, Vaahtomeri K, Ylikorkala A, Mäkelä TP. Growth arrest by the LKB1 tumor suppressor: induction of p21(WAF1/CIP1). *Hum Mol Genet*. 2002;11(13):1497–504.
52. Esteve-Puig R, Canals F, Colomé N, Merlino G, Recio JÁ. Uncoupling of the LKB1-AMPK $\alpha$  energy sensor pathway by growth factors and oncogenic BRAFV600E. *PLoS One*. 2009;4(3).
53. Spicer J, Ashworth A. LKB1 kinase: Master and commander of metabolism and polarity. *Curr Biol*. 2004;14(10):383–5.
54. Esteve-Puig R, Gil R, González-Sánchez E, Bech-Serra JJ, Grueso J, Hernández-Losa J, et al. A mouse model uncovers LKB1 as an UVB-induced DNA damage sensor mediating CDKN1A (p21WAF1/CIP1) degradation. *PLoS Genet*. 2014;10(10):e1004721.
55. Jeghers HMVKH. Generalized Intestinal Polyposis and Melanin Spots of the Oral Mucosa, Lips and Digits — A Syndrome of Diagnostic Significance. *N Engl J Med*. 1977;296(21):1194–200.
56. Denison FC, Hiscock NJ, Carling D, Woods A. Characterization of an alternative splice variant of LKB1. *J Biol Chem*. 2009;284(1):67–76.

57. Zhou W, Zhang J, Marcus AI. LKB1 tumor suppressor: Therapeutic opportunities knock when LKB1 is inactivated. *Genes Dis.* 2014;1(1):64–74.
58. Alessi DR, Sakamoto K, Bayascas JR. LKB1-Dependent Signaling Pathways. *Annu Rev Biochem.* 2006;75(1):137–63.
59. Xie Z, Dong Y, Zhang J, Scholz R, Neumann D, Zou M-H. Identification of the Serine 307 of LKB1 as a Novel Phosphorylation Site Essential for Its Nucleocytoplasmic Transport and Endothelial Cell Angiogenesis. *Mol Cell Biol.* 2009;29(13):3582–96.
60. Boudeau J, Scott JW, Resta N, Deak M, Kieloch A, Komander D, et al. Analysis of the LKB1-STRAD-MO25 complex. 2004;
61. Baas AF, Boudeau J, Sapkota GP, Smit L, Medema R, Morrice NA, et al. Activation of the tumour suppressor kinase LKB1 by the STE20-like pseudokinase STRAD. *EMBO J.* 2003;22(12):3062–72.
62. Boudeau J, Baas AF, Deak M, Morrice NA, Kieloch A, Schutkowski M, et al. MO25 $\alpha/\beta$  interact with STRAD $\alpha/\beta$  enhancing their ability to bind, activate and localize LKB1 in the cytoplasm. *EMBO J.* 2003;22(19):5102–14.
63. Lizcano JM, Göransson O, Toth R, Deak M, Morrice NA, Boudeau J, et al. LKB1 is a master kinase that activates 13 kinases of the AMPK subfamily, including MARK/PAR-1. *EMBO J.* 2004;23(4):833–43.
64. Shaw RJ, Kosmatka M, Bardeesy N, Hurley RL, Witters LA, DePinho RA, et al. The tumor suppressor LKB1 kinase directly activates AMP-activated kinase and regulates apoptosis in response to energy stress. *Proc Natl Acad Sci.* 2004;101(10):3329–35.
65. Sapkota GP, Deak M, Kieloch A, Morrice N, Goodarzi A a, Smythe C, et al. Ionizing radiation induces ataxia telangiectasia mutated kinase (ATM)-mediated phosphorylation of LKB1/STK11 at Thr-366. *Society.* 2002;516:507–16.
66. Rowan A, Bataille V, Mackie R, Healy E, Bicknell D, Bodmer W, et al. Somatic mutations in the Peutz-Jeghers (LKB1/STKII) gene in sporadic malignant melanomas. *J Invest Dermatol.* 1999;112(4):509–11.
67. Bardeesy N, Sinha M, Hezel AF, Signoretti S, Hathaway NA, Sharpless NE, et al. Loss of the Lkb1 tumour suppressor provokes intestinal polyposis but resistance to transformation. *Nature.* 2002;419(6903):162–7.
68. Ji H, Ramsey MR, Hayes DN, Fan C, McNamara K, Kozlowski P, et al. LKB1 modulates lung cancer differentiation and metastasis. *Nature.* 2007;448(7155):807–10.
69. Gupta R, Liu AY, Glazer PM, Wajapeyee N. LKB1 preserves genome integrity by stimulating BRCA1 expression. *Nucleic Acids Res.* 2015;43(1):259–71.
70. Wang Y-S, Chen J, Cui F, Wang H, Wang S, Hang W, et al. LKB1 is a DNA damage response protein that regulates cellular sensitivity to PARP inhibitors. *Oncotarget.* 2016;2(45):4–7.
71. Noonan FP, Dudek J, Merlino G, De Fabo EC. Animal models of melanoma: An HGF/SF transgenic mouse model may facilitate experimental access to UV initiating events. *Pigment Cell Res.* 2003;16(1):16–25.
72. Noonan FP, Recio JA, Takayama H, Duray P, Anver MR, Rush WL, et al. Neonatal sunburn and melanoma in mice. *Nature.* 2001;413(6853):271–2.
73. Dankort D, Filenova E, Collado M, Serrano M, Jones K, McMahon M. A new mouse model to explore the initiation , progression , and therapy tumors. *Genes Dev.* 2007;21(415):379–84.
74. Dankort D, Curley DP, Cartlidge RA, Nelson B, Karnezis AN, Damsky WE, et al. BrafV600E cooperates with Pten loss to induce metastatic melanoma. *Nat Genet.* 2009;41(5):544–52.
75. Damsky W, Micevic G, Meeth K, Muthusamy V, Curley DP, Santhanakrishnan M, et al. mTORC1 activation blocks brafV600E-induced growth arrest but is insufficient for melanoma formation. *Cancer Cell.* 2015;27(1):41–56.
76. Mann MB, Black MA, Jones DJ, Ward JM, Yew CCK, Newberg JY, et al. Transposon mutagenesis identifies genetic drivers of BrafV600E melanoma. *Nat Genet.* 2015;47(5):486–95.
77. Dhomen N, Reis-Filho JS, da Rocha Dias S, Hayward R, Savage K, Delmas V, et al. Oncogenic Braf Induces Melanocyte Senescence and Melanoma in Mice. *Cancer Cell.* 2009;15(4):294–303.
78. Viros A, Sanchez-Laorden B, Pedersen M, Furney SJ, Rae J, Hogan K, et al. Ultraviolet radiation accelerates BRAF-driven melanomagenesis by targeting TP53. *Nature.* 2014;511(7510):478–82.
79. Damsky W, Micevic G, Meeth K, Muthusamy V, Curley DP, Santhanakrishnan M, et al. mTORC1 activation blocks brafV600E-induced growth arrest but is insufficient for melanoma formation. *Cancer Cell.* 2015;27(1):41–56.
80. González-Sánchez E, Martín-Caballero J, Flores JM, Hernández-Losa J, Montero MÁ, Cortés J, et al. Lkb1 Loss Promotes Tumor Progression of BRAFV600E-Induced Lung Adenomas. *PLoS One.* 2013;8(6):4–11.
81. Zheng B, Jeong JH, Asara JM, Yuan Y, Granter SR, Chin L, et al. Oncogenic B-RAF Negatively Regulates the Tumor Suppressor LKB1 to Promote Melanoma Cell Proliferation. *Mol Cell.*

- 2009;30(2):237–47.
82. Fujimoto M, Basko-Plluska JL, Krausz T, Selim MA, Shea CR. Melanocytic tumors with intraepidermal melanophages: A report of five cases with review of 231 archived cutaneous melanocytic tumors. *J Cutan Pathol.* 2015;42(6):394–9.
  83. Green AC, Wallingford SC, McBride P. Childhood exposure to ultraviolet radiation and harmful skin effects: Epidemiological evidence. *Prog Biophys Mol Biol.* 2011;107(3):349–55.
  84. Recio JA, Merlino G. Hepatocyte growth factor / scatter factor activates proliferation in melanoma cells through p38 MAPK , ATF-2 and cyclin D1. *Oncogene.* 2002;21(June 2001):1000–8.
  85. Chen L, Li Z, Zwolinska AK, Matthew A, Cross B, Koomen J, et al. MDM2 recruitment of lysine methyltransferases regulates p53 transcriptional output. *EMBO J.* 2010;29(15):2538–52.
  86. Akbani R, Akdemir KC, Aksoy BA, Albert M, Ally A, Amin SB, et al. Genomic Classification of Cutaneous Melanoma. *Cell.* 2015;161(7):1681–96.
  87. Cells E, Katzenellenbogen RA, Egelkrout EM, Vliet-gregg P, Gewin LC, Gafken PR, et al. NFX1-123 and Poly ( A ) Binding Proteins Synergistically Augment Activation of Telomerase in Human Papillomavirus Type 16. 2007;81(8):3786–96.
  88. Han Y, Jin YH, Kim YJ, Kang BY, Choi HJ, Kim DW, et al. Acetylation of Sirt2 by p300 attenuates its deacetylase activity. *Biochem Biophys Res Commun.* 2008;375(4):576–80.
  89. Qin L, Wu Y, Toneff MJ, Li D, Liao L, Gao X, et al. NCOA1 Directly Targets M-CSF1 Expression to Promote Breast Cancer Metastasis. *Cancer Res.* 2015;74(13):3477–88.
  90. Recio JA, Noonan FP, Takayama H, Anver MR, Duray P, Rush WL, et al. Ink4a / Arf Deficiency Promotes Ultraviolet Radiation-induced Melanomagenesis 1. 2002;6724–30.
  91. Ikehata H, Ono T. The mechanisms of UV mutagenesis. *J Radiat Res.* 2011;52(2):115–25.
  92. Noonan FP, Otsuka T, Bang S, Anver MR, Merlino G. Accelerated ultraviolet radiation-induced carcinogenesis in hepatocyte growth factor/scatter factor transgenic mice. *Cancer Res.* 2000;60(14):3738–43.
  93. Krauthammer M, Kong Y, Ha BH, Evans P, Bacchiocchi A, McCusker JP, et al. Exome sequencing identifies recurrent somatic RAC1 mutations in melanoma. *Nat Genet.* 2012;44(9):1006–14.
  94. Patton EE, Widlund HR, Kutok JL, Kopani KR, Amatruda JF, Murphey RD, et al. BRAF Mutations Are Sufficient to Promote Nevi Formation and Cooperate with p53 in the Genesis of Melanoma. *Curr Biol.* 2005;15:249–54.
  95. Xu H, Zhai Y, Chen J, Lu Y, Wang J, Quan C, et al. LKB1 reduces ROS-mediated cell damage via activation of p38. 2014;(August):1–12.
  96. Xie X, Hu H, Tong X, Li L, Liu X, Chen M, et al. The mTOR–S6K pathway links growth signalling to DNA damage response by targeting RNF168 Xiaoduo. *Nat Cell Biol* [Internet]. 2018; Available from: <http://dx.doi.org/10.1038/s41556-017-0033-8>
  97. Kottakis F, Nicolay BN, Roumane A, Karnik R, Gu H, Nagle JM, et al. LKB1 loss links serine metabolism to DNA methylation and tumorigenesis. *Nature.* 2016;539(7629):390–5.
  98. Spender LC, Ferguson GJ, Liu S, Cui C, Girotti MR, Sibbet G, et al. Mutational activation of BRAF confers sensitivity to transforming growth factor beta inhibitors in human cancer cells. *Oncotarget.* 2016;7(50):81995–2012.
  99. Sanz-Moreno V, Marshall CJ. Rho-GTPase signaling drives melanoma cell plasticity. *Cell Cycle.* 2009;8(10):1484–7.
  100. Makrodouli E, Oikonomou E, Koc M, Andera L, Sasazuki T, Shirasawa S, et al. BRAF and RAS oncogenes regulate Rho GTPase pathways to mediate migration and invasion properties in human colon cancer cells: a comparative study. *Mol Cancer.* 2011;10:118.
  101. Fecchi K, Travaglione S, Spadaro F, Quattrini A, Parolini I, Piccaro G, et al. Human melanoma cells express FGFR/Src/Rho signaling that entails an adhesion-independent caveolin-1 membrane association. *Int J Cancer.* 2012;130(6):1273–83.
  102. Ahmad I, Muneer KM, Tamimi IA, Chang ME, Ata MO, Yusuf N. Thymoquinone suppresses metastasis of melanoma cells by inhibition of NLRP3 inflammasome. *Toxicol Appl Pharmacol.* 2013;270(1):70–6.
  103. Zeng PY, Berger SL. LKB1 is recruited to the p21/WAF1 promoter by p53 to mediate transcriptional activation. *Cancer Res.* 2006;66(22):10701–8.
  104. Shelly M, Cancedda L, Heilshorn S, Sumbre G, Poo M ming. LKB1/STRAD Promotes Axon Initiation During Neuronal Polarization. *Cell.* 2007;129(3):565–77.
  105. Barnes AP, Lilley BN, Pan YA, Plummer LJ, Powell AW, Raines AN, et al. LKB1 and SAD Kinases Define a Pathway Required for the Polarization of Cortical Neurons. 2007;1:549–63.
  106. Kuwako K, Okano H. Versatile Roles of LKB1 Kinase Signaling in Neural Development and Homeostasis. 2018;11(October):1–9.

107. Asada N, Sanada K, Fukada Y. LKB1 Regulates Neuronal Migration and Neuronal Differentiation in the Developing Neocortex through Centrosomal Positioning. 2007;27(43):11769–75.
108. Garman B, Anastopoulos IN, Krepler C, Brafford P, Sproesser K, Jiang Y, et al. Genetic and Genomic Characterization of 462 Melanoma Patient-Derived Xenografts, Tumor Biopsies, and Cell Lines. *Cell Rep.* 2017;21(7):1936–52.
109. Gray-Schopfer VC, Karasarides M, Hayward R, Marais R. Tumor necrosis factor- $\alpha$  blocks apoptosis in melanoma cells when BRAF signaling is inhibited. *Cancer Res.* 2007;67(1):122–9.
110. Madonna G, Ullman CD, Gentilcore G, Palmieri G, Ascierto PA. NF- $\kappa$ B as potential target in the treatment of melanoma. *J Transl Med.* 2012;10(1):53.
111. Estrada Y, Dong J, Ossowski L. Positive crosstalk between ERK and p38 in melanoma stimulates migration and in vivo proliferation. *Pigment Cell Melanoma Res.* 2009;22(1):66–76.
112. Kunz M, Ibrahim S, Koczan D, Thiesen HJ, Köhler HJ, Acker T, et al. Activation of c-Jun NH2-terminal kinase/stress-activated protein kinase (JNK/SAPK) is critical for hypoxia-induced apoptosis of human malignant melanoma. *Cell Growth Differ.* 2001;12(3):137–45.
113. Brancho D, Tanaka N, Jaeschke A, Ventura JJ, Kelkar N, Tanaka Y, et al. Mechanism of p38 MAP kinase activation in vivo. *Genes Dev.* 2003;17:1969–78.